ELECTROPHYSIOLOGICAL STUDIES OF ACQUIRED EPILEPSY AFTER PERINATAL HYPOXIA-ISCHEMIA

by

Jeffrey Bastar

A dissertation submitted to the faculty of
The University of Utah
in partial fulfillment of the requirements for the degree of

Doctor of Philosophy

Department of Physiology

The University of Utah

December 2016

Copyright © Jeffrey Bastar 2016

All Rights Reserved

The University of Utah Graduate School

STATEMENT OF DISSERTATION APPROVAL

The dissertation of **Jeffrey Bastar**

has been approved by the following supervisory committee members:

F. Edward Dudek	, Chair	**10/27/2016** Date Approved
K.C. Brennan	, Member	**10/27/2016** Date Approved
Michael C. Sanguinetti	, Member	**10/27/2016** Date Approved
Awais Riaz	, Member	**10/31/2016** Date Approved
Matthew Wachowiak	, Member	**10/27/2016** Date Approved

and by **Dean Li** , Chair/Dean of

the Department/College/School of **Physiology**

and by David B. Kieda, Dean of The Graduate School.

ABSTRACT

Perinatal hypoxic-ischemic (PHI) encephalopathy afflicts roughly 1-2 in every 1000 live births, predisposing affected infants to a higher probability of developing epilepsy, cerebral palsy, and other neurological disorders. In many forms of acquired epilepsy, including PHI, there is a seizure-free period of time between the injury and the onset of the first spontaneous recurrent seizure (SRS) termed the latent period. In animal models of PHI, we aim to better understand the mechanisms that lead to an epileptic network that occur during this latent period. Due to limitations in performing electrophysiological experiments in immature animals, this time period remains under-studied in the pediatric population. We start our study at the cellular level using immunohistochemistry and whole-cell patch clamp methods before moving to the whole brain level with magnetic resonance imaging and the electroencephalogram (EEG) to examine anatomical and physiological changes that precede the development of epilepsy. We find that immediately after injury, early cell loss results in a reduction in the amount of excitatory and inhibitory synaptic input to pyramidal cells within the peri-infarct region. However, this reduction is short term, as there is a rapid recovery in the synaptic inputs 2 weeks later without any identifiable increase in the number of cells. As the brain continues to develop, the cellular loss that occurs early on leads to atrophy, and sometimes complete loss of the cortex, hippocampus, and thalamus. Even with major cell loss, power spectral analysis of the EEG identified no obvious reduction or increase in the power of any of the various cortical rhythms (delta, theta, alpha, beta, and gamma). However, EEG analysis did reveal the earliest known time point at which seizures occur in this animal model, as well as a previously undescribed short-duration convulsive seizure. Our findings suggest that the mechanisms responsible for the development of SRSs begin immediately after injury and result in a variable and progressive latent period.

TABLE OF CONTENTS

LIST OF FIGURES

ACKNOWLEDGEMENTS

I would like to acknowledge my advisor, Dr. Ed Dudek, for his guidance and mentorship through the development and completion of this work. The knowledge imparted on me through him will serve me well both in my career and in my life. I would like to acknowledge my committee for providing me valuable feedback on this project, and for being such outstanding role models in the guidance of my career. I would like to acknowledge my collaborators and colleagues in the Dudek lab: Dr. Jay Spampanato for teaching me many things including slice electrophysiology, and most of all that there is such a thing as a dumb question; Dr. Mark Lehmkuhle for his work on the video-EEG acquisition and for always being prompt; Dr. Peter Roper for his assistance in the analysis of the EEG data, and for teaching me patience - you saved me years on the end of my life and took away just as many; Dr. Erika Scholl for her sympathy and support in keeping me going when I had little left in the tank; Dr. Petr Tvrdik for his mentorship and for asking the questions I didn't think to ask. I would like to acknowledge Vicki Skelton for all things administrative, for making sure all the i's were dotted and the t's were crossed, and for being the oil that kept the machine running. I would like to acknowledge the HHMI Med into Grad Program for providing multiple opportunities to share my work, and for the additional education in translational research. I would like to acknowledge my parents, in-laws, and siblings for the moral support and the many Sunday dinners, Friday night dinners, and the random meals that were of greater support than they will ever know. Last but not least, I would like to acknowledge my wife Brooke, who was with me every step of the way. Thank you for being by my side through all the good and the bad that this project had to offer, and for putting up with me when even I didn't want to put up with me. This project would not be completed without you. In the paraphrased words of the great electrophysiologist Buszaki, forgive me for all those times I was absent but more importantly for all those times my body was present but my mind was not.

CHAPTER 1

PERINATAL HYPOXIC-ISCHEMIC ENCEPHALOPATHY: A MODEL OF STROKE-INDUCED PEDIATRIC EPILEPSY

Jeffrey Bastar[1], Jay G. Spampanato[2], Shilpa D. Kadam[3], Andrew Zayachkivsky[4], Jeffrey Ekstrand[5], Kevin J. Staley[6], F. Edward Dudek[2]

[1]Department of Physiology, University of Utah School of Medicine, Salt Lake City, UT, USA

[2]Department of Neurosurgery, University of Utah School of Medicine, Salt Lake City, UT, USA

[3]Neuroscience Laboratory, Hugo Moser Research Institute at Kennedy Krieger, Baltimore, MD, USA

[4]Neurona Therapeutics, 650 Gateway Boulevard, South San Francisco, CA, USA

[5]Department of Pediatrics, University of Utah School of Medicine, Salt Lake City, UT, USA

[6]Department of Neurology, Massachusetts General Hospital, Harvard Medical School, Boston, MA, USA

Corresponding Author:

F. Edward Dudek, Ph.D.
Department of Neurosurgery
University of Utah School of Medicine
383 Colorow, Suite 383
Salt Lake City, UT 84108

Email: ed.dudek@hsc.utah.edu

Office phone: (801) 587-5880
FAX: (801) 581-8075
Cell: (970) 690-402

Abstract

Perinatal hypoxia-ischemia (PHI) in rodents (i.e., the Rice-Vannucci model) is associated with acute seizures, and can lead to a variable amount (moderate to severe) of neuronal injury. In immature rats at postnatal day 7 (P7), PHI or hypoxia alone (Ha) leads acutely to two distinct patterns of "early" electrographic seizures (i.e., maximal power in the alpha and delta bands) (Zayachkivsky et al., 2015). Long-term, continuous, wireless recordings from rats for periods of up to 6 months have revealed spontaneous recurrent seizures (SRSs; i.e., "late" seizures) and spikes in the Electroencephalogram (EEG), which progressively worsened over time after the PHI treatment (2-11 months) (Kadam et al., 2010). The SRSs that occurred after the PHI treatment had durations of 10s of seconds. Initially, most SRSs were nonconvulsive, but later, most of them were convulsive. The SRSs often occurred in clusters, where each seizure cluster could be separated by week and could contain a dozen SRSs over a 1-2 day period. Only those rats with a macroscopic infarct later developed SRSs; those rats without obvious lesions did not develop chronic epilepsy (i.e., had no detectable SRSs). The neuropathological features of this clinically relevant model recapitulate the pattern of neuronal loss in humans with PHI encephalopathy (PHIE); the SRSs and electrographic spikes in this animal model have a duration, frequency, and pattern that emulate this form of acquired human pediatric epilepsy.

General Description of the Model

Animal models of perinatal hypoxic-ischemic encephalopathy (PHIE) have long been used to study the underlying mechanisms and long-term consequences of birth-related brain injury. Rice, Vannucci, and Brierley (1981) adapted the Levine model of anoxic injury (Levine, 1960) to the 7-day postnatal (P7) rat pup, and thereby developed the basic protocol for production of the PHI model. PHI-induced brain injury involves unilateral ligation of the common carotid artery, which is followed by systemic hypoxia. Many variations of this model have been developed over the past few decades. It has long been known that PHI is a major cause of neurological disability in premature newborns and full-term infants that have undergone a prolonged or complicated birth (Volpe, 1998; Johnston et al., 2001). The goal of developing PHI

as an animal model was to provide insight into the underlying mechanisms of brain injury in order to develop early detection strategies and treatments to minimize or prevent neuronal damage, thus potentially mitigating the acquired epilepsy and developmental comorbidities that result from PHI. While several models of PHI, or ischemia alone, have been developed in different species, most research examining acute and subacute seizure activity and the development of epilepsy with spontaneous recurrent seizures (SRSs) has been performed in rodents. This review will therefore deal primarily with research concerning PHI-induced seizures in rats (and to some extent, mice), with only a limited discussion of other species. It will focus on seizures and epilepsy, although PHI models have been used to investigate many other related neurobiological problems.

The primary mechanism responsible for permanent brain damage in the PHIE model is oxygen and glucose deprivation (Perlman, 2006). PHI results in rapid neuronal injury manifest as necrosis (early stage) and apoptosis or programmed cell death (late stage). The injury is associated with membrane depolarization, excessive release of glutamate, an increase of intracellular [Ca^{2+}], generation of free radicals, and the activation of phospholipases and nucleases (Perlman, 2006). It is critical to differentiate the PHI model from alternative models of neonatal seizures (Sun et al., 2016), based on perinatal hypoxia alone (PHa). In *both* PHI and PHa, the rat pups acutely experience two types of behavioral and electrographic seizures *during* the treatment (i.e., EEG power is primarily in the alpha and delta bands) (Zayachkivsky et al., 2015). In PHIE, however, a variable percentage of the animals also develop a well-defined infarct and neuropathological changes that are similar to those observed clinically (Marín-Padilla, 2000, Kadam and Dudek, 2007). By contrast, in the PHa model (i.e., hypoxia without ischemia) the animals experience the acute seizures with no detectable neuronal death (e.g., Rakhade et al., 2011). The PHIE model has been shown to generate epilepsy, based on long-term (i.e., several months), continuous video-EEG monitoring of SRSs (Kadam et al., 2010). Importantly, and in contrast to PHa, only the PHI-treated animals that had an ischemic lesion developed chronic epilepsy (Kadam et al., 2010), even though all of the carotid artery-ligated animals experienced

seizures *during* the hypoxic treatment. These data establish the validity of PHI as a model of acquired pediatric epilepsy.

Methods of Generation of the Model

In the rat, both hypoxia and ischemia are required for the induction of an infarct, while some mouse strains are susceptible to an infarct with unilateral occlusion of the carotid artery alone. This is an important point for the PHI model, because the infarct appears to be necessary for the development of epilepsy (Kadam et al., 2010). Although it has been argued that hypoxia-induced seizures in immature rats leads to spontaneous recurrent seizures (Rakhade et al., 2011), the PHa model has been challenged based on the short duration and high frequency of the epileptiform events, and the presence of these events in control animals (Shaw, 2004, 2007). The overall method to produce PHI-induced neuronal damage consists of unilateral ligation of the common carotid artery, followed by systemic hypoxia of 8% oxygen and balanced nitrogen (Rice et al., 1981), while maintaining the animal at 37 °C. The duration of hypoxia has varied across different studies in the literature, ranging from 30 min to >3 hr. Our laboratory uses the following protocol. Sprague-Dawley rat pups 7 days of age (P7), weighing approximately 16-18 gm (male and/or female), are anesthetized with 2-4% isoflurane. The ventral cervical region is aseptically prepared with betadine scrub and the ventral midline infused with bupivacaine (0.5%, 0.25 ml). Under direct visualization with a dissecting microscope, a 1-cm midline incision is made over the trachea, and the right common carotid artery is isolated and permanently ligated with a cautery pen. The incision is closed with 4-0 Vicryl suture and the pup is allowed to recover with the dam and littermates for 2 hr. Age-matched sham-surgery controls have the right common carotid artery exposed under identical procedures, but it is not ligated. After the 2-hr recovery period, the rat pups with the ligated carotid artery are placed into an air-tight temperature- and humidity-controlled chamber. The rat pups are subjected to hypoxia (humidified 8% oxygen, balanced nitrogen) and maintained at 37 °C for 2 hr, and then allowed to recover in normal air before being returned to the dam and littermates. Age-matched sham-operated controls are placed into the same air-tight temperature- (37 °C) and humidity-controlled chamber for 2 hr, but the rodents are

not exposed to the hypoxic conditions (Kadam et al., 2010). To produce PHa animals in our group, the same treatment protocol is used with the hypoxic gas, but without unilateral ligation of the carotid artery (Zayachkivsky et al., 2015). However, other groups have developed other PHa protocols; for example, Rakhade et al. (2011) used only 15 min of hypoxia (7% oxygen for 8 min, 5% for 6 min, and 4% for 1 min).

The original developers of the model observed that rat pups could survive in the 8% O_2 hypoxic environment for $\geq$3 hr before substantial mortality occurred (Vannucci et al., 1999). We have observed that some animals begin to die at approximately 90 min, and the full 3-hr duration of hypoxia is not necessarily required for induction of the infarct. The size of the lesions that develop is variable and range from a slight reduction in the volume of the ipsilateral hemisphere to near complete loss of the entire affected hemisphere. Both cortical and subcortical structures, such as the hippocampus, may be damaged; however, the core of neuronal loss is parasagittal in location between the perfusion territories of the middle cerebral artery supplied by the common carotid artery (Kadam and Dudek, 2007). The cingulate cortex is spared, as it is perfused by the anterior cerebral artery.

Characteristics and Defining Features

Age- and Sex–related Issues

During development of the PHI model in the rat, the age of 7 postnatal days (P7) was chosen because the developmental stage of the brain was thought to best correlate with that of a 32-40-week infant (Semple et al., 2013). At this age, histological analysis shows that neuronal layering in the cerebral cortex is complete, the germinal matrix is undergoing involution, and white matter myelination is absent (Vannucci et al., 1999). Due to higher resistance to hypoxia, the concentration of oxygen must be decreased to 5% when using animals younger than P7 (e.g., P2-3) (Towfighi et al., 1997). Older animals become more sensitive to the HI insult, leading to increased severity and frequency of the lesion at higher ages between P7-30 (Towfighi et al., 1997), and older animals are more prone to die. The hippocampus is relatively resistant to HI before P7, but becomes progressively more vulnerable with age, and by P13, hippocampal injury

can exceed cortical damage (Towfighi et al., 1997). Both male and female animals can be and have been used in HI treatment, and both have shown vulnerability to developing cerebral lesions.

Seizure/Epilepsy Phenotype

Spikes

The relationship between interictal spikes and epileptogenesis in the PHI model has only been examined qualitatively. The earliest time point investigated was 2 months of age, about 7 weeks after induction of the infarct (Kadam et al., 2010). In all HI-treated animals that later developed SRSs in the work of Kadam and coworkers (2010), interictal events were already present at 2 months as spikes and sharp waves. The interictal activity was initially lateralized to the ipsilateral hemisphere; spike frequency increased over time as the interictal events became more widespread. The unilateral nature of the spiking coincided with the lateralization of the onset of electrographic seizure activity during SRSs. Interictal spikes were not observed in those animals that underwent PHI treatment but did not develop an infarct or SRSs. These data (Kadam et al., 2010) together support the hypothesis that interictal spikes are associated with epileptogenesis, offering potential predictive value to an epilepsy diagnosis (White et al., 2010). With the development of advanced techniques that enable EEG recordings in neonatal pups immediately after HI, the time course for the recovery of background suppression and for the development of interictal spikes relative to the onset of SRSs should be addressable using quantitative methods, with particular emphasis on early detection to determine the potential of background suppression and interictal spikes to serve as biomarkers for acquired epileptogenesis.

EEG/Behavioral Seizures

In the PHI model, seizures have been recorded with video-EEG both acutely at the time of the PHI brain insult (i.e., “early” seizures) and chronically as of 2 months after PHI (i.e., “late” seizures). Electrographic seizures (i.e., “early” seizures) occur during hypoxia, whether or not

ongoing ischemia is present (Zayachkivsky et al., 2015). Similarly, video-EEG has been used with radiotelemetry to study nonconvulsive and convulsive SRSs (i.e., “late” seizures), which progressively increase in frequency with time after the PHI insult and tend to occur in clusters (Williams et al., 2004; Kadam and Dudek, 2007; Williams and Dudek, 2007; Kadam et al., 2010). A unique finding of the PHI animal model is that only the animals that develop cortical damage as a result of HI will go on to experience spontaneous recurrent seizures. Seizures are seen as early as 2-3 months of age at a frequency of approximately 8 seizures/month (Kadam et al., 2010). However, this estimate of overall seizure frequency is quite variable because the seizures generally occur in clusters. Behaviorally, the animals exhibit forelimb clonus with some lordotic posturing, the equivalent of a grade 3 seizure on the Racine scale. Due to previous recording limitations (i.e., size of the DSI radiotelemetry transmitters was too large to implant in immature rats), 2-3 months of age is the earliest time point available to observe when seizures start. Improved recording techniques are currently allowing us to perform chronic recordings at a much earlier time point (i.e., miniature telemetry from Epitel, inc.). These studies, as described later in this thesis, might reveal a shorter latent period and an earlier onset of spontaneous seizures.

Seizures associated with the perinatal HI model are progressive. As the animal matures in age, seizure frequency increases to approximately 40 seizures/month by 1 year of age. Similarly, seizure severity increases in the same manner and the behavioral correlate evolves to include rearing and falling over, classified as grade 4-5 seizures (Kadam et al., 2010). As seen in patients with epilepsy and other animal models, the seizures in this model do tend to cluster. The initial increase in seizure frequency from 2 months to 6 months primarily results in a decrease in the intercluster interval before stabilizing. Intercluster intervals, the time *between* seizure clusters, can last from a few days up to a few weeks with seizures occurring in clusters of as few as 2 and up to as many as 22 within a 24-hr period (Kadam et al., 2010).

Due to a large infarct zone that encompasses many cortical and subcortical structures, including the hippocampus, the localization for the onset of seizures associated with PHI is currently unknown. The rate of seizure occurrence does not correlate with the amount of damage to the hippocampus, suggesting that the focal onset zone may be elsewhere (Williams et al.,

2004). Multi-electrode recordings of cortical EEG in 2-7 month-old rats have shown initial seizure activity in the peri-infarct region prior to spreading to the remaining ipsilateral and contralateral cortices (Kadam et al., 2010). Simultaneous EEG recordings from the ipsilateral hippocampus and the peri-infarct region will be necessary to identify the true focal point for seizure onset in this model. It is entirely possible that the variability in lesion size results in variability in seizure onset zone leading to onsets in different regions based on severity of the lesion. The progressive nature of the epileptogenesis in this model results in synchronous bilateral seizure onsets in older animals (Kadam et al., 2010).

Acute Seizures

Video-EEG analyses have been performed on the acute seizures that occur during PHI with tethered recordings (Cuaycong et al., 2011; Sampath et al., 2014) and with miniature wireless telemetry (Zayachkivsky et al., 2013, 2015). Sampath and coworkers (2014) reported seizures during PHI with variable duration and behaviors. Zayachkivsky et al. (2015) found two distinct types of seizures: convulsive seizures had electrographic activity in the delta band, while seizures with electrographic activity in the alpha band showed a tonic “shivering” type of behavior. These two distinct types of seizures could occur separately or together. Zayachkivsky and coworkers (2015) observed that the acute seizures during PHI appeared to be similar if not identical to the seizures during PHa (i.e., no ischemia), which strongly suggests that exposure to the hypoxic environment (rather than the ischemia *per se*) drives the acute seizures in these two models. The seizures began soon after onset of hypoxia (Zayachkivsky et al., 2015), and seizure frequency progressively decreased from the first hour through the second hour during exposure to the hypoxic conditions (Zayachkivsky et al., 2015). Simultaneously, the background EEG (i.e., EEG activity between seizures) became suppressed (Sampath et al., 2014; Zayachkivsky et al., 2015). Abnormalities in the background EEG have been proposed as potential predictors of ongoing brain damage (Watanabe et al., 1980; Tharp et al., 1989; Legido et al., 1991; Holmes and Lombroso, 1993; Zayachkivsky et al., 2015). A reduction in the background EEG signal should, in theory, be easier to detect in an EEG recording than infrequent and sporadic seizure

activity. Therefore, these data support earlier work suggesting that background suppression of the EEG is a more reliable and useful detector and predictor of ongoing brain injury and subsequent epilepsy, which is potentially important because the most promising treatments for prevention of epilepsy after brain injury presumably should be administered within this early phase.

Response to Induced Repetitive Seizures

The response of the PHI model to induced repetitive seizures has been studied by testing the effect of kainate-induced seizures superimposed on the PHI treatment (Wirrell et al., 2001). Kainate-induced seizures, which alone caused little or no neuronal death at P10, substantially augmented the PHI-induced histopathological brain damage. Therefore, even though kainate-induced seizures in the otherwise normal immature brain may not cause significant histopathological injury, these seizures can greatly augment PHI-induced brain injury (Wirrell et al., 2001). The PHI-treatment in the Wirrell et al. study was of a shorter duration than the PHI-treatment used in this dissertation (i.e., 30 min vs. 120 min). Therefore, the resulting damage measured in Wirrell et al. occurred exclusively in the hippocampus.

Epilepsy Including Epileptogenesis and Progression of Epilepsy

This model offers a unique opportunity to study mechanisms of epileptogenesis in real-time as they occur in the acute and latent phases, prior to the development of SRSs. As is seen in other animal models of acquired epilepsy, it is difficult to determine whether anatomical or physiological changes associated with the development of epilepsy are the cause of the SRSs, or are an effect from these seizures on the brain. Having a relatively long, slow progression compared to many other experimental models allows for the study of multiple time points during epileptogenesis.

Examination of the latent period has revealed that prior to the onset of SRSs, cortical evoked field potential recordings ipsilateral to the infarct at 3 weeks post-HI exhibit normal responses in standard solutions, but a hyper-excitable network in the presence of a $GABA_A$

receptor antagonist (Kadam and Dudek, 2016). However, 6 months later when the animal has ongoing SRSs, there is a break down in this balance of inhibitory GABAergic and excitatory glutamatergic transmission so that cortical slices are bilaterally hyperexcitable without the presence of a $GABA_A$ receptor antagonist (Kadam and Dudek, 2016). These findings suggest greater innervation early on from local excitatory circuits that are normally "masked" by GABAergic circuits. Additional electrophysiological analysis of the latent period is the primary focus of this thesis.

As mentioned earlier, the properties and patterns of SRSs that characterize PHI-induced epilepsy have been studied with long-term, continuous, radio-telemetric recordings obtained from 2 months to >1 year of age (Kadam et al., 2010). The duration of individual SRSs ranged from about 40 sec to 100 sec, with nonconvulsive seizures occurring at earlier times after the PHI insult and generally having slightly shorter durations, compared to convulsive seizures. The SRSs recorded after PHI were quite similar to those obtained in animal models of acquired epilepsy based on status epilepticus (e.g., repeated low-dose kainate; see Williams et al., 2009; Dudek et al., this volume); in addition to durations that were 10s of seconds, these events showed a progressive evolution during each seizure, and they were followed by a period of post-ictal depression. The SRSs were distinctly different from the spike-and-wave discharges (SWDs) reported after PHa (Rakhade et al., 2011), which appear identical to the "absence-like" seizures (i.e., typically seconds in duration) characterized extensively in sham-control animals of the same strain (i.e., Long-Evans "hooded" rats; see (Shaw, 2004, 2007)).

The SRSs associated with the PHI model have been shown to be progressive. By 1 year of age, seizure frequency increased to about 40 seizures per month (Kadam et al., 2010), as determined with long-term, continuous recordings from two different cohorts of rats (each recorded for about 5 months). Seizure severity also progressively increased from focal nonconvulsive seizures to convulsive seizures that appeared to have a bilateral onset (Kadam et al., 2010). The behavioral correlates of these convulsive seizures evolved to include rearing and falling, which are classified as grade 4-5 seizures (Kadam et al., 2010) with the Racine scale. As seen in patients with epilepsy and in other animal models, the seizures in this model can exhibit

profound clustering. Intercluster intervals can last from a few days to a few weeks, and the SRSs occurred in clusters of as few as 2 and up to as many as 22 seizures within a 24-hr period (Kadam et al., 2010).

Reflex Epilepsy

Reflex seizures are initiated when an external stimulus provokes a seizure. The perinatal HI model exhibits profound neuronal malformations within the ipsilateral somatosensory cortex and it is therefore plausible that the HI-treated animals could experience reflex seizures, although this has not been specifically tested. Kadam et al. (2010) reported that the handling of 2 animals during cage change resulted in a reflex convulsive seizure. One of these rats later went on to have one spontaneous convulsive seizure followed by more reflex seizures, but the other one progressed to develop spontaneous seizures unrelated to handling with no additional reflex seizures. Although only two rats were seen to develop reflex seizures in that study, it is possible that all of the animals with the PHI model would show reflex seizures if given the appropriate stimulus.

Neuropathology

Neuron Loss

Neuronal loss associated with the Rice and Vannucci model of PHIE is similar to the human condition. Although variable across individual animals, the core of the infarct is parasagittal in location, lying within the perfusion territory of the middle cerebral artery. The ipsilateral paracingulate cortex, which is perfused by the anterior cerebral artery, is unaffected by the lesion. Cell death starts to occur soon after the onset of the HI treatment, with a diffuse loss of neurons throughout the ipsilateral cortex after the insult (Kadam and Dudek, 2007). At 30 days post-HI, neocortical cell death appears less diffuse, and columns of surviving neurons are formed and separated by bands of glial scar tissue, including the presence of deep-laminar loss of cortical neurons (Kadam and Dudek, 2007). At 6 months of age, the extensive atrophy of the ipsilateral hemisphere is associated with parasagittal microgyri. Some of the pyramidal neurons

have transformed their morphology, which includes an increase in cell body size, as well as distorted and sometimes increased branching of apical and basal dendrites (Kadam and Dudek, 2007). In the spared paracingulate cortex, there are cytomegalic pyramidal neurons with dysmorphic dendritic branching, and a large amount of pedunculated and mushroom spines on the dendrites (Kadam and Dudek, 2007). White matter hypercellularity occurred in the region of the corpus callosum underlying ipsilateral and contralateral cortex, as well white matter dysplasia (blurring of the border between white and layer VI gray matter).

The ipsilateral hippocampus is atrophied, particularly in the more rostral or dorsal region (Kadam and Dudek, 2007). The lesion of the dorsal hippocampus is variable in size and severity: from minimal loss of neurons in CA3, CA1, or the dentate gyrus, to severe loss in those regions, or complete loss of the hippocampus (Kadam and Dudek, 2007). The ventral hippocampus is relatively spared in this model, except that Timm staining of mossy fiber sprouting is present bilaterally in both the dorsal and ventral hippocampus (Williams et al., 2004; Kadam and Dudek, 2007; Williams and Dudek, 2007).

Reactive Gliosis

Most research on glial cells after PHI has focused on the mechanisms underlying injury to the oligodendrocytes, which results in damage to the developing white matter leading to cerebral palsy (Sen and Levison, 2006). Relatively little is known about reactive gliosis during PHIE. A common belief is that astrocytes have a strong resistance to ischemia, yet astrocyte death may precede neuronal loss after a stroke, at least in adult HI models (Garcia et al., 1993; Liu et al., 1999; Lukaszevicz et al., 2002). As early as 12 hr post-HI, degenerating astrocytes are present in both the white and gray matter. For up to 24 hr, these cells show signs of shortened dendritic processes, chromatin condensation, and apoptotic bodies (Villapol et al., 2008). In the HI animal model, astrocytes represent 30-60% of apoptotic cells within the first 72 hr after HI (Villapol et al., 2008). The formation of the glial scar begins around 24 hr post-HI from a dense network of reactive GFAP-positive astrocytes. For the first week following HI, the astrogliosis remains at the periphery of the infarcted region. As the surviving neurons coalesce into columns of living tissue

at 1 month of age, the astrogliosis is observed surrounding the fluid-filled cavity (Benjelloun et al., 1999). The presence of reactive astrocytes this far into cortical development suggests that astrogliosis may play an active role in the formation of the cystic infarct.

Whether reactive astrocytes are beneficial or detrimental to cortical recovery after a HI event is still unknown. Immediately after the injury, during inflammation of the tissue, reactive glia and invading immune cells produce reactive oxygen species, release excitatory amino acid agonists, proinflammatory cytokines, chemokines, and tumor necrosis factors which further contributes to neuronal death through apoptosis (Bona et al., 1999; Hagberg and Mallard, 2005). However, after adult ischemia, reactive astrocytes protect neurons and oligodendrocytes by restricting inflammation (Sofroniew, 2005), and in the absence of reactive astrocytes, the brain is more susceptible to injury (Nawashiro et al., 2000).

Similar to reactive astrocytes, it is unknown whether activated microglia are beneficial or detrimental to the infarcted tissue. Activation of microglia is detected at the periphery of the infarcted region by 72 hr post-HI, and progressively infiltrates the tissue increasing in number over the course of a week (Benjelloun et al., 1999). Studies from other stroke models suggest a negative impact of microglia, based on the finding that inhibition of microglia activation attenuates ischemia-induced brain injury (Villapol et al., 2008). Infiltration of microglia leads to blood-brain barrier disruption, and edema formation (Sheehan and Tsirka, 2005). Microglia also releases inflammatory cytokines and cytotoxic substances that can further exacerbate tissue injury (Sheehan and Tsirka, 2005). Contrary to this, some studies suggest a beneficial role of microglia in increasing functional recovery after cerebral ischemia (Neumann et al., 2006, 2009). Microglia release metalloproteinases (MMPs), which are important in extracellular matrix remodeling and angiogenesis. Furthermore, microglia aid in the repair of tissue through phagocytosis of cellular debris and producing anti-inflammatory cytokines and growth factors (Shi and Pamer, 2011). Additional studies directly focusing on microglia activation in the perinatal HI model are necessary to fully understand the role of microglia activation to the development of the infarct.

Imaging

The use of advanced imaging techniques in the PHI model is not widespread, but interest in their use continues to increase because it would provide a clinically relevant means to non-invasively measure infarct volume, hemispheric atrophy, structural loss (van der Aa et al., 2013; Aggarwal et al., 2014), and to track changes over time. Obviously, imaging offers the ability to make comparisons between lesion size/location to different outcomes without euthanizing the animal, which would be useful for testing the effectiveness of potential antiseizure and neuroprotective treatments. Various applications of magnetic resonance imaging (MRI) that can be used include T1-wieghted imaging, T2-wieghted imaging, and diffusion tensor imaging (DTI)(Wang et al., 2006; Lodygensky et al., 2008; Tuor et al., 2013). Compared to human infants, however, the spatial resolution of MRI in P7 rat pups is significantly lower (Lodygensky et al., 2008) because of the small brain volume in the pups. For analysis of the pathological changes after PHI, MR imaging has the potential to identify similar structural abnormalities as seen with immunohistochemical staining.

Co-morbidities

Cognitive/Behavioral

Only a limited amount of published data are available on cognitive and behavioral deficits associated with PHIE in rodents. In comparison to sham controls, PHI rats tested in the open field test had significantly decreased traveling distance and speed, had a lower score for rearing/leaning and grooming, and spent more time in the center of the maze, thus indicating impairment in motor and exploratory activity (Qu et al., 2014; Sanches et al., 2015). When tested on the Morris water maze for spatial reference memory, they performed worse than sham controls with increased escape latency and distance traveled (Qu et al., 2014; Sanches et al., 2015). On inhibitory avoidance tests, PHI animals performed worse than shams, suggesting memory impairment (Rojas et al., 2013; Sanches et al., 2015).

Mortality

The most critical time in regard to mortality is during the hypoxia phase of treatment. The cause of death during hypoxia is cessation of respiration during acute seizures. Respiration becomes visibly strained during the hypoxic treatment as the diaphragm and intercostal muscles become constricted, thus preventing the animals from breathing. During prolonged seizures, respiration may stop and not start again, resulting in death. It is rare for pups to die *after* the hypoxic treatment (after the oxygen levels are returned to normal), and thus mortality rates are not often reported. We have observed that up to half of the pups may die during any particular PHI treatment procedure, with an average mortality of about 25%. Finally, temperature of the chamber is an extremely important variable that must be monitored routinely and kept well-controlled; higher temperatures (e.g., >37 °C) greatly increase mortality.

Strain/Genetic Variations

Most research on PHIE has been done in Sprague-Dawley rats at P7, but other studies with Wistar rats at P7-12 (Levison et al., 2001; Cuaycong et al., 2011) have shown similar results. No known differences between different rat strains or other genetic variations seem to alter the formation of the lesion, or the development of epilepsy. An important issue relevant to previous studies on acquired epileptogenesis is the confounding interpretations based on the reported induction of brief (mostly a few seconds in duration), frequently occurring (a few or several per minute, but quite variable) spike-and-wave discharges (SWDs) that have been attributed to epileptogenesis after hypoxia-induced “neonatal seizures” (Rakhade et al., 2011). These studies have been performed in the “hooded” rat (Long-Evans strain), which is well known to have high occurrence of SWDs in *controls* (Shaw, 2004, 2007), which progressively increase in frequency and duration as the animal ages (i.e., unlike *absence* epilepsy in humans, where the *absence* seizures often undergo remission as the child matures) (Pearl et al., 2001). Therefore, the greater occurrence of SWDs in control animals of Long-Evans rats compared to Sprague-Dawley is an important confound for the studies claiming that Ha treatment leads to epilepsy (Rakhade et al., 2011; Lippman-Bell et al., 2013).

Species Variations

Use of the Rice-Vannucci PHI model in animals other than rats offers numerous potential benefits. Adaptation of the PHI model to mice, in particular, would allow the use of novel genetic tools in the design of experiments intended to address basic mechanisms related to the PHI-induced development of acute seizures and chronic epilepsy. Genetic background may have a significant influence on the amount of brain damage; for example, CD1 mice appear to be more susceptible and 129Sv being more resistant to HI treatment (Sheldon et al., 1998). When monitored for 4 hr following treatment, CD1 mice at P12 had a higher incidence of lesions and higher percentage of seizures than P7 pups (Kadam et al., 2008). Chronic convulsive SRSs were later detected with video monitoring during a 7-month monitoring period. C57/BL6 mice that received the HI treatment at P7 and underwent limited video and EEG monitoring appeared to exhibit a lower propensity to develop chronic seizures with the rate of occurrence at 2 out of 9 animals that had an infarct (Peng et al., 2015). Due to the limited monitoring in this study, however, the number of animals that were determined to have had either early (acute and subacute) seizures was almost certainly underestimated. These data suggest that PHI models would be quite effective in mice, and in conjunction with the genetic tools available in mice, this approach could be particularly useful for mechanistic studies on epileptogenesis.

The greater size of large-animal models allows a wide range of experiments that are either not feasible or are much more difficult in a rodent. Most research with large animals has been focused on preventing brain damage during various PHI protocols. The most commonly used large-animal models are pigs (Kyng et al., 2015) and sheep; the closer similarity of their brains to that of a human (e.g., a white/gray matter ratio similar to human brain) has allowed for improved development of neuroprotective therapies, such as hypothermia (Thoresen et al., 1995; Gunn et al., 1997). The methods for inducing PHI in pigs and sheep are different from rats, but the resulting injury is similar. Neuropathological assessment of neuronal loss has identified lesions in pigs and sheep that are similar to those seen in humans, with degeneration in the hippocampus, thalamus, striatum, cortex, and subcortical white matter (Aridas et al., 2014). These large-animal models develop acute background EEG suppression and SRSs (Williams et

al., 1990; Björkman et al., 2010). An additional benefit to using large animals in studying HI-induced epilepsy is the ease of implementing multi-electrode EEG devices to monitor neural activity from the onset of the injury all the way through epileptogenesis. Even though these models are not widely used, they mimic the human disease and offer a range of benefits.

Response to Antiepileptic Drugs

The use of the PHI model has been limited when it comes to antiepileptic drug (AED) testing. The majority of the testing that has been done has focused on the acute period (i.e., PHI-treatment) and the response of these acute seizures (initial seizures occurring during treatment) to AEDs. Even though PHI results in a high risk to develop chronic seizures in the human population, this disorder is often looked at as a pediatric condition, as if treating the early (acute) seizures will prevent development of chronic epilepsy. However, in the PHI model we have experimentally identified a stronger correlation between SRSs with brain damage, than with the occurrence of acute seizures (Kadam et al., 2010).

Levetiracetam is a 7-yr-old antiepileptic drug that is gaining popularity in the treatment of the pediatric population. It is already approved for clinical use in infants older than 4 weeks of age (Beaulieau, 2013), and is often recommended for the treatment of neonatal seizures (Silverstein and Ferriero, 2008). Levetiracetam has a favorable pharmacokinetic profile in the pediatric population and appears to have neuroprotective properties (Kilicdag et al., 2013). When tested in the PHI model, the results were mixed. A few studies suggest that levetiracetam was neuroprotective when measuring neuronal apoptosis histopathologically (Kilicdag et al., 2013; Komur et al., 2014), and others found that administration of levetiracetam exacerbated injury resulting in greater cell loss from PHI-treatment (Griesmaier et al., 2014). All of these studies administered levetiracetam after PHI-treatment. These results suggest that there is a potential for levetiracetam, but further research is necessary to draw any further conclusion.

PHI is partly mediated by excitotoxicity, providing another target pathway to reduce neuronal loss and the subsequent epilepsy. Topiramate, an AMPA receptor antagonist, prevents over activation during excess accumulation of glutamate, as occurs during HI. In various models

of focal ischemic models, topiramate has been reported to reduce infarct volume by 50-80% (Yang et al., 1998). Specifically looking at the perinatal HI model, administration of topiramate reduced brain damage and improved cognitive impairments (Noh et al., 2006). However, this treatment was only efficacious if given within the first 2 hr post-HI. Similar to studies with levetiracetam, there are no studies measuring the effects of topiramate on SRSs.

A common drug studied in neonatal models (not PHI), and worth mentioning here, is the loop diuretic bumetanide, which blocks the NKCC1 cotransporter. In immature brains, the concentration of Cl^- is higher intracellularly so that GABA is depolarizing, and thus possibly excitatory. This is a direct result of the NKCC1 cotransporter that pumps Cl^- into the cell. This, potentially, is the hypothetical reason pediatric epilepsies are refractory to AEDs that act as GABA receptor agonists. The use of the bumetanide shifts the reversal potential for Cl^- more negative, resulting in GABA becoming inhibitory. Bumetanide has been shown to be efficacious in some models of immature seizures by suppressing hippocampal epileptiform activity and attenuating electrographic seizures (Dzhala et al., 2005). Currently, bumetanide has only be tested in the PHa model with misleading results (Wang et al., 2015), but warrants investigation in the PHI model.

Use in Therapy and Biomarker Development

The pathophysiological cascade that leads to neuronal death is not confined to the hypoxic event, but lasts for days after the insult (Vannucci et al., 2004). This time window allows for the application of several different types of therapeutic treatments and interventions. However, it can be difficult to determine if there has been an HI event leading to neuronal death and subsequent epilepsy. To determine if and when therapeutic treatment is necessary, biomarkers that are effective within the first 2 days after injury are required. The use of noninvasive imaging techniques and quantitative EEG offer potential benefit for identifying brain damage. EEG monitoring over the first 4 days starting at the onset of HI has identified a significant reduction in the integrated power of the beta and gamma frequencies from P8 to at least P10 in animals that developed an infarct (Zayachkivsky et al., 2011, 2015). These results suggest that quantitative

EEG – in addition to imaging – could potentially identify when injury is occurring in real time and allow for immediate treatment to reduce or prevent further neuronal damage.

The PHI model may also be useful to gain additional evidence whether interictal spiking is a biomarker for the development of acquired epilepsy. Monitoring the presumed latent period with EEG to identify interictal spiking or subclinical nonconvulsive seizures may help to determine the electrographic abnormalities that precede clinically recognizable seizures. Abnormalities that identify when epileptogenesis is occurring could further increase the potential therapeutic time frame for the treatment of epilepsy with anti-epileptogenic drugs, even after a lesion has formed.

There are currently no approved effective therapeutic treatments for PHI (Fathali et al., 2011). However, numerous types of therapies in development are aimed at improving neuroprotection within the first 2 days after PHI. Of the physiological manipulations, hypothermia is the most potent and promising treatment for preventing energy depletion (Ohmura et al., 2005). A reduction in body temperature to 3-5°C below normal temperature is sufficient to decrease brain energy utilization, thus leading to reduced neuronal loss and lesion size (Sirimanne et al., 1996).

Pharmacological interventions are being tested as alternatives to hypothermia or in combination with hypothermia. These treatments can be administered after the identification of the injury, but within that 2-day time window of neuronal loss. All of these treatments show promising results by reducing infarct volume and ultimately preserving hemispheric brain volume. Pharmacological treatments are numerous and include haemopoietic growth factors (Maiese et al., 2008), nitric oxide synthase inhibitors (Johnston et al., 2000), neuronal growth factors (Holtzman et al., 1996; Hossain et al., 1998), the inhibition of caspase enzymes (Cheng et al., 1998; Kawamura et al., 2005), glutamate receptor antagonists (Alkan et al., 2001; Noh et al., 2006), calcium channel blockers (Zhu et al., 2011), and free radical scavengers (Yasuoka et al., 2004; Miura et al., 2006).

Limitations

The PHI model is widely used for multiple reasons, such as very little equipment or time is required to perform the treatment (Taniguchi and Andreasson, 2008). One of the limitations with this model is the variability in lesion size, ranging from 0 to 83% of the affected hemisphere (Cuaycong et al., 2011). The wide range in cerebral matter lost to the lesion adds complexity to interpreting the results between researchers. Increased reporting of the range of lesion sizes and the extent of cortical damage observed in each study would help to address this complication. In addition to lesion size variability, some animals completely fail to develop a detectable cortical infarct (Towfighi et al., 1997; Kadam et al., 2009; 2010). When performing chronic epilepsy studies without live-animal imaging, it has not been possible to know which animal has developed a lesion until histopathological studies have been performed. As a result, it might be necessary to increase the number of animals undergoing treatment to increase the likelihood that you will have a large enough sample size with lesions, which could prolong its overall duration. However, the possibility that only half of the HI-treated animals will have an infarct creates an improved experimental design because those animals subjected to HI that do not develop an infarct (and thus also do not develop epilepsy) can provide an important control group (e.g., see Kadam et al., 2010)

Model Optimization Considerations

As mentioned throughout this chapter, an inherent difficulty with the PHI model is the variability that exists with the lesion size. While the lesion always occurs within the perfusion territory of the MCA, it does not always involve the same amount of damage. The lesion can encompass various amounts of cortical and subcortical structures, or spare those same regions. For example, the ipsilateral hippocampus in one PHI animal might be completely missing, and then unaffected in another. This variability in lesion size adds complexity to interpreting results from different labs. Future research with this model will benefit from further optimization of the PHI techniques. A standard hypoxia chamber used between labs could be of use to ensure that

temperature, oxygen flow, and CO_2 venting remains the same between labs as a way to minimize the factors that could potentially affect lesion size.

Insights into Human Disorders – What Does the Model Model?

After the elderly, the perinatal period is the most susceptible to stroke and HI brain injury. PHIE is a major cause of acute mortality and chronic neurological morbidity in infants and children. In rodents, this condition has been studied extensively with the Rice-Vannucci model; with this method, unilateral occlusion of the common carotid artery leads to a unilateral infarct, which is accompanied by acute and subacute nonconvulsive and convulsive seizures and also with chronic epilepsy. Thus, as has been described in this chapter and will be briefly summarized below, this variant of the Rice-Vannucci model shows seizures and epilepsy with many similarities to the human condition. As with humans, the rodent is variable in terms of the nature and site of the injury, although a typical injury pattern within the perfusion territory of the MCA is common in both the rodent and human. Thus, a highly characteristic pattern of brain damage provides a model of PHIE with many of the detailed histopathological characteristics found in human neonates. In the rodent, the insult is generally administered at postnatal day 7 (P7-P10), which is qualitatively similar to the human perinatal period. Nearly one-quarter to one-half of affected infants will die in the acute period, during or directly after the HI injury (Graham et al., 2008); thus, the mortality associated with PHIE in the rodent is similar to human neonates.

Similar to the human, the PHI insult causes acute and subacute seizures, which have been difficult to study rigorously in rodent pups. Using miniature wireless telemetry, the electrographic seizures were observed in at least two distinct forms, each of which persisted for tens of seconds to minutes. Experiments with Ha showed that the seizures do not cause any obvious histopathological damage, whereas PHI leads to robust damage that culminates in a macroscopic cystic infarct and appears to be an important if not essential feature of acquired epileptogenesis. The pattern of the acute seizures was very similar during the two treatment protocols (i.e., PHa and PHI), which suggests that the 2-hr hypoxia treatment *per se* drives the acute seizures, or at least plays a prominent role in their generation under these conditions. The

total acute seizure burden during the hypoxia treatment phase was actually greater for the PHa group compared to the PHI group. The subsequent brain injury in the form of an infarct is associated with background suppression during and after the insult, which persists for days after the PHI and maybe longer. Thus, as in the human, background suppression is almost certainly a better indicator or biomarker of subsequent negative outcomes, such as overt brain damage and chronic epilepsy, because neonatal seizures alone are not necessarily associated with brain injury and subsequent epilepsy. Furthermore, imaging of the lesion may be a good structural biomarker for PHIE-induced epileptogenesis in humans. Finally, the observation that the acute seizure burden was higher during Ha (no infarct and no epilepsy) compared to HI (ultimately had an infarct, and later developed epilepsy) argues that it is the infarct - *not the acute seizures* - that causes the subsequent SRSs and epilepsy.

In the PHI model, the chronic epilepsy shows a latent period for the development of SRSs that may be partially obscured by the subacute seizures and the slow buildup and probabilistic occurrence of the SRSs. As with all epilepsy, the latent period is difficult to determine with certainty (i.e., requires continuous long-term seizure monitoring to be certain that a prior seizure was not missed), but available data suggest it is on the order of a few weeks. EEG spikes appear to precede the SRSs, and spikes were only observed in those animals that later developed SRSs (Kadam et al., 2010). Thus, electrographic spikes may be a good electrophysiological biomarker for PHIE-induced epileptogenesis in humans. The individual seizures have the electrophysiological properties, particularly the seizure duration, similar to nonconvulsive seizures in humans derived from brain injury, as opposed to spike-and-wave discharges (SWDs) or *absence* seizures. Other potentially relevant models, such as neonatal hypoxia without concordant ischemia (i.e., PHa) (Rakhade et al., 2011) and lateral fluid percussion (D'Ambrosio et al., 2009), have brief seizures (typically only a few seconds, but rarely 10s of seconds) at a much higher frequency (i.e., many per minute as opposed to one or a few per day), but these events are readily apparent in control animals. Thus, the individual seizures - in terms of duration, waveform, and pattern in these other models (e.g., D'Ambrosio et al., 2009; Rakhade et al., 2011) are extremely dissimilar to what is observed in the PHI model and human

patients that have suffered perinatal brain damage. In addition, another important point is that seizures typically occur in clusters in the PHI-induced model, which is often seen in children with PHI-induced epilepsy. Therefore, the PHI model models perinatal brain damage and leads to a form of epilepsy very similar to what is often seen in children with perinatal brain injury.

CHAPTER 2

SHORT-TERM SYNAPTIC RECOVERY IN THE RAT NEOCORTEX AFTER PERINATAL HYPOXIA-ISCHEMIA

J.D. Bastar[1], J. Spampanato[2], F.E. Dudek[2]

Departments of Physiology[1] and Neurosurgery[2]

University of Utah School of Medicine

Salt Lake City, UT

Corresponding Author:

F. Edward Dudek, Ph.D.
Department of Neurosurgery
University of Utah School of Medicine
383 Colorow, Suite 383
Salt Lake City, UT 84108

Email: ed.dudek@hsc.utah.edu

Office phone: (801) 587-5880
FAX: (801) 581-8075
Cell: (970) 690-402

Abstract

Perinatal hypoxia-ischemia (HI) is common and predisposes the infant to later-in-life neurological impairments, such as cognitive deficits, cerebral palsy, and epilepsy. The HI-induced, anatomical, and physiological changes in the neocortex that subsequently contribute to the development of spontaneous recurrent seizures (i.e., chronic epilepsy) remain unknown. Previous data from our group (Kadam et al., 2010) demonstrate that a commonly used model of HI encephalopathy can produce a robust infarct, and rats with HI-induced brain damage develop epilepsy. We hypothesized that the neocortical pyramidal cells in the peri-infarct region have dramatically reduced synaptic innervation, due to local neuronal death, when compared to sham controls.

HI was induced in rat pups at postnatal day 7 (P7) using the Rice-Vannucci model (Levine, 1960; Rice et al., 1981). Whole-cell recordings were performed on brain slices from HI-treated animals and sham controls: (1) at 24-48 hr after HI (i.e., P8-9), (2) 2 weeks later (P21-23), when cell loss is complete (Lai and Yang, 2011), and (3) adulthood (P120), a time point when spontaneous recurrent seizures are thought to have started to occur (Kadam et al., 2010). Specifically, we recorded miniature inhibitory postsynaptic currents (mIPSCs), miniature excitatory postsynaptic currents (mEPSCs), and tonic inhibition (at P8-9 and P21-23 ages) converging onto pyramidal neurons within the peri-infarct region that surrounds the damage. Immunohistochemistry for GAD67 and NeuN labeling was used to confirm gross anatomical loss of interneurons and pyramidal neurons in the damaged area. The frequency of both mIPSCs and mEPSCs onto superficial cortical pyramidal cells in the HI-treated animals was significantly decreased within 24-48 hr after HI. At 2 weeks after HI, however, the frequency of the mIPSCs and mEPSCs had recovered to control levels. The amplitudes and decay constants of the mIPSCs and mEPSCs were unchanged at all time points. Likewise, tonic inhibition did not differ between HI and sham-control animals at P8-9 or P21-23. At P21-23 ages, isolated groups of cells could clearly be seen in and around the cortical infarct. The GAD67 and NeuN labeling confirmed that these islands of cortex contained both pyramidal cells and interneurons; however, their contribution to normal and abnormal cortical function is unclear. Our data suggest that one of the

first functional changes in the damaged cortex following HI is a loss of inhibitory and excitatory synaptic innervation, which appears to recover within 2 weeks after HI. Considering the extensive damage that results from HI, it is remarkable that so much functional recovery in synaptic innervation occurs so quickly. Previous studies have suggested that the initial spontaneous recurrent seizures that begin to occur a few weeks after HI appear to be generated primarily within the peri-infarct region (Kadam et al., 2010). The present studies provide evidence that substantial re-innervation of both excitatory and inhibitory synaptic connections has already occurred by this point. Continued synaptic reorganization may contribute to a hyperexcitable network and progressive epileptogenesis.

Introduction

Perinatal hypoxia-ischemia (HI) is a common neurological insult occurring in approximately 1-2 per 1000 live births (Kurinczuk et al., 2010). The overall occurrence of HI in surviving infants is about 1.1%. Neonatal mortality occurs in 15-20% of these births with 25% of the survivors developing neurological sequelae that include cognitive deficits, cerebral palsy, and epilepsy (Pisani et al., 2009). Epilepsy associated with cerebral palsy and HI is frequently refractory to medication (Hadjipanayis et al., 1997), and is therefore of a particular concern. The best strategy for new treatments for HI-induced epilepsy is to target mechanisms that occur during the latent period, which is after the injury but before the onset of spontaneous recurrent seizures. Metabolic effects of HI have been extensively studied, identifying pathogenic mechanisms of cell death through necrosis and apoptosis as a result of energy deficiencies within the first 6-48 hr (Lai and Yang, 2011). Weeks later, this cellular death contributes to the morphological abnormalities within the cerebral hemisphere leading to chronic recurrent seizures, which progressively become more severe and more frequent (Kadam et al., 2010). It is still unknown how neuronal loss and the other anatomical and physiological changes lead to spontaneous recurrent seizures.

Our group has extensively characterized an etiologically appropriate animal model with a perinatal insult that is comparable in many ways to HI injuries in the human. Histopathological

features of the neocortical lesion in this animal model correspond to the clinical findings of the human condition, which include porencephalic cysts, microgyri, dislamination of cortical cytoarchitecture, and neuronal dysmorphisms (Kadam and Dudek, 2007). Even though infarct size is variable between animals, the core of the infarct is primarily located between the perfusion territories of the major arteries supplied by the middle cerebral artery (MCA). Due to immaturity of penetrating cerebral vasculature at the age of HI onset (Rorke, 1992), the neocortical neuronal cell death is predominantly columnar at 1 month. Morphological changes continue over time, creating isolated patches of neurons at 6 months (Kadam and Dudek, 2007). The hippocampus, the major focal point of seizures in temporal lobe epilepsy, is atrophied and shifted to a more caudal location. Histological analysis of the hippocampus after the development of chronic seizures has identified the presence of mossy fiber sprouting in the ipsilateral, and even contralateral, hippocampi associated with the severity of the lesion (Williams et al., 2004; Kadam and Dudek, 2007). However, the amount of hippocampal damage does not correlate with the seizure occurrence, suggesting that the focal point may be elsewhere (Williams et al., 2004). A possible site for the onset of electrographic seizures is within the peri-infarct region, where the remaining cells have a hypothetical reduction in synaptic innervation from local neuronal death. EEG data with recording channels near the infarct, the peri-infarct region, and the contralateral cortex suggest an electrographic seizure onset zone within the peri-infarct cortex (Kadam et al., 2010).

To assess the degree of loss and recovery of excitatory and inhibitory synaptic inputs onto neocortical pyramidal cells after perinatal HI, we recorded miniature inhibitory and excitatory postsynaptic currents (mIPSCs and mEPSCs) along with tonic inhibition in layer 2/3 pyramidal neurons within the peri-infarct region of the lesion at P8-9, P21-23, and P120. Experimental time points were selected to represent various stages in the epileptogenic process: (1) P8-9 is during the process of cell loss due to necrosis and apoptosis, (2) P21-23 is early within the estimated latent period, and (3) P120 is thought to be after the onset of spontaneous recurrent seizures. Studying changes in synaptic function *prior* to the development of spontaneous seizures will support the hypothesis that any changes identified would be epileptogenic in nature, and not a

consequence of the spontaneous recurrent seizures themselves. Because the recordings were performed prior to the development of seizures, or in animals that were not monitored for seizures (P120), the presence of a cortical infarct was used as presumptive evidence that these animals would develop epilepsy based on prior evidence that 100% of animals with an infarct developed spontaneous recurrent seizures, while none of the animals without an infarct did (Kadam et al., 2010).

Methods

Animals

All surgical procedures were performed under protocols approved by the University of Utah Animal Care and Use Committee. Pregnant Sprague-Dawley adult female rats (14 days gestation) were received from Charles River (Wilmington, MA). Pups were born in the animal facility ~1 week after the arrival of the pregnant female (University of Utah, Salt Lake City, UT). The litter size was culled to 8 pups at P3. Animals were housed with the dam and littermates, and at P7, they were treated with HI. The weight of the pup at the time of treatment was 16-18 g.

Perinatal HI

To model human neonatal hypoxic-ischemic encephalopathic cortical infarcts, the modified Levine's method (Levine, 1960; Rice et al., 1981) was performed on P7 rat pups. Both male and female rat pups 7 days of age were anesthetized with 2-4% isoflurane. The ventral cervical region was aseptically prepared with betadine scrub and the ventral midline infused with bupivacaine (0.5%, 0.25 ml). A 1-cm midline incision was made over the trachea, and the right carotid artery isolated and permanently ligated with a cautery pen. The incision was closed with 4-0 vicryl suture and the pup was allowed to recover for 2 hr with the dam and littermates. Age-matched sham controls had the carotid artery exposed under identical procedures but was not ligated.

After a 2-hr recovery period, the rat pups with the ligated carotid artery were placed into an air-tight temperature and humidity controlled chamber. They were subjected to hypoxia

(humidified 8% oxygen, balanced nitrogen) and maintained at 37 °C for 2 hr, and then allowed to recover in normal air before being returned to the dam and littermates. Age-matched sham-operated controls were placed into a separate air-tight temperature (37 °C) and humidity controlled chamber for 2 hr, but did not receive hypoxic conditions.

Slice Preparation

Coronal slices were cut from P8-9 HI (n = 6) and sham-operated (n = 4), and P21-23 HI (n = 5) and sham-operated (n = 5) Sprague-Dawley rats. Brains were quickly removed and placed into ice-cold normal artificial cerebrospinal fluid (aCSF) containing (in mM): 118 $C_5H_{14}ClNO$, 2.5 KCl, 1.3 $MgCl_2$, 1.2 NaH_2PO_4, 25 $NaHCO_3$, 10 glucose, 2.5 $CaCl_2$ with pH 7.3-7.4 when bubbled with 95% O_2-5%CO_2. Slices (400 µm thick) containing regions with cortical infarct were cut in the coronal orientation using a Leica VT1200 Vibratome (Leica Microsystems, Wetzlar, Germany). The slices were then transferred to a submerged holding chamber containing normal aCSF composed of (in mM): 125 NaCl, 3 KCl, 1.3 $MgSO_4$, 1.2 NaH_2PO_4, 25 $NaHCO_3$, 25 glucose, 1.3 $CaCl_2$ aerated with 95% O_2 and 5%CO_2 at 32 °C and allowed to recover for at least 1 h prior to experimentation.

Whole cell electrophysiological recordings in adult animals are more difficult, so the preparation was modified for coronal slices cut from P120 HI (n = 9) and sham-operated (n = 9) Sprague-Dawley rats. Brains were quickly removed and placed into ice-cold normal artificial cerebrospinal fluid (aCSF) containing (in mM): 92 $C_5H_{14}ClNO$, 2.5 KCl, 1.2 NaH_2PO_4, 30 $NaHCO_3$, 20 HEPES, 25 glucose, 5 sodium ascorbate, 2 thiourea, 3 sodium pyruvate, 10 $MgSO_4$, 0.5 $CaCl_2$ with 300-310 mOsm and pH 7.3-7.4 when bubbled with 95% O_2-5%CO_2. Slices (350 µm thick) containing regions with cortical infarct were cut in the coronal orientation using a Leica VT1200 Vibratome. The slices were then transferred to a submerged holding chamber containing NMDG-HEPES recovery solution composed of (in mM): 93 NMDG, 2.5 KCl, 1.2 NaH_2PO_4, 30 $NaHCO_3$, 20 HEPES, 25 glucose, 5 sodium ascorbate, 2 thiourea, 3 sodium pyruvate, 10 $MgSO_4$, 0.5 $CaCl_2$, 1.5 GSH-EE with 300-310 mOsm and pH 7.3-7.4 when bubbled with 95% O_2-5%CO_2 at 32 °C and allowed to recover for 15 min before being transferred to another submerged

holding chamber containing normal aCSF composed of (in mM): 92 NaCl, 2.5 KCl, 1.2 NaH_2PO_4, 30 $NaHCO_3$, 20 HEPES, 25 glucose, 5 sodium ascorbate, 2 thiourea, 3 sodium pyruvate, 10 $MgSO_4$, 0.5 $CaCl_2$ with 300-310 mOsm and pH 7.3-7.4 when bubbled with 95% O_2-5%CO_2 at 32 °C and allowed to recover for at least 1 h prior to experimentation.

Whole-Cell Voltage-Clamp Electrophysiology

Slices were placed in a submerged recording chamber and perfused with an extracellular recording solution containing (in mM): 125 NaCl, 3 KCl, 1.3 $MgSO_4$, 1.2 NaH_2PO_4, 25 $NaHCO_3$, 25 glucose, 1.3 $CaCl_2$, and 1 µM tetrodotoxin (Abcam, Cambridge, MA, USA). For adult slices, the extracellular recording solution contained 5 mM HEPES to aid in balancing pH and osmolarity (not used for juvenile slices). The recording solution was aerated with 95% O_2 and 5%CO_2 and a bath temperature was maintained at 33-34 °C. Microelectrodes (3-6 MΩ when filled) were pulled from fire-polished borosilicate glass (Sutter Instrument, Novato, CA, USA) and filled with internal recording solution containing (in mM): 135 Cs-methyl sulfonate, 8 NaCl, 10 HEPES, 0.5 EGTA, 2 MgATP, 0.3 NaATP, 7 Phosphocreatine Tris, 8 Biocytin (pH=7.3, 300 mOsmol). Whole-cell recordings were performed in voltage clamp mode on visually identified layer 2/3 pyramidal cells. In most cases, both mEPSCs and mIPSCs were recorded in the same cell by first holding the membrane potential at -70 mV to record mEPSCs, and then depolarizing to +10 mV to record mIPSCs. Whole-cell capacitance and series resistance were monitored and recordings were made with >70% series resistance compensation using the Axon Instruments MultiClamp 700A (Molecular Devices Corporation, Sunnyvale, CA, USA) at 10 kHz sampling frequency and digitized by an Axon Instruments Digidata 1440A. Recordings were terminated if the series resistance exceeded 25 MΩ. Events were detected from 8-10 min raw data. Kinetics of decay were measured by fitting the unitary averaged traces from isolated single events with an exponential function. Some events were best fit with a double exponential of the form: $A(t) = A_f exp\left(-t/\tau_f\right) + A_s exp(-t/\tau_s)$ where A_f and A_s are the amplitudes of the fast and slow decay components, and τ_s and τ_f are their respective decay time constants. The weighted time constant was calculated as:

$$\tau_\omega = \left\{ A_f \Big/ (A_f + A_s) \right\} \tau_f + \left\{ A_s \Big/ (A_f + A_s) \right\} \tau_s$$

This was used for comparisons of the decay times of the mEPSCs and mIPSCs.

Tonic inhibitory currents (I_{tonic}) recordings were performed identical to the whole-cell recordings with a few exceptions. We recorded tonic GABA at the typical V_{rest} of the cell. In order to achieve this, we needed high intracellular [Cl^-], making glutamatergic and GABAergic currents indistinguishable. Therefore, we used Kynurenic acid to block glutamatergic currents, and GABA was added to the extracellular solution to induce a strong I_{tonic}, and ensure that there would be a sufficient GABA-activated current to record. For recording I_{tonic} at -70 mV, a high CsCl-based internal solution was used, containing (in mM): 140 CsCl, 1 $MgCl_2$, 4 NaCl, 10 HEPES, 5.5 EGTA, 2 MgATP, 0.3 NaGTP, 2 Qx-314, 10 phosphocreatine, 8 biocytin (pH=7.2; 300 mOsmol). I_{tonic} was measured as the reduction in baseline holding currents after bath-applying a saturating amount (1 mM) of the $GABA_A$-receptor channel blocker, picrotoxin.

Immunohistochemistry

Rat pups P8-9 and P21-23 were anesthetized with isoflurane then transcardially perfused with 25 ml 0.9% saline followed by 50 ml of 4% paraformaldehyde (PFA) in 0.1 M phosphate buffer (PB, pH 7.4%). Brains were removed and post-fixed overnight in PFA at 4°C then washed in 0.1M phosphate buffered saline (PBS) and stored at 4°C. Brains were cut as 50-µm thick coronal sections on the Vibratome (VT1200; Leica). All sections were blocked in 5% BSA and 0.1% Triton in PBS for 1 h then incubated with one of the following primary antibodies (in 0.5% BSA, 0.05% sodium azide in PBS at RT for >60 h):mouse monoclonal anti-GAD-67 (1:10,000; Millipore), or mouse monoclonal anti-NeuN (1:10,000; Millipore) combined with rabbit polyclonal anti-GAD-65/67 (1:1,000; Sigma). Sections were then washed in PBS and incubated with either biotinylated anti-mouse (1:500; Vector) for GAD-67 sections, or biotinylated anti-rabbit (1:500, Vector) for GAD-65/67 sections (in 0.5% BSA, 0.05% sodium azide in PBS at RT for 3-5 h). For visualization, sections were washed in PBS and incubated with one or both of the following fluorescence conjugated secondary antibodies (in 0.5% BSA, 0.05% sodium azide in PBS at RT for 12-15 h): Alexa Fluor 488 goat anti-mouse (1:2000; Molecular Probes), and/or streptavidin

Alexa Fluor 555 (1:2000; Molecular Probes). After additional PBS washes, sections were mounted onto glass slides and coverslips in Flouromount-G (Southern Biotech) for imaging on an Imager Z1 microscope (Zeiss), with necessary filter sets for two-color epifluorescence.

Statistical Analysis

All values are expressed as means ± SEM. If the data followed a normal distribution based on an F-test, a homoscedastic Student's t-test was used to determine statistical significance between groups. When data displayed significantly different variances according to an F-test then a heteroscedastic t-test was used.

Results

A perinatal hypoxic-ischemic event in the neonatal pups creates cortical damage covering a large, but variable region of ipsilateral cortex perfused by the MCA (Kadam and Dudek, 2007). Previous work has reported that all of the animals that develop macroscopic infarcts will develop seizures, occurring as early as 2-3 months later (Kadam et al., 2010). This result suggests that at least some of the anatomical and physiological changes that occur within the cortex during this latent period contribute to the mechanisms of epileptogenesis. During perinatal HI, an infarct develops as the result of the death of both interneurons and pyramidal cells. On these grounds, one would expect a decrease in both excitatory glutamatergic and inhibitory GABAergic synaptic inputs; however, because interneurons make dense local-circuit connections, one might expect a proportionally larger effect on mIPSCs than on mEPSCs for the remaining neurons surrounding the infarct. Therefore, we hypothesized that the HI-induced infarct leads to a greater decrease in the frequency of mIPSCs than mEPSCs within the peri-infarct region.

Synaptic Activity Was Decreased 24-48 hr after Perinatal HI

To test for alterations in synaptic excitation or inhibition in rats with an HI infarct, we performed whole-cell voltage-clamp recordings on layer 2/3 pyramidal neurons within the peri-

infarct region (Figure 2.1). Focusing on presynaptic mechanisms, we first recorded mEPSCs and mIPSCs to test for alterations in the properties of the mEPSCs and mIPSCs, particularly changes to their frequency. Our first goal was to examine acute changes that occurred within the first 24-48 hr after induction of the infarct. This time point is during profound cell death; therefore, we obtained our recordings in slices from P8 and P9 (P8-9) animals (Figure 2.2). Measuring interevent interval (IEI) to report event frequency, we identified statistically significant differences in IEI at P8-9 in HI-treated animals compared to sham controls of mEPSCs (2610.83 ± 793.46 and 669.18 ± 120.52 msec, respectively, $p < 0.05$), and mIPSCs (6184.14 ± 1494.35 and 1271.86 ± 316.14 msec, respectively, $p \leq 0.005$).

Peak Amplitude and Decay Times Were Unchanged in HI-treated Animals at 24-48 Hours after Perinatal HI

To measure changes in the postsynaptic response, individual synaptic events were analyzed for peak amplitude (Figure 2.2) and decay times (Figure 2.3) at P8-9. Peak amplitude provides an indication of postsynaptic receptor density. No significant differences in amplitude were found at P8-9 between HI treated animals and sham controls for mEPSCs (-41.54 ± 2.61 and -45.66 ± 3.34 pA, respectively, $p > 0.05$), or mIPSCs (60.91 ± 5.29 and 51.78 ± 4.25 pA, respectively, $p > 0.05$) (Figure 2.4). The time course of decay reflects the time it takes for deactivation or desensitation of the postsynaptic ion channel. Overall, it is a measure of the kinetics (i.e., receptor subunits) of the postsynaptic receptor. We found no significant difference in decay time of events at P8-9 for HI-treated animals compared to sham controls of mEPSC (1.56 ± 0.15 and 1.66 ± 0.12 msec, respectively, $p > 0.05$), or mIPSC (9.00 ± 1.72 and 11.31 ± 2.21 msec, respectively, $p > 0.05$) (Figure 2.4).

Synaptic Activity Was Normalized 2 Weeks after Perinatal HI

We next determined whether the reduction in mIPSC and mEPSC frequency was present during the presumed latent period of epileptogenesis. Thus, we recorded mEPSCs and mIPSCs 2 weeks post-HI at P21, P22, and P23 (P21-23) (Figure 2.2). No significant difference was

observed at P21-23 for IEI in the HI-treated animals compared to the sham controls of mEPSCs (187.93 ± 75.60 and 159.22 ± 26.57 msec, respectively, $p > 0.05$), or mIPSCs (225.91 ± 50.25 and 230.89 ± 37.70 msec, respectively, $p > 0.05$) (Figure 2.4). This suggests that the difference observed at P8-9 normalized in the older animals.

Peak Amplitude and Decay Times Were Unchanged in HI-treated Animals at 2 Weeks after Perinatal HI

To determine any delayed changes to postsynaptic receptor density and/or composition, peak amplitude (Figures 2.2) and decay times (Figure 2.3) of synaptic events were measured at 2-weeks post-HI. Similar to what was observed at P8-9, no significant difference was observed for peak amplitude at P21-23 between HI-treated animals and sham controls for mEPSCs (-39.97 ± 4.06 and -41.59 ± 2.99 pA, respectively, $p > 0.05$), or mIPSCs (57.52 ± 6.21 and 56.26 ± 3.63 pA, respectively, $p > 0.05$) (Figure 2.4). The decay time was not significantly different at P21-23 between HI-treated animals compared to sham controls for mEPSCs (2.19 ± 0.25 and 1.67 ± 0.35 msec, respectively, $p > 0.05$), or mIPSC (6.36 ± 0.73 and 5.57 ± 0.43 msec, respectively, $p > 0.05$) (Figure 2.4, C).

Synaptic Activity Was Unchanged 4 Months Post-HI

Having measured a recovery of synaptic events from P8-9 to P21-23, we were interested if the synaptic modifications would continue long term into the period of spontaneous recurrent seizures, or if the changes were complete by P21-23. We know that as early as the third month of age, HI-treated animals begin having spontaneous seizures (Kadam et al., 2010); therefore, we chose to repeat the whole-cell voltage-clamp experiments in approximately 4-month-old adult animals (P120). Previous immunohistological evidence has shown an increase in synaptic GAD67/synaptophysin ratio in nerve endings of HI-treated adult rats (Romijn et al., 1994a). Based on this observation, we hypothesized there would be an increase in mIPSC frequency in our adult HI animals. No significant difference was observed in IEI between HI-treated animals and sham controls for either mEPSC (1151 ± 345.38 and 782.78 ± 120.27, respectively, $p > 0.05$)

or mIPSC (300.30 ± 66.57 and 172.41 ± 39.93, respectively, $p > 0.05$) (Figure 2.4). As with the other time points, no significant difference was found at P120 for mEPSCs between HI-treated animals and sham controls in peak amplitude (-40.92 ± 1.81 and -40.89 ± 2.65, respectively, $p > 0.05$) (Figure 2.4) or decay time (3.42 ± 0.58 and 2.49 ± 0.38, respectively, $p > 0.05$) (Figure 2.4), or for mIPSC's between HI-treated animals and sham controls in peak amplitude (38.15 ± 1.94 and 38.04 ± 2.27, respectively, $p > 0.05$) (Figure 2.4) or decay time (10.98 ± 1.88 and 8.12 ± 0.73, respectively, $p > 0.05$) (Figure 2.4).

Tonic Inhibition Is Unaffected after Perinatal HI

In an adult model of stroke, it was observed that an increase in GABA-mediated tonic inhibition was measured in the peri-infarct region after a stroke (Clarkson et al., 2010). Although that experiment was performed in adult mice, we were interested in seeing if the same was true in our pediatric model of stroke. Using an all-points histogram measurement of whole-cell voltage clamp recordings (Figure 2.5), we compared tonic inhibition levels before and after the addition of picrotoxin to block $GABA_A$ receptors. No significant difference was found in the absolute difference of tonic inhibition between HI-treated animals compared to sham controls at P8-9, or at P21-23 (Figure 2.6).

Immunohistological Labeling of GAD67 and NeuN

Immunohistological labeling of interneuron somas and synaptic terminals was performed with GAD67 as a way to visually confirm alterations to the number of interneurons and the relative density of inhibitory synaptic terminals. Immunolabeling with NeuN was used to identify changes to the numbers of pyramidal neurons. At P8-9, there was an obvious loss of somas labeled with NeuN and GAD67 within the infarct region (Figure 2.7). At this early time point, the cystic infarct is most likely still developing and has yet to coalesce with clearly defined borders. However, it was abundantly clear from the immunohistochemistry that fewer cell bodies were labeled with NeuN and GAD67 in the region affected by HI in the ipsilateral cortex. Furthermore, in regions

surrounding the developing cystic infarct, there was a reduction in the diffuse labeling of GAD67 puncta, the putative synaptic terminals of interneurons (Figure 2.7).

Two weeks later at P21-23, the cystic infarct was fully developed with well-defined borders delineating an open cavity filled with cerebral spinal fluid from the peri-infarct region identified from a high density of NeuN-labeled pyramidal cell bodies (Figure 2.7). At this time point, there were columns of intact pyramidal cell bodies that make up viable tissue of the peri-infarct region extending into the infarct. Examination of the immunolabeled tissue suggested that there was no difference in pyramidal cell density in the peri-infarct tissue compared to the contralateral cortex. Immunolabeling of GAD67 shows the fully developed infarct surrounded by peri-infarct tissue that has a similar number of interneuron cell bodies as the contralateral cortex (Figure 2.7). Furthermore, the diffuse synaptic terminal labeling of GAD67 appears to have recovered from the reduction seen in the acute period, to a level similar to that in the contralateral cortex.

Proximity of Electrophysiology Recording Sites to HI-induced Infarct at P8-9 and P21-23

As the animal ages after undergoing a HI-induced infarct, the lesion progresses from a diffuse injury of widespread neuronal loss without a distinct boarder at P8-9 into a more well-defined lesion at P21-23, with zones of complete cell loss. Because of this coalescing of viable neurons into specific regions separated by areas of scar tissue and cerebral spinal fluid, it was difficult to prepare acute slices for whole-cell electrophysiology. This can lead to the unintended consequence that the recording sites in older animals (P21-23) are farther away from the damage and out of the peri-infarct region or are in different regions of the brain, thus leading to an artificial recovery of synaptic events. To assess and control for this, we filled each recorded cell with biocytin and immunohistochemically colabeled with NeuN to visualize how close the recording site was to the infarct (Figure 2.8). A comparison of all recording sites of mEPSCs and mIPSCs for HI-treated animals and sham controls at P8-9 and P21-23 indicates that most of the patched cells were in the posterior frontal cortex and anterior parietal cortex within the motor and

somatosensory cortex (Figure 2.9). Assessing individual recording sites on their proximity to cortical damage showed that mEPSCs and mIPSCs recorded at P8-9 (Figure 2.10) and P21-23 (Figure 2.11) were at least within regions of reduced cell density and most were in close proximity to complete cell loss, in slices that exhibit that extent of damage.

Although no change was observed in tonic inhibition, we made the same comparisons of recording sites to each other and to the proximity of the infarct. Similar to the previous recordings, recordings of tonic inhibition were all done in the same brain region, which was also the posterior frontal cortex and anterior parietal cortex within motor and somatosensory cortex (Figure 2.12). All recording sites for tonic inhibition at P8-9 (Figure 2.13) and P21-23 (Figure 2.14) were also within regions of reduced cell density and in close proximity to complete cell loss, in slices where complete cell loss was present.

Discussion

Our results demonstrate that in neonatal rats, synaptic recovery occurs during the presumed latent period of epileptogenesis following perinatal HI. As early as 24-48 hr post-HI, there was a significant decrease in the frequency of mEPSCs and mIPSC with no alteration in amplitude or decay time of those events. Surprisingly, this deficit recovered 2 weeks postinjury with no additional changes observed. This recovery occurred during a time at which the neocortex was undergoing rapid development. Remarkably, the increase in synaptic events in damaged cortex overcame the deficit seen immediately after HI. When the animal reached a period where spontaneous recurrent seizures have been observed to occur in a portion of animals (Kadam et al., 2010), at P120, the recovery of synaptic events was sustained and there was no discernable difference in the frequency, amplitude, or decay time between HI and sham controls. Having measured a decrease in mIPSCs, we questioned whether tonic inhibition would be affected, but found no difference in levels of tonic inhibition between HI-treated and sham control animals at P8-9 or P21-23. This recovery in synaptic events occurred even with the presence of a large lesion created from the loss of neurons and interneurons, leading us to

speculate on the homeostatic mechanisms involved in maintaining basal levels of activity in a diseased brain.

Seizure Focus in HI

We focused on epileptogenic mechanisms within the peri-infarct region of the experimental stroke, based on evidence from electroencephalogram recordings performed in this animal model that identified this region as an apparent site of seizure onset (Kadam et al., 2010). This evidence is further supported by the photothrombosis stroke animal model that identified the peri-infarct region as the site of seizure generation (Witte et al., 2000). It is generally thought that the area surrounding the infarct shows increased neuroplasticity and is critical for rehabilitation (Dijkhuizen et al., 2003; Cramer, 2008; Brown et al., 2009).

Selection of Recording Time Points

In order to get a good sampling of the various stages in the epileptogenic process, we chose to perform our experiments at P8-9, P21-23, and P120. The first time point (P8-9) occurs during active cell death in which a portion of cells have already died as a result of necrosis, and other cells are in the process of dying from apoptosis (Lai and Yang, 2011). This time point reveals how the HI injury results in an initial reshaping of network activity. Furthermore, this time point provides a baseline for the comparison of any other changes leading to epilepsy that we may observe at the later time points. Because epileptogenesis is progressive in nature, it was necessary to sample early on in the process (P21-23), prior to the presumed development of spontaneous recurrent seizures, and later on (P120), after the occurrence of spontaneous recurrent seizures. Performing experiments at P21-23, we were able to relate any identifiable changes to being potentially causative in the development of epilepsy. At P120, we could confirm any sustained changes to synaptic activity as being epileptogenic, and parse out additional results as possibly being a result of the seizures.

HI Reduces Synaptic Innervation

At the onset of our study, we hypothesized that there would be a reduction in mIPSC events in the peri-infarct region that was a result of local interneurons dying off during perinatal HI. The loss of interneurons would reduce the amount of synaptic inhibition to the surrounding areas. This reduction in inhibition to the peri-infarct region would hypothetically be the mechanism driving seizure generation. In agreement with our hypothesis, we found a reduction in inhibition, and excitation, which recovered within 2 weeks. These results led us to consider two possible explanations for the recovery of synaptic events: neurogenesis and/or axonal sprouting. We subsequently discuss why these modifications may ultimately lead to seizures.

HI-induced Cell Death

Our results have identified a loss of synaptic activity within 24-48 hr after the induction of the insult. This time frame would appear to be too soon for substantial neuronal death from apoptosis to have occurred. While apoptosis does occur in this model of perinatal stroke, the initial neuronal loss is likely due to necrosis (Lai and Yang, 2011). A massive reduction in oxygen during hypoxia leads to decreased production of ATP during the first 8-48 hr after treatment. This leads to failure of the ATP-dependent Na^+/K^+ pumps, causing both cellular necrosis (early stage) and apoptosis (late stage). As the Na^+/K^+ pumps fail, there is an influx of Na^+, Cl^- and water causing cell swelling, cell lysis, and early cell death by necrosis (Lai and Yang, 2011). Our initial electrophysiological recordings were at 24-48 hr after the induction of the infarct and are well within the necrosis stage. This is evident from our NeuN and GAD67 labeling of the infarcted tissue. Based on these conditions, we are confident that our experiments represent neuronal death due to necrosis during the subacute period following HI.

Use of Miniature Currents as a Measure of Synaptic Activity

The measurement of miniature excitatory/inhibitory postsynaptic currents (mEPSCs/mIPSCs) is the best and most direct electrophysiological method for testing our hypothesis. Recording postsynaptic currents in the presence of tetrodotoxin (TTX) to block

voltage-gated sodium channels reflects the postsynaptic response to single vesicles released by spontaneous exocytosis of excitatory neurotransmitters glutamate and the inhibitory neurotransmitters y-aminobutyric acid (GABA) (Brown et al., 1979; Ceccarelli and Hurlbut, 1980; Ropert et al., 1990). These single quantal events give direct measurements of the interactions between postsynaptic receptors and presynaptic transmitter release (Katz and Miledi, 1970). The strength of this technique is that it filters out multisynaptic network activity and provides the ability to observe local release from synaptic terminals. Spontaneous release is a stochastic/probabilistic function, and measuring in the presence of TTX removes circuit function and activity. The power of this technique is that all synapses have some probability of release that is normally distributed so that a small sample of the population is representative of the whole population. However, this takes on the assumption that all synapses have uniform distribution of probability of release and that we can measure each mEPSC/mIPSC event accurately. The frequency of events are an indirect measure of the presynaptic connections. It is often interpreted to be a measurement of the number of synapses onto the cell of interest (Vautrin and Barker, 2003), or as the probability of quantal release for a population of synapses. The large amount of cell loss created from the lesion supports the conclusion that the decrease in the frequency of events in our data are from lost synaptic terminals as opposed to a change in release probability. The peak amplitude measurement of individual events typically represents the number of postsynaptic receptors (Nusser, 1999; Vautrin and Barker, 2003). This is certainly true, but the sizes can vary greatly based on the distribution of those events (Williams and Mitchell, 2008) and the density of receptors. The size of the soma of the layer 2/3 pyramidal cells in our recordings is consistently similar based on morphology from biocytin-filled cells. This allows us to assume that the density of the receptors is similar between cells. However, as a consequence of the cable properties of the dendritic arborization, there is a degradation of the synaptic events the farther away they are from the soma (Williams and Mitchell, 2008). This limits our method to measuring mostly synaptic events that are at the soma or near to the soma.

Recording Site Location

The argument can be made that the recovery in synaptic events might be an artificial result of recording farther away from damage in the older animals, ultimately being out of the peri-infarct region. The cortical infarct in the P8-9 animals is still in the phase of experiencing cellular loss, which leads to more diffuse damage interspersed with viable neurons. This allows for easier slice preparation in the younger animals because the tissue does not fall apart when sliced. The diffuse damage also makes finding “patchable” cells within or near the damaged areas easier as there are no regions of complete cell loss void of any live cells. In the older animals, HI-induced cell death is complete and the lesion essentially formed. This results in columns of surviving neurons separated by glial scarring (Kadam and Dudek, 2007). With the damage being more coalesced and having large gaps in the neocortical structure, the tissue is more difficult to slice. This is easily overcome by reducing the speed of the vibratome and modifying the slicing technique. A potential outcome of the larger lesion and glial scarring is that it could be difficult to find viable cells next to or within the damaged area. This would result in patching cells that were farther from the lesion in more stable tissue. In order to observe if this occurred, all recorded cells were filled with biocytin, labeled with NeuN, and imaged (Figure 2.11). The peri-infarct region was defined as being in close proximity to complete neuronal loss, and within a region of partial neuronal loss. Based on the images and these criteria, it was determined that all patched cells were within the peri-infarct region for both P21-23 (Figure 2.13 and 2.16) and P8-9 animals (Figure 2.14 and 2.17). Furthermore, all recorded cells are within the same general anatomical region (Figures 2.12 and 2.15). As it turns out, all HI-treated brains with lesions had an easily definable peri-infarct region based on an obvious reduction in cell density.

Temporal Resolution

In this study, each recording of mIPSCs/mEPSCs was approximately 5 min long, which has the potential of not being an adequate amount of time to get a large enough sample size to accurately depict synaptic activity. Using TTX to block action potential dependent release reduces the possibility of this happening, as it prevents our measurement from being affected by

fluctuations in network activity. Data from our lab addressing this issue have shown that the frequency of mIPSC events remain stable from minute to minute over a 35-min recording period (unpublished, Spampanato), suggesting that for at least mIPSCs, sampling for 5 min results in the same IEI as sampling for 35 min.

Neurogenesis

Aberrant Neuron Migration in the Epileptic Brain

Neuronal migration in the mammalian brain is nearly complete at the end of the embryonic period. However, it is known that neuronal migration continues in the postnatal brain in two particular regions of the brain: the hippocampus (Jessberger and Parent, 2015), and the subventricular zone (Lim and Alvarez-Buylla, 2016). This led us to postulate whether neurons generated from an endogenous germinal zone, particularly the subventricular zone, could have been translocated to regions of injury in an HI-damaged postnatal brain. Evidence of this is present in temporal lobe epilepsy where newly generated granule cells in the dentate gyrus migrate ectopically into the inner molecular layer and the hilar region of the hippocampus in both humans (Houser, 1990; Hauser, 1992) and animal models (Parent et al., 1997; Scharfman et al., 2000). In these cases, ectopic granule cells have been associated with the development of epilepsy (Parent et al., 1997).

Rostral Migratory Stream (RMS)

Of particular interest to this study is neurogenesis along the rostral migratory stream (RMS), which involves the migration of neural progenitor cells from the subventricular zone (SVZ) to the olfactory bulb (Lim and Alvarez-Buylla, 2016). This population of neural precursors within the SVZ is capable of differentiating into neurons, astrocytes, or oligodendrocytes (Lois and Alvarez-Buylla, 1993; Goldman, 1995). Under normal conditions, these SVZ stem cells migrate along the RMS to the olfactory bulb where they differentiate into GABA-containing and dopaminergic local circuit interneurons (Lois and Alvarez-Buylla, 1993; Luskin, 1993). However, after injury, it has been postulated that these cells can migrate towards damaged areas and

differentiate into neurons, interneurons, and glia, as seen in animal models of adult stroke (Jin et al., 2001; Zhang et al., 2001; Parent et al., 2002).

Neurogenesis after HI

The literature is conflicting on whether or not SVZ neurogenesis contributes to cellular recovery following an HI injury. One study looking at severe HI injuries found acutely depleted neural precursors in the SVZ (Skoff et al., 2001) while another study found an increase in cell proliferation and stimulation of neurogenesis in the ipsilateral SVZ 1-3 weeks after moderate HI injury (Plane et al., 2004). These conflicting results might be a result of the extent of the damage where a severe injury encompasses a portion of the SVZ, limiting its anatomy and ability to function properly. A more recent study using the same HI animal model as our study looked for SVZ cell proliferation and neurogenesis 1-3 weeks post HI by measurement of the SVZ size, incorporation of bromodeoxyuridine (BrdU) into proliferating cells, and by immunoassay of doublecortin which is only expressed in immature neurons (Ong et al., 2005). They further determined cell phenotypes of newly differentiated cells with antibody labeling of mature neurons, astrocytes, and oligodendroglia. The results of their study found that there was an increase in SVZ size, an increase in BrdU labeled cells within the SVZ, and an increase in neurogenesis based on doublecortin labeling as early as 1 week post-HI (Ong et al., 2005). Despite the increased activity of the SVZ, at 4-weeks post-HI, only markers of astrocytes and oligodendroglia were identified within the lesioned striatum, and no neuronal markers (Ong et al., 2005). These results suggest that even though HI injury stimulates SVZ proliferation and neurogenesis, it is unlikely that these cells are migrating and differentiating into neurons and interneurons in the peri-infarct region. Therefore, the recovery of synaptic activity at the same post-HI ages in our study is most likely a result of something other than neurogenesis.

Axonal Sprouting

Stroke-induced Axonal Sprouting

Axonal sprouting as it pertains to stroke, has primarily been studied in adults. It is known that after stroke, human patients will exhibit 80% to 90% unilateral body weakness that improves to 45% to 62% over time (Carmichael, 2003). Some of this is attributed to resolution of tissue damage, but late improvements are thought to be due to axonal sprouting. In rat models of stroke, axonal sprouting has been shown to occur as intracorticostriatal projections (Carmichael et al., 2001), as well as corticostriatal projections from contralateral cortex to ipsilateral striatum (Napieralski et al., 1996) and the peri-infarct region (Carmichael and Chesselet, 2002). More specifically, in the PHI animal model, mossy fiber sprouting has been observed in epileptic animals within the ipsilateral and contralateral hippocampi (Williams et al., 2004; Kadam and Dudek, 2007; Williams and Dudek, 2007).

Brain-Derived Neurotrophic Factor (BDNF)

One protein involved in the growth and differentiation of new neurons is brain-derived neurotrophic factor (BDNF). It is known that BDNF increases neurogenesis (Lee et al., 2002), induces morphological changes in dendritic spines (Tyler and Pozzo-Miller, 2003), and stimulates axonal growth (Danzer et al., 2002). Based on the physiological effects of BDNF, and its association with epilepsy (Binder et al., 2001; Kanemoto et al., 2003; Scharfman, 2005), it is important to consider its potential role in the recovery seen in our study. A previous study used enzyme-linked immunosorbent assay performed 6, 24, 48, 72 hr after HI treatment and 7 days later to measure levels of BDNF after HI injury. They discovered that BDNF levels significantly increased in HI animals within the first 2 days, but peaked at 48 hr before downregulating to normal levels at 7 days (Wang et al., 2013). The increase in BDNF levels is relatively transient, yet it still fits in with our data that found a recovery in synaptic activity after injury. It is plausible that following the initial loss of cells from HI-treatment, upregulation of BDNF stimulates neurons to increase growth and synapse formation beginning 24-48 hr after injury and completing by 14 days postinjury.

Time Course of Axonal Sprouting in our Experiments

Epilepsy is often described as a disorder involving either too much neuronal excitation or too little inhibition. This was the dogma asserted in an older study that hypothesized a decrease in GABAergic synapses would be present in HI animals at 4-6 months of age (Romijn et al., 1994b), a time that coincides with spontaneous seizures (Kadam et al., 2010). Contrary to their hypothesis, they found that there was actually an increase in synaptic GABAergic immunohistochemical labeling at this time point (Romijn et al., 1994b). This led us to speculate if the axonal sprouting and synapse formation would continue beyond 14 days postinjury. Our electrophysiological experiments performed in 4-month-old animals found that there was no significant increase or decrease in the amount of excitatory or inhibitory synaptic events. If there was a significant increase in GABAergic synapses beyond control levels, we did not measure them. Therefore, we conclude that by age P21, the majority of the axonal sprouting has already occurred and that the mechanisms of seizure generation are most likely due to improper rewiring of the network.

Future Directions

Immunohistochemistry alone is not sensitive enough to study if axonal sprouting is occurring. We would like to do paired recordings of layer 2/3 pyramidal neurons within the peri-infarct region. These recordings will involve pyramidal to pyramidal connections and interneuron to pyramidal neuron connections. By stimulating the activity of one cell and recording the amplitude of the evoked response, we get an idea of the number of synapses being formed onto the postsynaptic cell. Comparing HI to Sham controls at the P21 time point will enable us to detect if sprouting is playing a role in the recovery of synaptic events.

Conclusions

Overall, we have shown evidence for homeostatic plasticity in a model of perinatal stroke. Knowing that the animals that present with a cortical infarct will ultimately develop later-in-life spontaneous seizures, we are able to infer these results as mechanisms of epileptogenesis. Here

we showed that there was neither an increase in excitation nor a decrease in inhibition that persisted into the chronic epilepsy phase, but a balancing of the two. These results imply that physiologically, the neuronal matrix is trying to maintain normal levels of activity that most likely occurs through axonal sprouting of the remaining neurons. Future research will be needed to understand how this rewiring ultimately leads to epilepsy, whether it is through fewer interneurons controlling more pyramidal neurons causing hypersynchronous rhythms, more interneuron-interneuron interactions leading to transient decreases in inhibition, pyramidal neuron-neuron interactions leading to transient increases in excitation, or other aberrant connections.

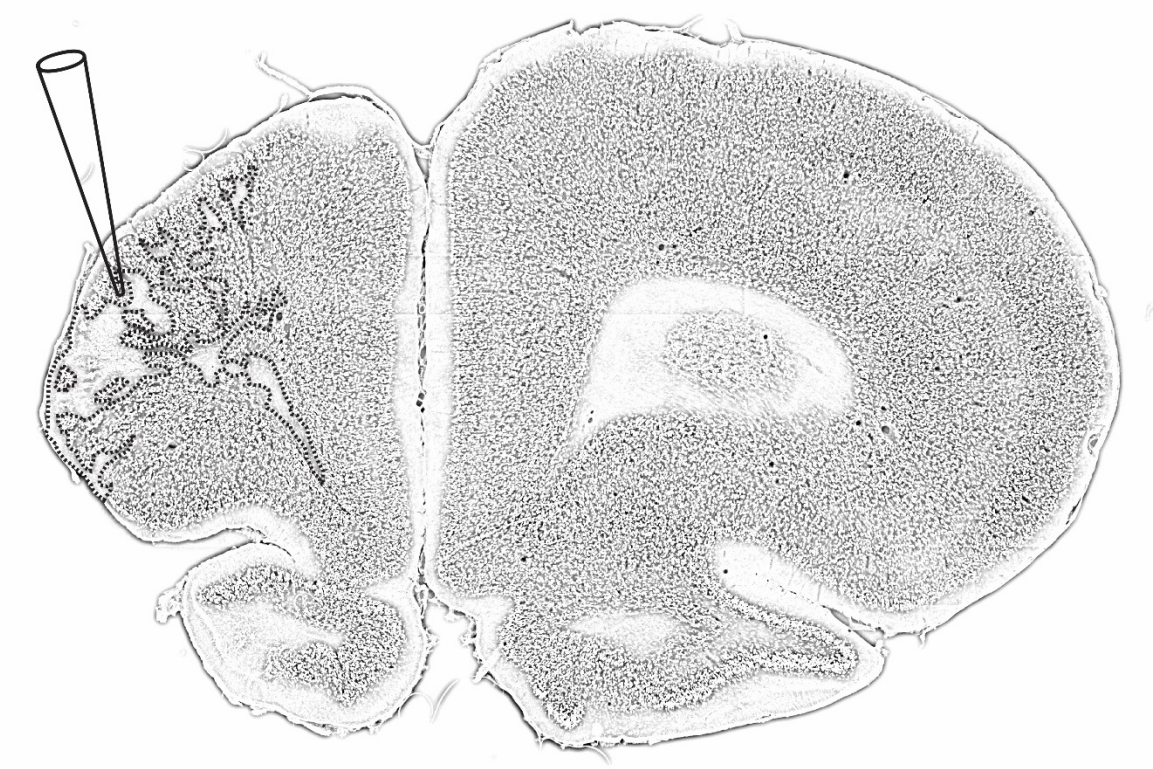

Figure 2.1: Coronal brain section indicating the experimental protocol of whole-cell recordings from HI-treated rats. HI induced at P7 results in a unilateral infarct with cell loss. Whole-cell patch clamp recordings of miniature inhibitory and excitatory postsynaptic currents (mIPSCs and mEPSCs), as well as tonic inhibition, were performed within the peri-infarct region as indicated by the silhouetted pipette. An infarct is apparent by the large reduction in hemisphere size and the presence of cell loss (outlined by dotted line). Equivalent recordings were obtained from anatomically similar regions in neocortical slices of sham control animals

Figure 2.2: Whole-cell recordings of mIPSCs and mEPSCs in layer 2/3 pyramidal cells of neocortical slices from control and HI-treated rats at P8-9 and P21-23. Successive traces indicate the amount of synaptic activity of a representative cell recording. The mIPSC frequency was reduced in HI-treated animals (**A1**) when compared to sham controls (**A2**). A decrease in mEPSC frequency was observed in the same cells for HI-treated animals (**B2**) compared to sham controls (**B2**). Two weeks after induction of an HI infarct, levels of synaptic activity are similar between HI-treated animals and sham controls. The mIPSC frequency was not different in HI-treated animals (**C1**) when compared to sham controls (**C2**). No change in mEPSC frequency was observed in the same cells for HI-treated animals (**D2**) compared to sham controls (**D2**).

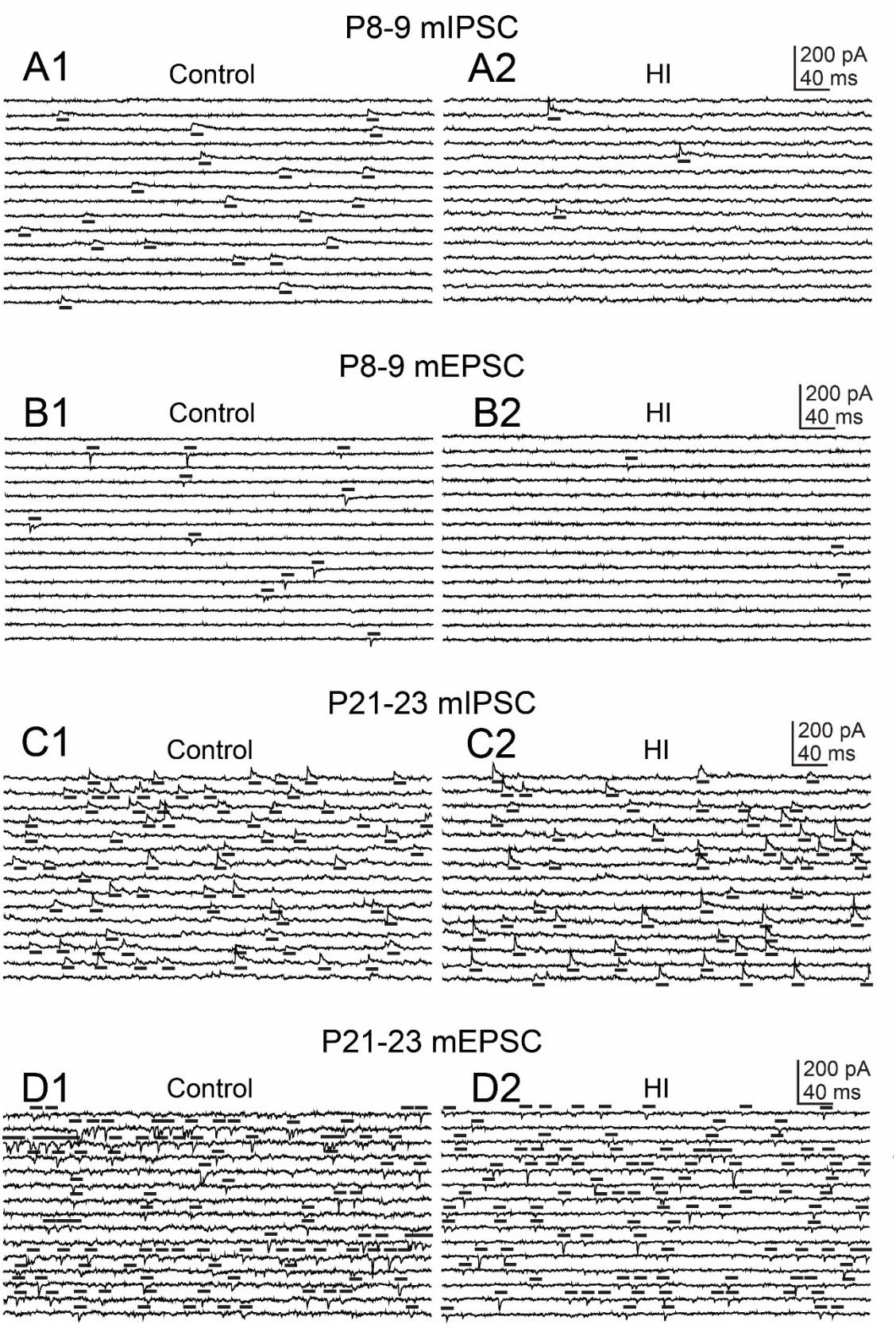
P8-9 mIPSC
A1
Control
A2
HI
200 pA
40 ms
P8-9 mEPSC
B1
Control
B2
HI
200 pA
40 ms
P21-23 mIPSC
C1
Control
C2
HI
200 pA
40 ms
P21-23 mEPSC
D1
Control
D2
HI
200 pA
40 ms

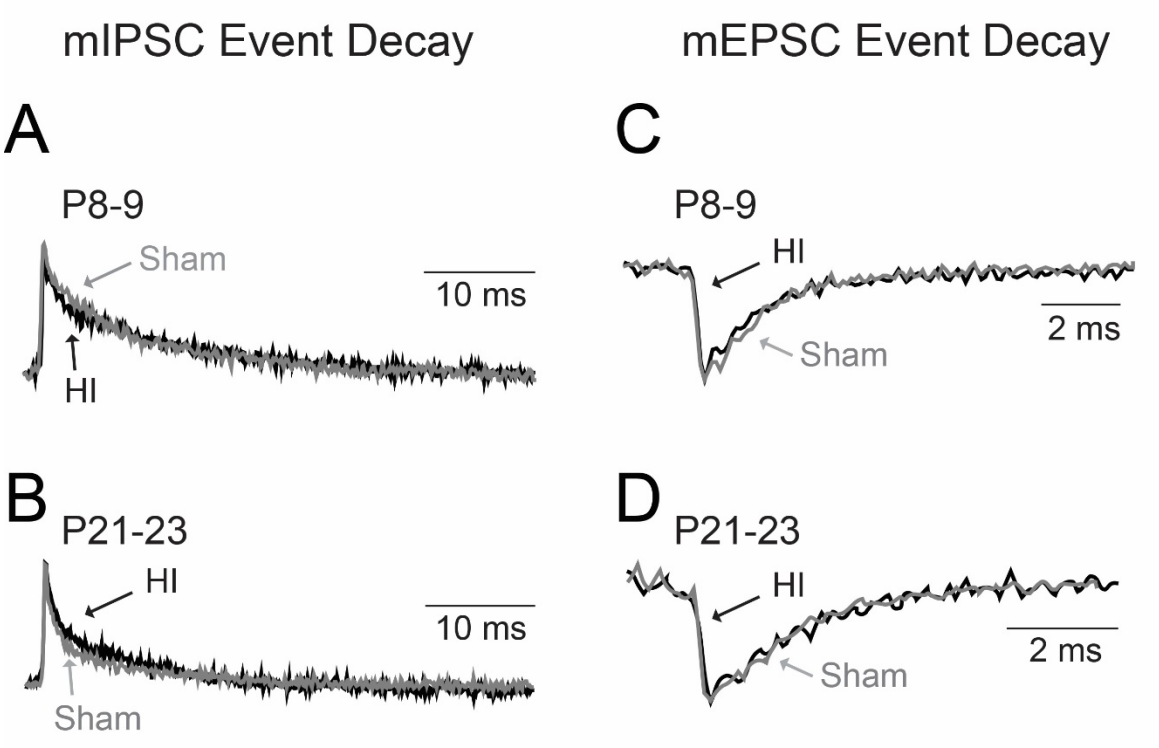

Figure 2.3: mIPSC and mEPSC averaged events indicated similarities in the rate of event decay between HI-treated and sham control rats. No difference in the rate of mIPSC decay was detected between HI and sham controls at both time points, at P8-9 (**A**) and later at P21-23 (**B**). Recording mEPSCs in the same cells, no difference in the rate of event decay was found between HI and sham controls at P8-9 (**C**) and later at P21-23 (**D**).

Figure 2.4: Quantification of mEPSC and mIPSC event frequency, amplitude, and decay time at P8-9, P21-23, and P120. Event amplitude (top row), interevent interval (IEI) (middle row), and decay time (bottom row) for mEPSC (left) and mIPSC (right) events for HI-treated animals (grey) compared to sham controls (black) at P8-9 (left 2 columns), P21-23 (middle 2 columns), and P120 (right 2 columns). Mean peak amplitude does not significantly differ between HI and sham controls for mEPSCs or mIPSCs at any time point. Comparison of mean IEI indicates a significant increase for HI compared to sham controls for mEPSCs, *$p<0.05$ and mIPSCs, *$p<0.05$ at P8-9, with no difference at P21-23 or P120. Mean decay time does not significantly differ between HI and sham controls for mEPSCs or mIPSCs at any time point. Error bars are SEM.

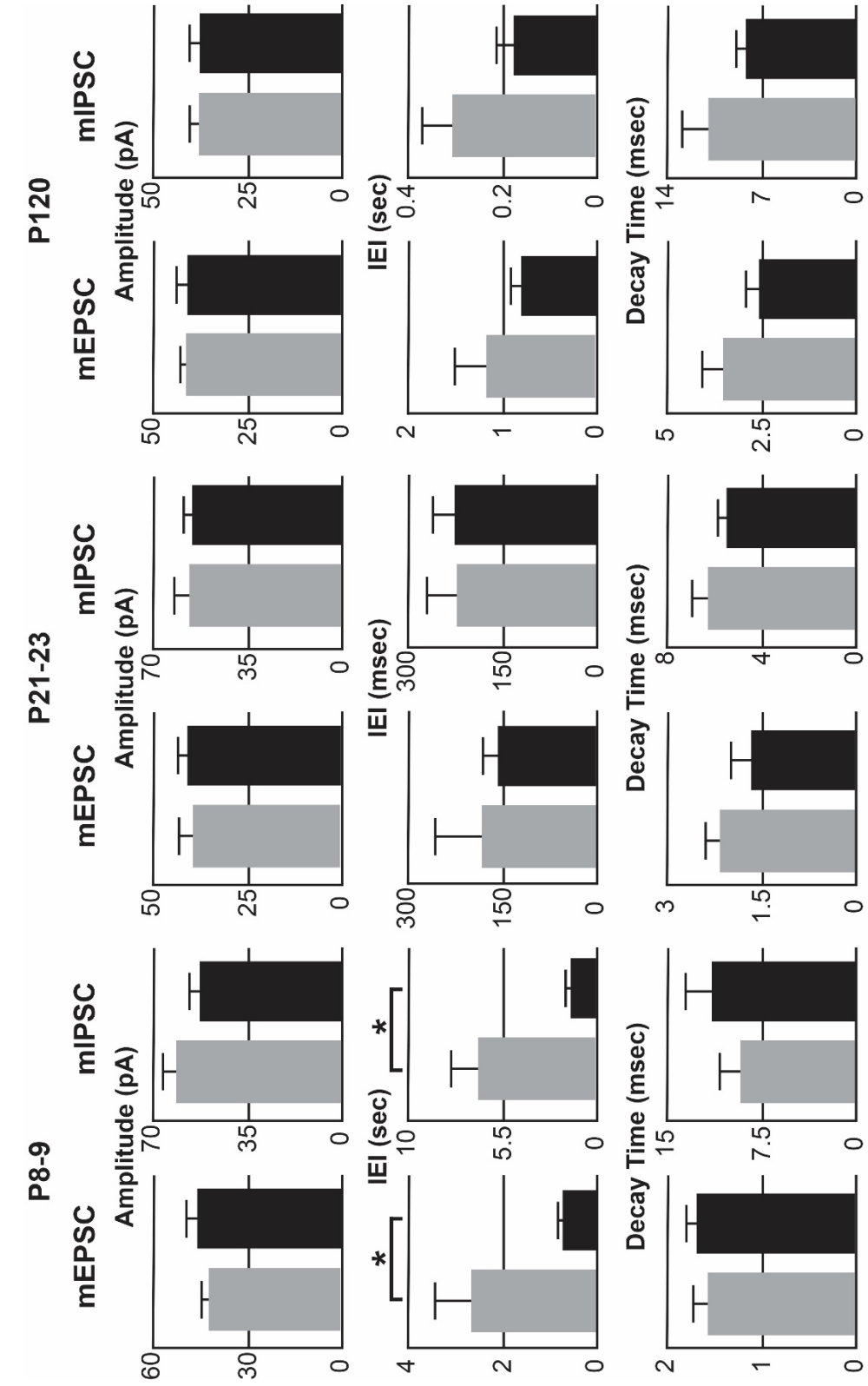
P8-9
P21-23
P120
mEPSC
mIPSC
Amplitude (pA)
IEI (sec)
IEI (msec)
Decay Time (msec)
*
*

Figure 2.5: Measured levels of tonic inhibition in treatment and sham control animals at P9 and P23. Individual whole-cell recordings measuring levels of tonic inhibition in HI and sham control animals at P9 and P23. Right side of the figure is an all-points histogram of the raw electrophysiology recording. The mean of the histogram is a direct measurement of the baseline level of tonic current before and after the addition of picrotoxin (arrows) to block $GABA_A$ receptors. The absolute difference in the means indicates that no difference was detected between HI and sham animals at either time point, P9 (**A1**,**A2**) or P23 (**B1**,**B2**).

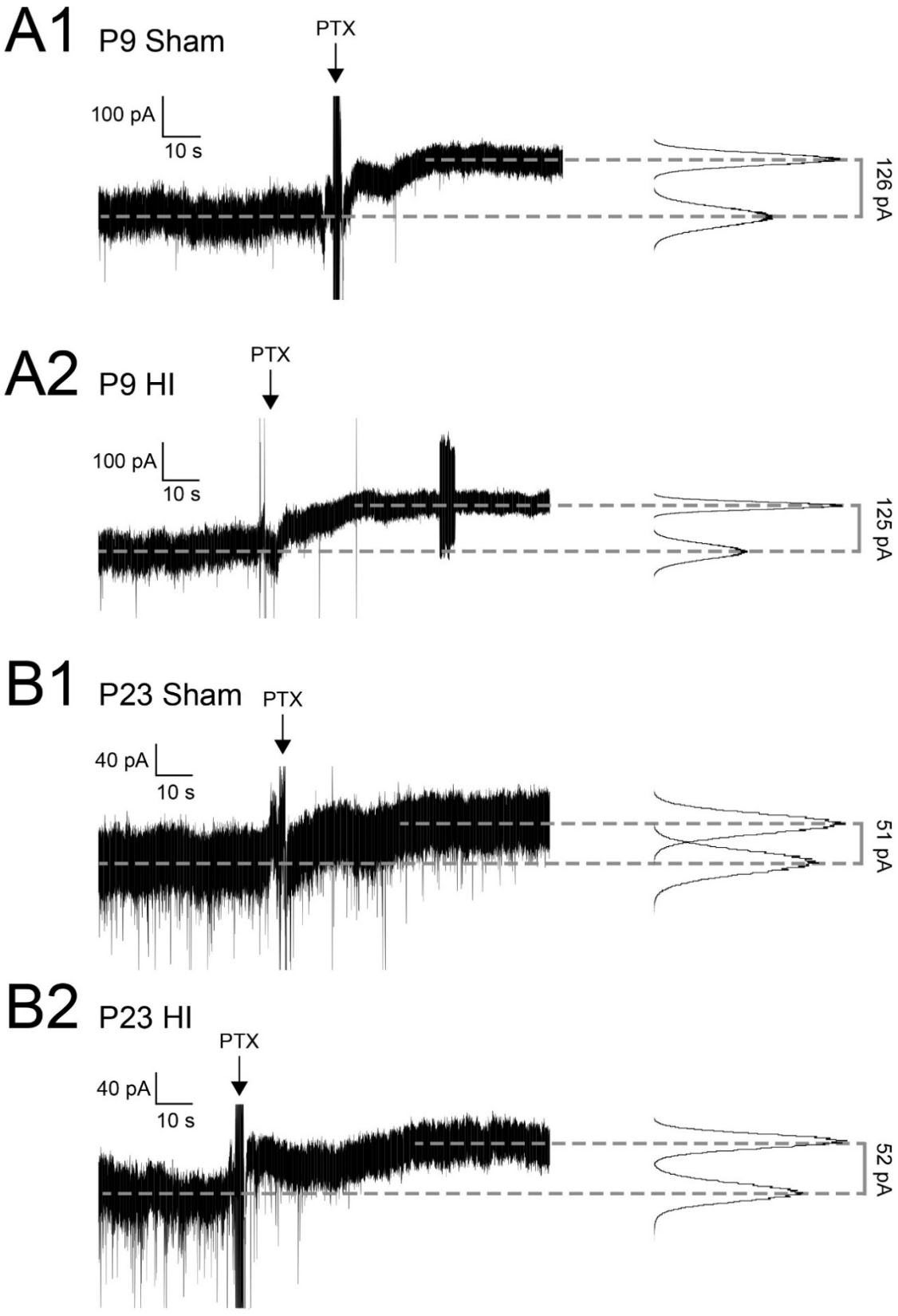
A1
P9 Sham
PTX
100 pA
10 s
126 pA
A2
P9 HI
PTX
100 pA
10 s
125 pA
B1
P23 Sham
PTX
40 pA
10 s
51 pA
B2
P23 HI
PTX
40 pA
10 s
52 pA

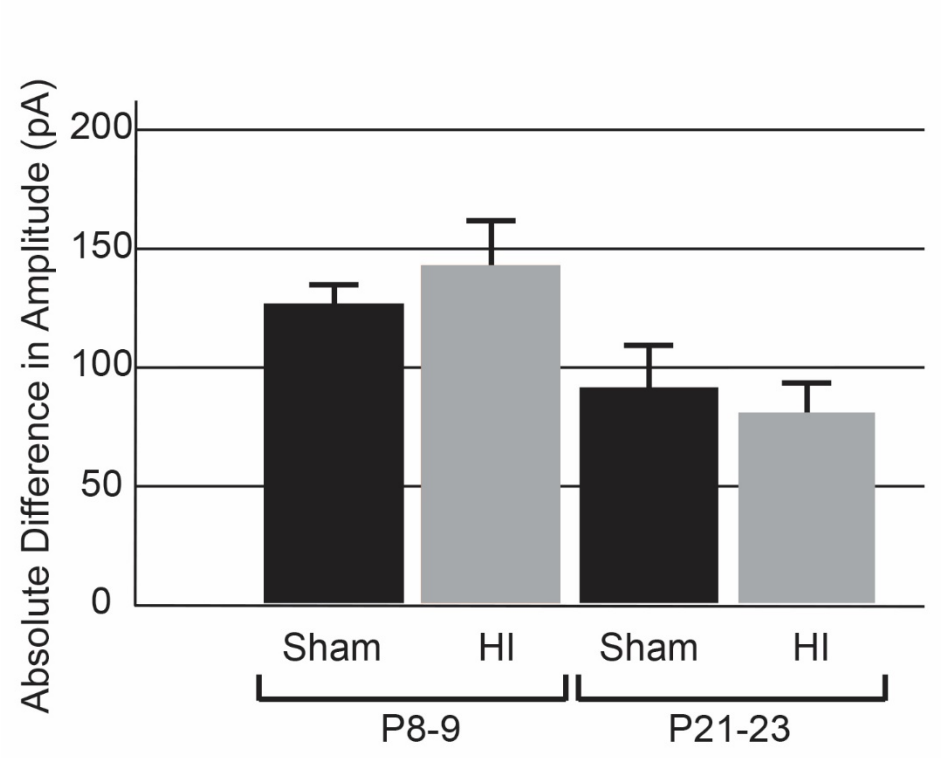

Figure 2.6: Quantified levels of tonic inhibition. Mean levels of tonic inhibition calculated from all-points histograms of electrophysiology recordings and measured as absolute difference in amplitude pre- and postpicrotoxin application. Quantification indicates that no significant difference in levels of tonic inhibition was detected between HI-treated animals and sham controls at P8-9, or at P21-23. Error bars are SEM.

Figure 2.7: Immunohistochemical analysis of neuron and interneuron density with NeuN and GAD67 labeling. Coronal vibratome sections were incubated in antibodies to identify regions of neuron (NeuN), and interneuron (GAD67) loss and survival. **A**, At 24-48 hr post-HI insult, there is a reduction in the diffuse, background labeling of GAD67 that is correlated with synaptic terminals in the region of the infarct. This loss of synaptic labeling is wide spread and covers a large region of the ipsilateral cortex (dotted white outlines), while the contralateral cortex maintains uniform GAD67 labeling throughout. At 2-weeks post-HI, the peri-infarct region (dotted white outlines) has formed into columns of viable tissue separated by scar tissue and cerebral spinal fluid. The diffuse synaptic labeling of GAD67 in the peri-infarct region is recovered to similar levels compared to the contralateral cortex. An absence of interneuron cell bodies (bright fluorescently labelled dots) within the infarct suggest a reduction in the number of remaining interneurons at P21-23. **B**, At 24-48 hr post-HI insult, NeuN labeling of neuron cell bodies demonstrates a similar wide spread reduction in neuronal density in the region of the infarct (dotted white outlines) compared to the contralateral cortex. At 2-weeks postinjury, columnar cortical structures are prominent and easily identifiable via NeuN labeling in the peri-infarct ipsilateral cortex (dotted white outlines). Qualitative analysis reveals a similar size and density of neurons in the remaining live tissue compared to the contralateral cortex.

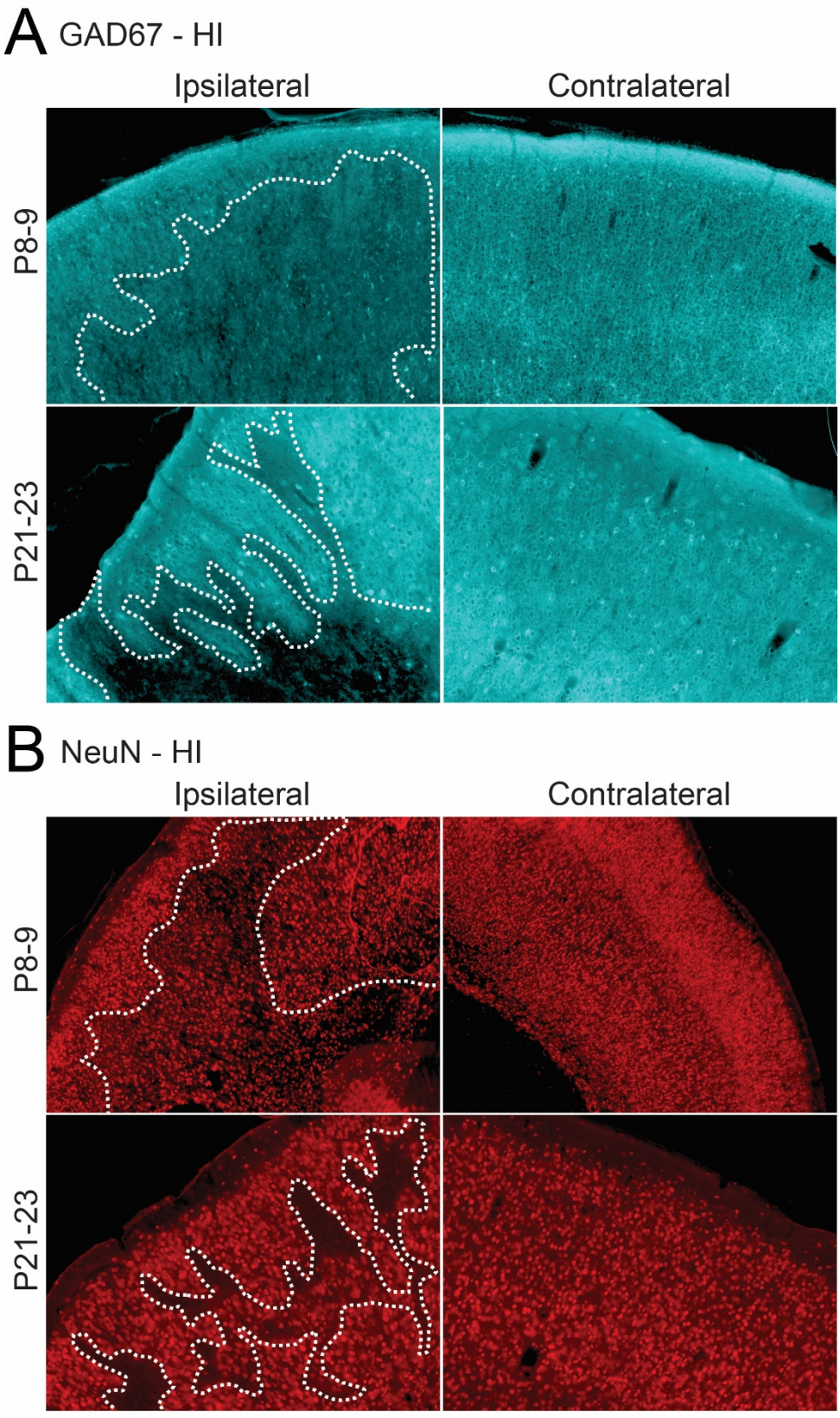
A GAD67 - HI
Ipsilateral
Contralateral
P8-9
P21-23
B NeuN - HI
Ipsilateral
Contralateral
P8-9
P21-23

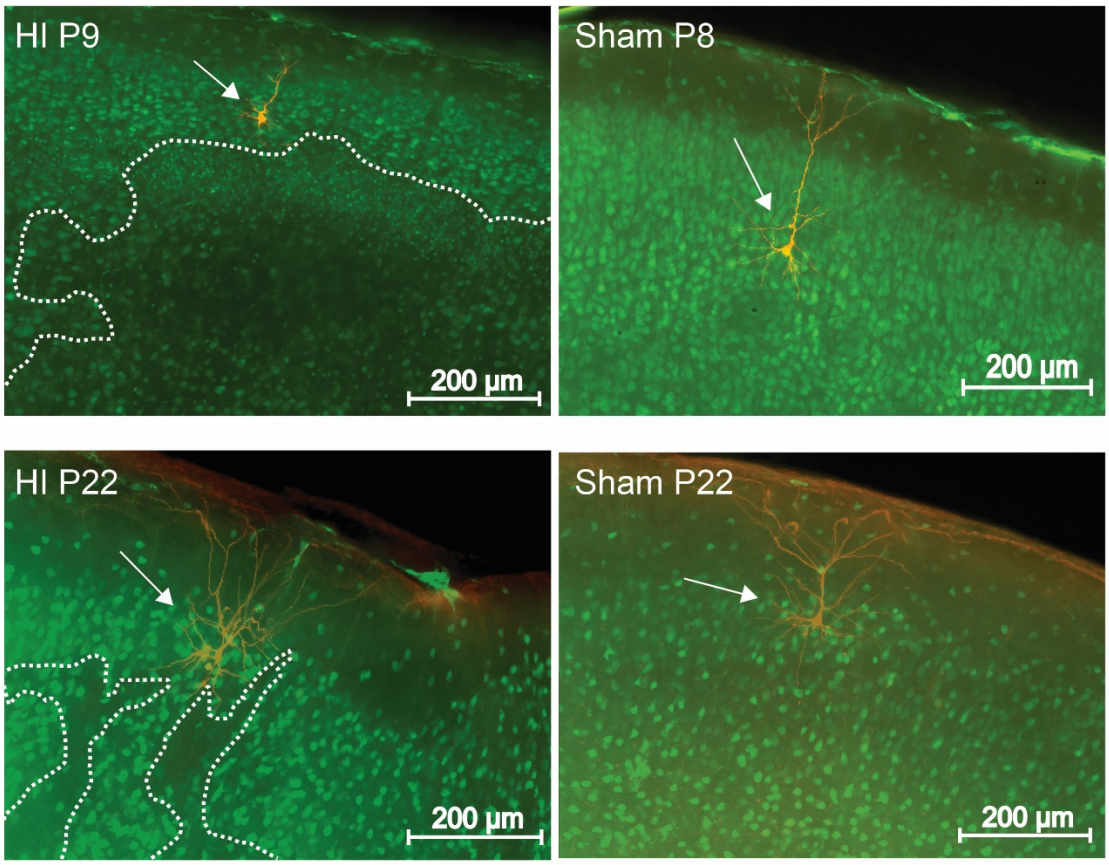

Figure 2.8: Visualization of recorded cells in proximity to the infarct. Cells were filled with biocytin (orange) during whole-cell recordings and later developed for light microscopy to control for morphological changes and to identify proximity to cortical damage. To visualize cortical damage, sections were stained with NeuN (green). In cells (white arrows) recorded 24-48 h (top left) and 2 weeks (bottom left) postinjury, it is evident that they were in close proximity to the infarct (dotted white outline).

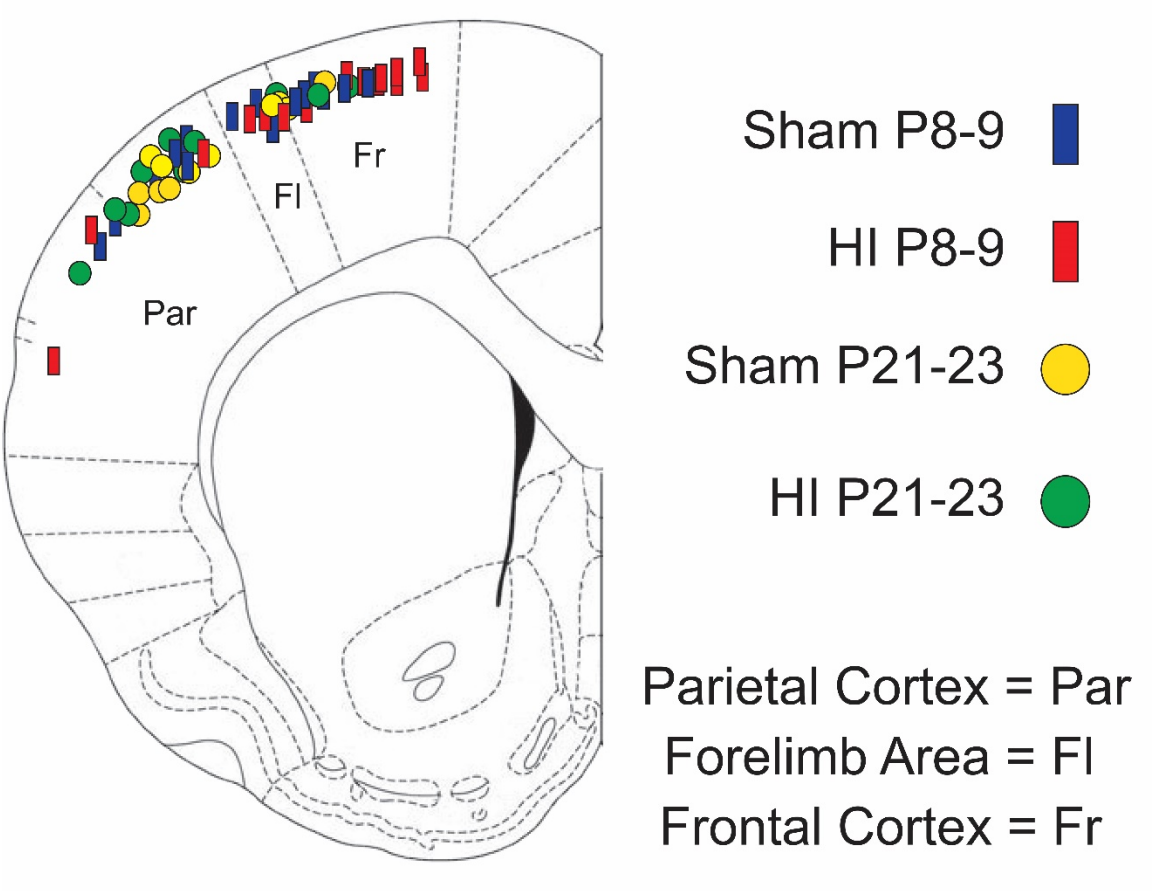

Figure 2.9: Diagram of mIPSC and mEPSC recording sites. This cartoon image shows serial coronal sections of a rat brain with colored shapes representing the mIPSC and mEPSC recording site for P8-9 sham (blue rectangle), P8-9 HI (red rectangle), P21-23 sham (yellow circle), or P21-23 HI (green circle), as well as HI (black) or sham (gray). All of the recording sites for mIPSC and mEPSC were in cortical layers 2/3 and mostly clustered within the same regions with similar spread throughout the cortex. Most recordings were in the posterior frontal cortex and the anterior parietal cortex primarily within motor and somatosensory cortex.

Figure 2.10: Drawn images detailing the proximity of mIPSC and mEPSC recording sites in relation to neuron loss within the peri-infarct region of P8-9 rats. The image on the right shows an overlay of the sketched image onto an actual image of the tissue illustrating how the shaded areas correspond to amounts of cell loss (light gray = reduced cell density, dark gray = complete cell loss) and where the recording site (orange biocytin filled cell, and black square) is in relation to it. Each coronal section contains a single neuron, with all recorded cells in this study at P8-9 being represented in this image. Based on these images, it is evident that all recording sites are within regions of reduced cell density and are in close proximity to complete cell loss, in slices with that degree of damage.

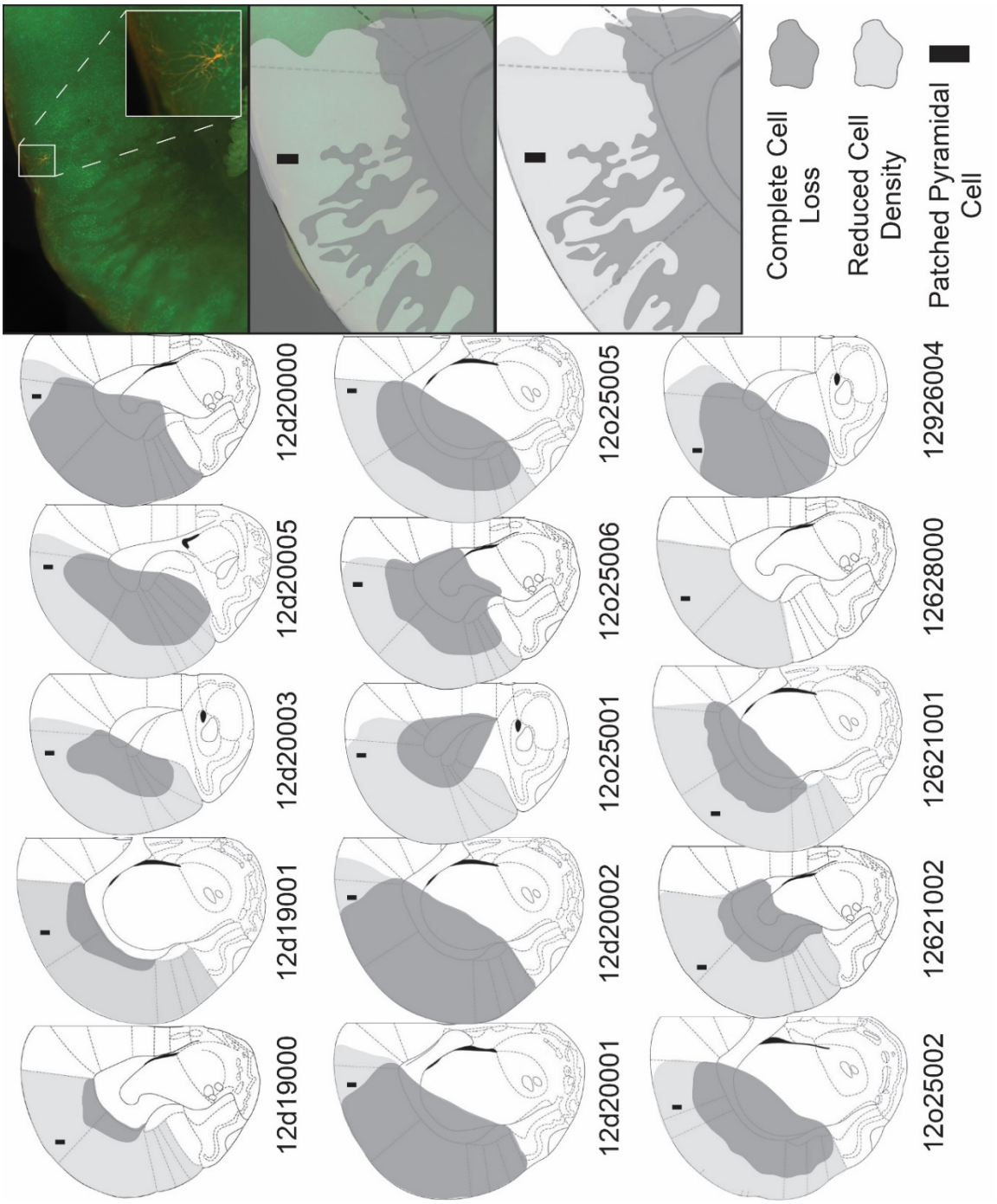
Complete Cell Loss
Reduced Cell Density
Patched Pyramidal Cell
12d19000
12d19001
12d20003
12d20005
12d20000
12d20001
12d20002
12o25001
12o25006
12o25005
12o25002
12621002
12621001
12628000
12926004

Figure 2.11: Drawn images detailing the proximity of mIPSC and mEPSC recording sites in relation to neuron loss within the peri-infarct region of P21-23 rats. The image on the right shows an overlay of the sketched image onto an actual image of the tissue illustrating how the shaded areas correspond to amounts of cell loss (light gray = reduced cell density, dark gray = complete cell loss) and where the recording site (orange biocytin filled cell, and black circle) is in relation to it. Each coronal section contains a single neuron, with all recorded cells in this study at P21-23 being represented in this image. Based on these images, it is evident that all recording sites are within regions of reduced cell density and are in close proximity to complete cell loss.

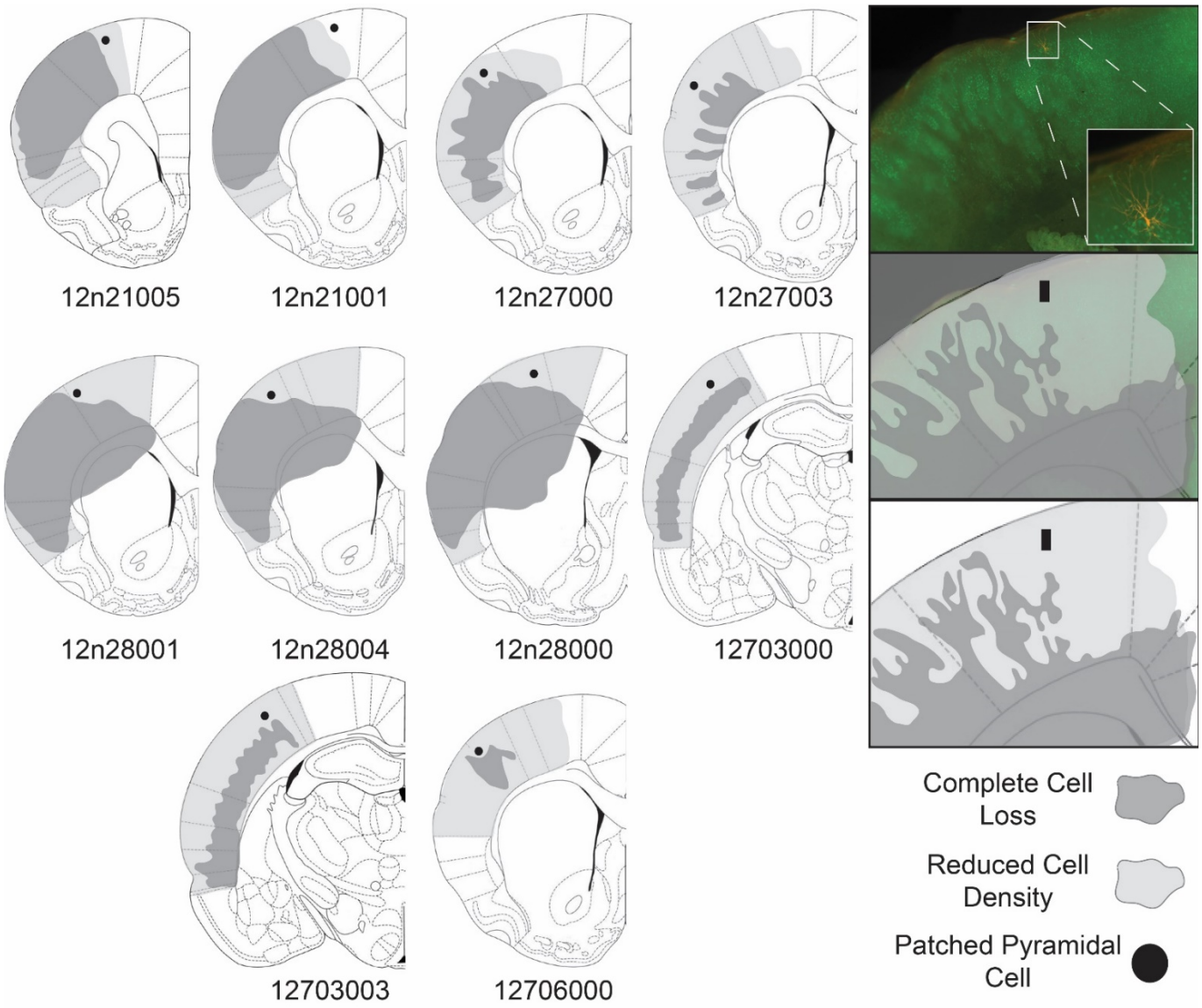
12n21005
12n21001
12n27000
12n27003
12n28001
12n28004
12n28000
12703000
12703003
12706000
Complete Cell Loss
Reduced Cell Density
Patched Pyramidal Cell

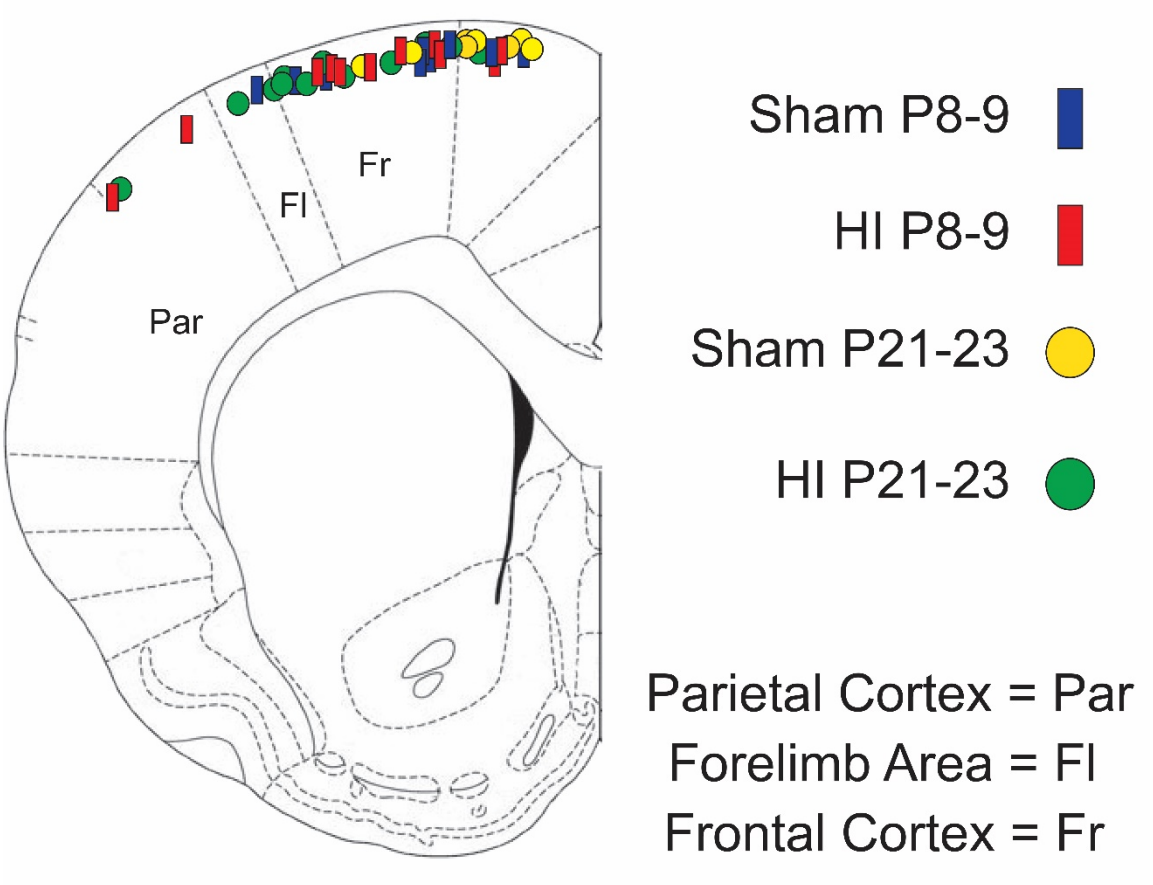

Figure 2.12: Diagram of tonic inhibition recording sites. This cartoon image shows serial coronal sections of a rat brain with colored shapes representing the mIPSC and mEPSC recording site for P8-9 sham (blue rectangle), P8-9 HI (red rectangle), P21-23 sham (yellow circle), or P21-23 HI (green circle), as well as HI (black) or sham (gray). All of the recording sites for tonic inhibition were in cortical layers 2/3 and clustered within the same regions with similar spread throughout the cortex. Most recordings were in the posterior frontal cortex and the anterior parietal cortex primarily within motor and somatosensory cortex.

Figure 2.13: Drawn images detailing the proximity of tonic inhibition recording sites in relation to neuron loss within the peri-infarct region of P8-9 rats. The image on the right shows an overlay of the sketched image onto an actual image of the tissue illustrating how the shaded areas correspond to amounts of cell loss (light gray = reduced cell density, dark gray = complete cell loss) and where the recording site (orange biocytin filled cell, and black square) is in relation to it. Each coronal section contains a single neuron, with all recorded cells in this study at P8-9 being represented in this image. Based on these images, it is evident that all recording sites are within regions of reduced cell density and are in close proximity to complete cell loss, in slices with that degree of damage.

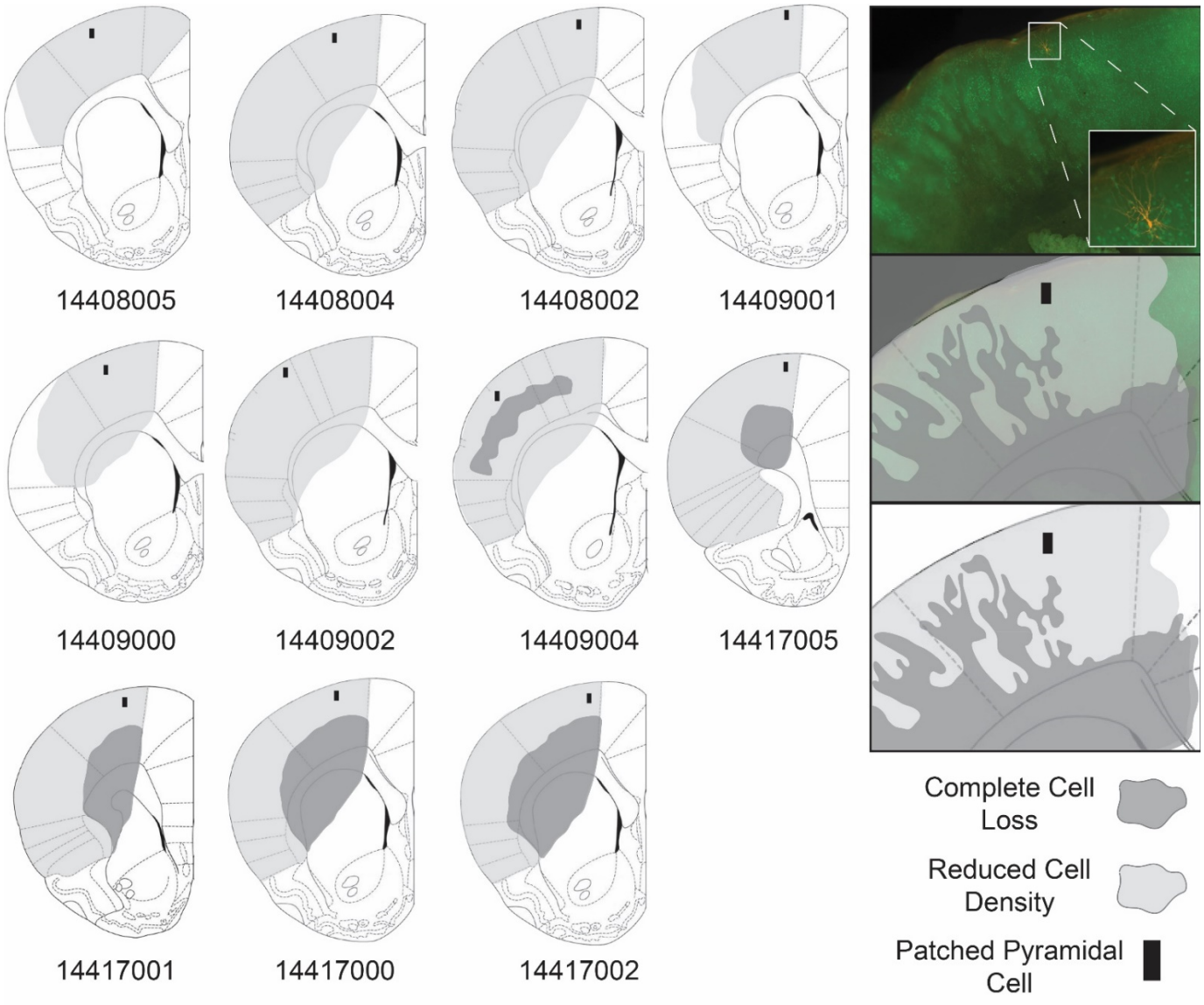
14408005
14408004
14408002
14409001
14409000
14409002
14409004
14417005
14417001
14417000
14417002
Complete Cell Loss
Reduced Cell Density
Patched Pyramidal Cell

Figure 2.14: Drawn images detailing the proximity of tonic inhibition recording sites in relation to neuron loss within the peri-infarct region of P21-23 rats. The image on the right shows an overlay of the sketched image onto an actual image of the tissue illustrating how the shaded areas correspond to amounts of cell loss (light gray = reduced cell density, dark gray = complete cell loss) and where the recording site (orange biocytin filled cell, and black circle) is in relation to it. Each coronal section contains a single neuron, with all recorded cells in this study at P21-23 being represented in this image. Based on these images, it is evident that all recording sites are within regions of reduced cell density and are in close proximity to complete cell loss, in slices with that degree of damage.

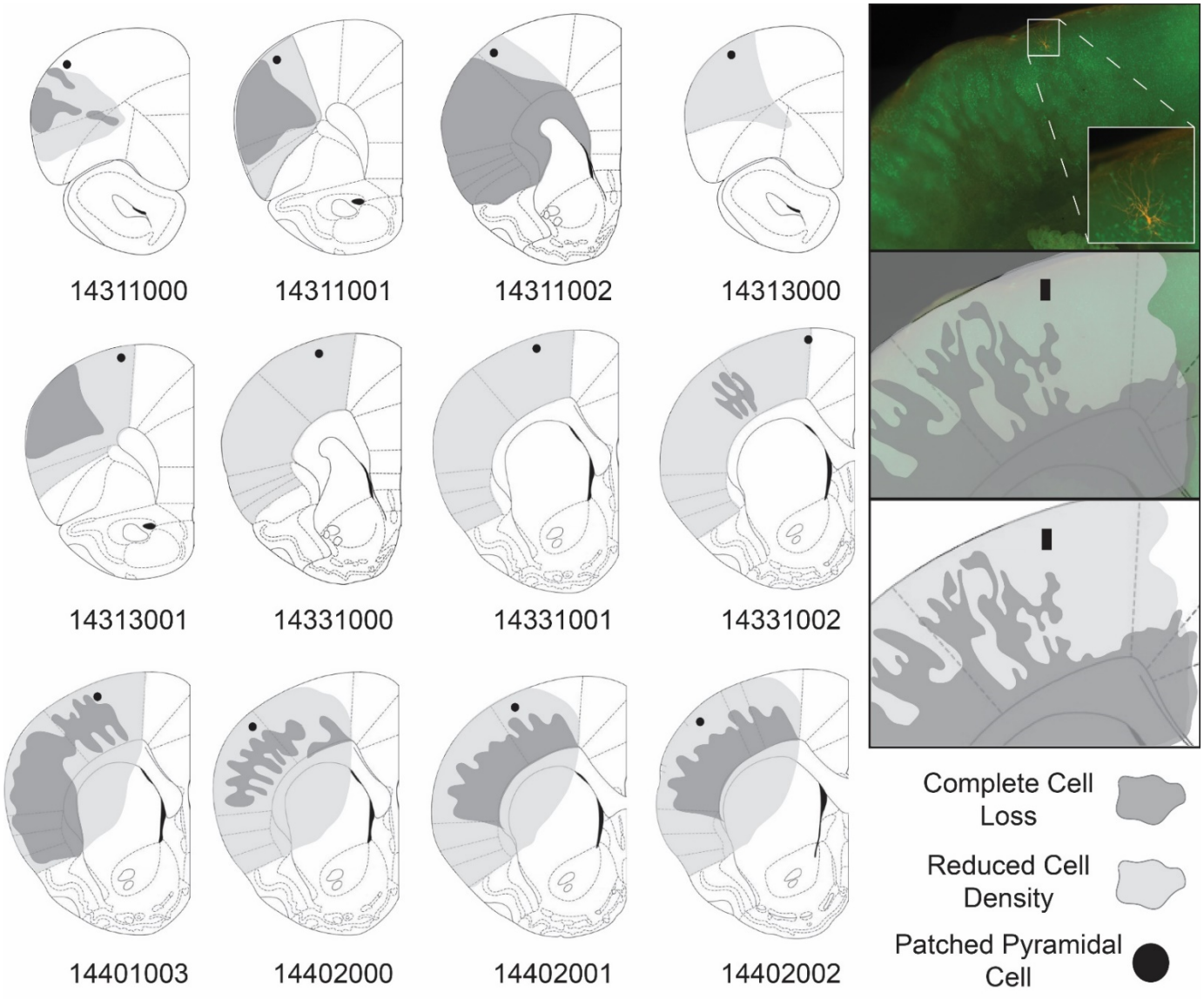
14311000
14311001
14311002
14313000
14313001
14331000
14331001
14331002
14401003
14402000
14402001
14402002
Complete Cell Loss
Reduced Cell Density
Patched Pyramidal Cell

CHAPTER 3

VIDEO-EEG ANALYSIS WITH MINIATURE TELEMETRY OF EPILEPTOGENESIS AFTER PERINATAL HYPOXIA-ISCHEMIA IN THE RAT: POWER SPECTRAL DENSITY AND SEIZURES

J.D. Bastar[1], P. Roper[2], M.J. Lehmkuhle[2], F.E. Dudek[2]

Departments of Physiology[1] and Neurosurgery[2]

University of Utah School of Medicine

Salt Lake City, UT

Corresponding Author:

F. Edward Dudek, Ph.D.
Department of Neurosurgery
University of Utah School of Medicine
383 Colorow, Suite 383
Salt Lake City, UT 84108

Email: ed.dudek@hsc.utah.edu

Office phone: (801) 587-5880
FAX: (801) 581-8075
Cell: (970) 690-4022

Abstract

It is commonly accepted that in acquired epilepsy, there is a seizure-free period termed the latent period where unknown changes lead to the generation of spontaneous recurrent seizures. Difficult to study in the human population, the majority of research on the latent period has focused on young adult rodents. However, in the immature brain, the pathogenesis of epilepsy might be quite different. Limitations in the ability to record continuous video-EEG from immature animals has led to greater interest in projects aimed at filling this void. In this study, we use a newly developed miniature wireless telemetry device that allows us to implant immature animals shortly after a perinatal hypoxic-ischemic injury and record video-EEG continuously in to adulthood. This approach uncovered difficulties associated with device implantation in immature animals being reared with their dam, and the solutions to mitigate them. Analysis of the EEG in this study revealed the earliest known time point of spontaneous recurrent seizures (SRSs) in this animal model, and gives us an understanding of the variability of the latent period. The use of power spectral analysis monitored the development of cortical frequency rhythms during the maturation of the animal from juvenile to adulthood as a way to identify any early biomarkers of epileptogenesis. This study shows the feasibility of performing continuous video-EEG monitoring from immature animals, and sets up the frame work for further research.

Introduction

Hypoxic-Ischemic Encephalopathy

Perinatal hypoxic-ischemic (PHI) encephalopathy is a relatively common injury affecting term infants, occurring 1-2 in every 1000 live births (Kurinczuk et al., 2010). Individuals who have been subjected to a PHI injury are predisposed to developing epilepsy, cerebral palsy, and other neurological deficits (Volpe, 1998, 2009; Johnston et al., 2001). Current treatments for PHI-induced epilepsy are limited to mitigating seizures with anti-epileptic drugs (AEDs) after the onset of spontaneous recurrent seizures (SRSs). This approach is insufficient at controlling the SRSs, as a high percentage of these patients have seizures that are refractory to AEDs (Hadjipanayis et al., 1997). The next best treatment is to induce hypothermia within the first 24-48 hr after the PHI

injury in order to prevent neuronal damage by reducing the metabolic activity of neurons (Ohmura et al., 2005). This method is still in the experimental phase, and is difficult to implement because (1) it requires knowing that a PHI event has occurred and (2) it is difficult to cool the brain. To improve treatment options for PHI-induced epilepsy, it is necessary to understand how it develops, and for this we need to know what occurs during the latent period.

Latent Period

The latent period in acquired epilepsy is the time between a precipitating insult and the first epileptic seizure. During this time, it is believed that the mechanisms required for epileptogenesis are in progress. The classic hypothesis is that epileptogenesis and its latent period represent a step function of time from the initial injury to the first SRS. Another more recent hypothesis about this time course is that epileptogenesis occurs as a continuous function, which is slow and gradual, and leads to a progressive development of epilepsy (Dudek and Staley, 2011). This hypothesis is supported by data showing that even after the onset of epilepsy, the disorder is progressive, becoming more frequent and severe over time clinically (Engel, 1996) and experimentally (Hellier et al., 1998; Williams et al., 2009; Kadam et al., 2010). Therefore, understanding the time course of the latent period is critical to discovering the mechanisms that lead to epilepsy. Almost all of the research data on the latent period of acquired epilepsy is from adult rodents, yet the mechanisms of epileptogenesis may be very different in the immature brain (Shorvon and Guerrini, 2010). While the need for 24-hr video-EEG monitoring studies determining the latency period of acquired epilepsy in the immature brain exists, it is technically demanding with many technical limitations due to the need for the pup to be reared by the dam.

New Approach

To address the need for more monitoring during the latent period, we implanted neonatal pups within 24-72 hr after PHI with a wireless EEG transmitter and recorded video-EEG continuously for 2-3 months. Previous research with the PHI animal model has shown that SRSs can occur by the third month of age (Kadam et al., 2010). However, the lack of smaller EEG

recording devices previously prevented long-term continuous monitoring any earlier than 2 months of age. The recent development of a miniature wireless telemetry device enabled us to implant and monitor electrical activity from neonatal pups as early as P6 (Zayachkivsky et al., 2013). A major goal of this study was to more accurately determine the true latent period of epileptogenesis in the PHI animal model, and to find the distribution of times between the HI insult and onset of SRSs. Furthermore, based on the finding that only PHI animals with brain damage (regardless of treatment) developed SRSs (Kadam et al., 2010), we hypothesized that if there is an identifiable lesion, then there will be a persistent alteration to the power of one or more EEG frequency bands (delta, theta, alpha, beta, or gamma). It is plausible that through the loss of local pyramidal neurons and interneurons within the cortical and subcortical network of the affected hemisphere, the evolution and development of the various EEG frequencies will lead to epileptogenesis. This finding would introduce a new diagnostic marker of epileptogenesis and provide a potential mechanistic target for treatment.

Methods

Animals

All surgical procedures were performed under protocols approved by the University of Utah Animal Care and Use Committee. Pregnant Sprague-Dawley adult female rats (14 days gestation) were received from Charles River (Wilmington, MA). Pups were born in the animal facility ~1 week after the arrival of the pregnant female (University of Utah, Salt Lake City, UT). The litter size was culled to 8 pups at postnatal day 3 (P3). Animals were housed with the dam and littermates, and at P7, they were treated with PHI. The weight of the pup at the time of treatment was 16-18 g. Due to high mortality rates when the transmitter was implanted at P6, most pups were implanted at P8-10 to allow for an adequate increase in body weight to compensate for transmitter weight. At the time of transmitter implantation, the litter was further culled to a total of 4 pups to enhance survival of the implanted pup. Environmental enrichment items, such as a block of wood, were added to the cage to occupy the dam’s desire to chew and entice her away from chewing the transmitter.

Perinatal HI

To model in rat pups the human condition of neonatal hypoxic-ischemic encephalopathy with cortical infarcts, the modified Levine's method (Levine, 1960; Rice et al., 1981) was performed on P7 rat pups. Both male and female rat pups were anesthetized with 2-4% isoflurane. The ventral cervical region was aseptically prepared with betadine scrub and the ventral midline infused with bupivacaine (0.5%, 0.25 ml). A 1-cm midline incision was made over the trachea, and the right carotid artery isolated and permanently ligated with a cautery pen. The incision was closed with 4-0 Vicryl suture and the pup was allowed to recover for 2 hr with the dam and littermates. Age-matched sham controls had the carotid artery exposed under identical procedures, but the carotid artery was not ligated.

After a 2-hr recovery period, the rat pups with the ligated carotid artery were placed into an air-tight temperature- and humidity-controlled chamber. They were subjected to hypoxia (humidified 8% oxygen, balanced nitrogen) and maintained at 37 °C for 2 hr, and then allowed to recover in normal air before being returned to the dam and littermates. Age-matched sham-operated controls were placed into a separate air-tight temperature- and humidity-controlled chamber (37 ˚C) for 2 hr, but did not receive the hypoxic treatment.

Implantation of the Telemetry Unit

Pups were housed and reared with the dam and implanted at 8-10 days of age with a 2-channel miniature wireless telemetry device. During this procedure, animals were anesthetized with 2-4% isoflurane, and placed onto a water-circulating heating pad on a stereotaxic unit. The stereotaxic unit was sprayed with 70% alcohol, and surgical tools were sterilized by autoclaving and maintained in 70% ethanol. The rat pup was placed in the stereotaxic unit using small-animal ear bars. The surgical site was prepared with betadine scrub and solution, and the incision site was isolated with sterile surgical drapes. Once the pup was anesthetized, a 1-cm incision was made on the top of the head using a scalpel, and the skin was separated using hemostats. Periosteum was removed from the skull, and surface bleeding was cauterized. Three holes were drilled using a 0.7mm burr, one over each bilateral hemisphere at approximately 3 mm caudal to

bregma and 2.5 mm lateral to the sagittal suture for the recording electrodes, and one over the cerebellum at approximately 1 mm caudal to lambda and along the midline for the reference electrode. The electrode wires of the transmitter were trimmed to an adequate length and placed at a target depth of the dura. The transmitter was attached to the skull using a cyanoacrylate adhesive (Loctite 454) with accelerator (Loctite 7452). The skin was then closed with Vicryl 4-0 around the implant and cleaned with betadine solution. Animals were treated with local application of bupivacaine and allowed to recover with the dam and littermates (Figure 3.1).

Data Acquisition and Recording

Animals began 24-hr video-EEG monitoring immediately after the implantation of the transmitters. The unsexed male and female Sprague Dawley rat pups were housed with their dam and 3 littermates in cages under a 12 h light/dark cycle (6:00am – 6:00 pm), until the age at which they could be weaned and individually housed. The transmitters (three Platinum-Iridium alloy electrodes) had two channels referenced to a common electrode. Using capacitive coupling, the EEG was transmitted wirelessly on a frequency-modulated carrier centered at 6 kHz to a receiver base situated below the animal's housing. Signals were bandpass filtered (0.1 - 100 Hz, 8 dB per octave), amplified (2000x gain), digitized at 500 Hz per channel (BIOPAC MP150, Goleta, CA), and stored on a PC computer using Acqknowledge software version 4.1.1. (BIOPAC). Each animal was simultaneously video monitored with video cameras and infrared lighting for the duration of the EEG recording. Video and EEG recordings were time stamped and new recordings were started at 1-hr and 2-hr epochs, respectively, to maintain temporal congruency. Video was stored on 4-TB external desktop hard drives (WD Green).

Experimental Design

Unsexed male and female rats were monitored (n=24, 13 male, 11 female). Implantation times were staggered as a result of high mortality when implanted early: 3 rats were implanted at P6, 1 rat was implanted at P8, 14 rats were implanted at P9, and 6 rats were implanted at P10. Of the 24 implanted rats, 9 were randomly selected male and female sham controls, and 15 were

randomly selected male and female PHI-treated animals all from separate litters. Random inclusion of animals into a treatment group was made by implanting both an HI and a sham animal each week, and due to random variables (death, dam chewing transmitter, and battery dying) not all animals that were implanted made it to the end of the study. All rats yielded data for the duration of the battery life of the wireless transmitter, which was estimated to be approximately 2 months. Animals were monitored for an average of 75.8 ± 1.3 d (minimum 62, maximum 88). The total number of video-EEG recording days in this study was 1820 (Figure 3.2).

EEG Data Analysis

EEG analysis was blinded to treatment and the degree of brain damage. Seizure detection was performed 50% by manual visual inspection, and 50% using a custom written computer algorithm based on auto-correlation. Any seizures that were identified by the algorithms were visually confirmed by eye on the EEG and video. Analysis with the computer algorithm yielded high coverage of the total EEG trace by visual inspection; therefore, the overall analysis by visual inspection is closer to 80%. Due to the large amount of data collected, and the time necessary for full analysis, only the first week and the last 4 weeks of collected data were analyzed to detect continuation of acute and subacute seizures (first week), or the onset of chronic seizures (last 4 weeks), respectively. If seizures were detected in either time period, then further analysis was performed on the entire data set for that animal to determine the earliest time that SRSs began to occur.

Grading of Seizures

Behavioral movements associated with electrographic seizures were classified using the Racine scale (grades 1-5) to determine the severity of the motor seizure (Racine, 1975): grade 1, immobility with open eyes and/or “wet-dog shakes” associated with facial automatisms; grade 2, same behaviors as grade 1 with head bobbing; grade 3, forelimb clonus with a lordotic posture; grade 4, continued forelimb clonus with rearing; grade 5, same behavior as grade 4 with falling

over from rearing. Electrographic seizure activity associated with no abnormal behavior was classified as a grade 0.

Power Spectral Density Analysis

Data were analyzed using custom designed software written in Python version 2.7.10 (64 bit), from the Continuum Analytics distribution 2.3.0. Estimates of the power spectral density (PSD) for each EEG signal were computed using the standard Welch method, called from the SciPy library version 0.17.1 with 4096 FFT points, and segment length 2048 points, and across the frequency range 1-100Hz. The PSD was then interpolated using a cubic spline interpolation, and resampled to divide it into 1-Hz bins. The initial 1-100 Hz frequency range was then further subdivided into the standard EEG frequency bands with ranges: delta (1-4 Hz), theta (5-7 Hz), alpha (8-12 Hz), beta (13-30 Hz), gamma (31-100 Hz). Time is measured in number of days post-HI, or alternatively as number of days post-P7. Results are presented as mean EEG activity (± 95% confidence interval) across the cohort. In the event that an individual recording either started more than 24 hr post-HI or terminated prior to the rest of the cohort then that signal was only included in the mean when it was active, and thus the n of the cohort, was not necessarily constant throughout the duration of the experiment, but could vary, and hence is not given in the legend. To analyze the data, the signal was first divided into 30 min windows, and the PSD across the entire 1-100 Hz range, for each 30 min window, was computed. The resulting averaged PSD for each cohort was first plotted as a three-dimensional plot, and also as a two-dimensional heat-map where the upper amplitude limit was chosen to show the best contrast across the range of amplitudes. Subsequently, to show temporal trends in each frequency band, for each cohort, the power in each frequency band was first integrated between the upper and lower frequency band limit (e.g. delta: 1-4 Hz) for each of the 30-min windows. Then to mitigate the effect of transient changes in EEG activity, the trends were smoothed using a running mean computed over a 20-hr window.

Experimental Difficulties

Successful chronic EEG recordings from immature animals have not been previously performed. This is the direct result of difficulties and limitations associated with implanting and recording from immature animals while they are being reared by the dam. In order to perform the work in this study, we developed alternative solutions to the difficulties we encountered. Of the 24 implanted animals included in this study, there were 58 animals (70% failure rate) that were not included for various reasons: died from not feeding, dam chewed the transmitter, transmitter ripped off by the dam, or the transmitter's battery failed too early.

In the early phase of this study, we adapted the single-channel transmitter into a two-channel transmitter. The single-channel transmitter provided successful studies on the acute and subacute phase of PHI (Zayachkivsky et al., 2015). However, when adapted to two-channels, the power needed to run the transmitter for 2-3 months required an increase in battery size. This led to necessary beta testing to determine the proper battery size needed to provide sufficient power. Even after the battery size was determined, there was little consistency to the duration of the battery life. While most transmitters worked for 2-3 months (predicted life was 2 months), occasionally the battery would die earlier, preventing the animals inclusion into the study.

The increase in battery size also led to an increase in transmitter weight. The single-channel transmitter weighed less than 1 g, while the two-channel transmitter weighed 2.2 g and was twice the size. The increase in weight and size resulted in the inability of the implanted pup to maneuver into position to suckle from the dam. The initial experimental design was to implant the pup at P6, prior to treatment, when the weight of the pup was 14-16 g. This worked fine for the single-channel transmitter, but the increase in the transmitter's weight made it difficult for the pup to lift its head, or to get under the dam and past its litter mates to feed. This was further complicated from the dam rejecting the only implanted pup in her litter. The transmitter was too heavy for these pups and they ended up losing weight, and dying, from expending all of their energy attempting to crawl over the bedding while having their heads weighed down. The first attempt to mitigate this was to cull the remainder of the litter. This did not work, because the dam was uninterested in nursing the single implanted pup. We then culled the litter to a total of 4 pups,

thus encouraging the dam to nurse, while giving the implanted pup a better chance of reaching a nipple. This worked occasionally, but it did not fix the issue of the pup being unable to move over the bedding with the weight of the transmitter on its head. Therefore, to increase the chance of survival for the pup, we waited until the pup was P8-10 once it had grown enough to be able to move itself to the dam to feed. Implanting the slightly older pup, and culling the litter to four, worked to prevent pups from dying due to starvation.

The more difficult problem to solve was that the transmitters would get chewed to the point of breaking. This would occur from both the dam and the littermates once they were old enough to have their eyes open. The solution to prevent the littermates from chewing the transmitter was to sac the remainder of the litter when they were about P14. This worked at preventing the littermates from destroying the transmitter, however, the bigger issue was the dam's intolerance to the implanted transmitter. This generally occurred within the first 24 hr, mainly at night when the dam was active, but it happened anywhere from 3 to11 days post-implantation. The first attempt to prevent the dam from chewing the electrode was to implant a second pup with a dummy transmitter. These attempts failed immediately as the dam completely removed the transmitter from the pup's skull. This could have been due to a problem with surgical attachment of the dummy transmitter, but it still demonstrates the dam's curiosity with the transmitter. Second attempts used an animal deterrent spray called "bitter apple spray" which was coated over the electrode. The electrodes are made with a hard epoxy, preventing liquids from absorbing in, but the bitter apple spray was allowed to dry, leaving a film of bitter apple taste on the transmitter to deter the dam from chewing it. When the pup was returned to the dam after surgery, a spare electrode was put in to the cage to satisfy the dam's curiosity of novel objects. Chocolate feeding pellets were also added to the cage to give the dam something to chew on. This worked for some dams, but not others. The final attempt was to include some environmental enrichment to the cage to fulfill the dam's desire to chew. This was done in the form of a wooden block, and hard dog chew bones that could be replaced when worn down. This reduced the occurrence of the transmitters getting destroyed, but did not prevent it. Once the pup reached

P21, they were weaned from the dam and individually housed in their own cage, eliminating further issues with the dam.

Results

Seizures

Prior to this study, the earliest time point that seizures were observed in this animal model was within the third month of age (P60-90) (Kadam et al., 2010). In the first phase of analysis, we found that no PHI-treated animals (n = 0/15) had observable seizures within the first week of monitoring, analyzed as early as P7, and as late as P17. The second phase of analysis (last 4 weeks of data recorded per animal), we identified seizures in 1 PHI-treated animal (n=1/15) (Figure 3.3). This analysis covered ages from P7-10 to P43-P96. For the animal that had seizures, we observed 77 seizures within the 4 weeks analysis period (P50-77). No clustering was observed for the seizures, as every day except 5 had at least 1 seizure, with an average 3 seizures per day and a maximum of 9 seizures in a single day. Every seizure had an electrographic and behavioral component. All seizures were behaviorally a grade 3 or 4 on the Racine scale, but varied in duration from as brief as 6 sec to as long as 56 sec (Figure 3.4). Seizure duration and electrographic morphology appeared to occur in two distinct types: less than 10 sec or longer than 20 sec (described in chapter 4). When the analysis for this animal was expanded to the entire recording period, it was found that it had its first spontaneous seizure at P-32, which was 25 days post-PHI, and had a total n=128 seizures. A more in-depth analysis and description of this animal will be in Chapter 4. There were no seizures observed at either time point of analysis for sham controls (n = 0/9) (Figure 3.3).

Spikes

It has been hypothesized that interictal spiking may precede, and even predict, epileptic seizures (White et al., 2010; Staley et al., 2011). The detection of spikes was not the focal point of this study, nor did we analyze a sufficient amount of data to have a definitive conclusion; however, we did identify spiking in 2 of the PHI-treated animals (n = 2/15) (Figure 3.3), neither of

which were the animal that had seizures. The morphology of spiking was different in each animal. One type of spiking was similar in morphology and duration to the spikes that occur during the clonic phase of the seizures (Figure 3.5). Surprisingly, these spikes were only present in the contralateral side, and not in the ipsilateral side to the damage. Subsequent analysis of this animal's brain revealed that the ipsilateral hemisphere was largely destroyed, which suggests that ipsilateral damage was so great that no spike occurred. Therefore, the spiking originated in the contralateral hemisphere. The second type of spiking consisted of a large-amplitude spike, and a large-amplitude slow wave (Figure 3.5). These spike-wave discharges occurred at a low frequency with a long interspike interval. These spikes were only present in the ipsilateral hemisphere. Spikes were only observed within the last 4 weeks of the recordings, and not in the first week. No spikes were observed at either time point of analysis for sham controls (n = 0/9) (Figure 3.3).

Spike Artifact

We were able to identify four types of spiking artifact in our recordings that occurred in PHI-treated animals and sham controls both within the first week and the last 4 weeks of analysis. The transmitter had to be perpendicular to the receiver base in order to transmit properly. Two types of spiking artifact arose from the transmitter being parallel to the base, which often occurred when the animal was sleeping. The first type of artifact consisted of repetitive high-amplitude, high-frequency synchronous biphasic spiking activity that occurred simultaneously in each channel (Figure 3.6 A). The second type was more subtle than the first type, and had a slightly higher amplitude than baseline with high-frequency spiking in both channels (Figure 3.6 B). When the animal touched the wire top, it led to a disruption in the transmission of the EEG signal (short circuited), which caused the third type of spiking artifact. This event resulted in realistically looking high-amplitude intermittent triphasic spikes that occurred in both channels, but not always synchronous (Figure 3.6 C). Lastly, the fourth type of artifact was a high-amplitude, high-frequency nonsynchronous spiking that would often appear in the ipsilateral channel more than the contralateral channel (Figure 3.6 D). This spiking activity occurred whenever the animal drank

from the water bottle, most likely causing a short-circuit of the wireless transmission. All of these spiking artifacts were common throughout the recordings. Interestingly, the spiking artifact caused by touching the wire top and drinking were present in the early recordings, when the non-implanted dam performed those activities.

Gross Anatomical Assessment of the Brains

After the HI treatment, the anatomical lesion that developed was quite variable (Kadam and Dudek, 2007). The resulting effect of the HI treatment ranged from no detectable damage to approximately 90% loss of the ipsilateral hemisphere. Using gross anatomical inspection, we first determined if an identifiable lesion was present and if we could categorize the brains into three groups: sham control, minor damage from PHI, and major damage from PHI (Figure 3.7). Sham controls were expected to have no obvious infarct and to have bilaterally symmetrical hemispheres. Based on this criterion, 2 sham control brains (n = 2/9) were excluded from further analysis beyond the seizure/spike detection due to small but detectable lesions that formed from the implanted electrode. For the PHI-treated animals, 5 had a reduction in the volume of the ipsilateral hemisphere with no obvious cystic infarct, and were included into the PHI minor damage group (n = 5/15). Six HI-treated animals had large amounts of atrophy, complete cellular loss, and the formation of a cystic infarct (n = 6/15). The remaining 4 HI-treated brains had no apparent damage and were further analyzed with magnetic resonance imaging (MRI) to determine whether any subtle damage had occurred (n = 4/15).

Magnetic Resonance Imaging

The use of gross anatomy alone was clearly not sufficient to determine cell loss or the presence of atrophy to deep cortical layers or subcortical structures. Therefore, we used MRI to obtain an analysis at a higher resolution of the entire brain for the previously described categories of sham control, minor PHI damage, and major PHI damage. Of the sham control brains that had no damage at the gross anatomical level (n = 7/9), the MRI confirmed that there was no cellular loss to the deep cortical layers and hippocampal atrophy (Figure 3.8). MRI of the PHI-treated

brains in the group with major PHI damage (n = 6/15) was consistent with the results from the anatomical inspection, which was a lack of cortex, dorsal hippocampus, thalamus, and any other subcortical structures on the ipsilateral side (Figure 3.8). However, even with the massive amounts of damage, small remnants of the ventral hippocampus were still present. The contralateral hemisphere for these brains did not appear to have any cell loss or atrophy. For the HI-treated brains that appeared from gross observation to have only minor damage (n = 5/15), MRI revealed much more damage than was visible with the gross inspection. For all of the brains considered to have minor damage from gross inspection, the dorsal hippocampus was clearly atrophied, and cellular loss was present within deeper cortical layers in the ipsilateral hemisphere (Figure 3.8). The ipsilateral ventral hippocampus was still structurally intact in these brains. The contralateral hemisphere had no obvious signs of damage and appeared similar to sham control brains. Of the PHI-treated brains that showed no signs of any damage with the gross anatomical assessment (n = 4/15), the MRI revealed that 2 of them actually had what appeared to be possible atrophy to the ipsilateral cortex and dorsal hippocampus. However, these brains were excluded from the PHI group with minor damage because the injury was considered too subtle to properly categorize.

Power Spectral Density

To determine if the brains of PHI-treated animals develop differently than sham control animals, we chose to determine how traditional EEG frequency bands (delta, theta, alpha, beta, and gamma) change over the course of the life of the rat, from the time of implantation (P8-10) to 70 days later. The data analyzed with reference to the two groups was based on gross anatomical observation and confirmed by MRI: major PHI damage (n = 6) and minor PHI damage (n = 5). The first comparison was between hemispheres (ipsilateral vs contralateral) in both the major (Figure 3.9) and minor damage (Figure 3.10) groups. For both groups, no significant difference was found between the running means of EEG power in any frequency band at any point over the 70 days analyzed. For the ipsilateral hemisphere, no significant difference at any time point for any of the frequency bands was found between the running means for the sham-

control, minor-damage, and major-damage groups for up to 70 days postimplantation (Figure 3.11). However, the minor-damage group showed a consistent, but not significant, increase in the total power for the running means in the delta, theta, and alpha frequency bands, which encompasses the 1-12 Hz range (Figure 3.12). To determine whether the power of each frequency band changed immediately after treatment with PHI, a small subset of sham and PHI-treated animals, which were implanted at P6, were included in the analysis from P7-21 (Sham n = 13, PHI n = 17). Although not significant, a trend was found toward an increase in theta, alpha, beta, and gamma bands compared to sham controls immediately after treatment with PHI (Figure 3.13). This difference lasted for 2 days (P7 to P9) before returning to similar levels as the controls for the remainder of the analysis (P21).

Discussion

In this study, we set out to better identify the latent period of epileptogenesis after PHI injury by monitoring for subacute background suppression, interictal spikes, early onset SRSs, and the reduction in the power of EEG PSD. Although we did not identify any subacute background suppression or changes to PSD of any EEG rhythm, we did identify interictal spikes in 2 HI-treated animals and SRSs in 1 HI-treated animal. Based on previous research that found interictal spikes always preceded SRSs (Kadam et al., 2010), and all the animals with HI-induced lesions developed seizures (Kadam et al., 2010), we expected to observe more animals with interictal spikes and seizures. The fact that we did not have more animals with interictal spikes or seizures implies that our study was performed within the latent period of epileptogenesis.

Background Suppression

A suppression in cortical EEG rhythms after injuries, such as perinatal stroke, have clinically been shown to be associated with worse outcomes (Amorim et al., 2016; Latal et al., 2016; Topjian et al., 2016; Weitzel et al., 2016). Corroborating those findings experimentally, previous work in our lab (unpublished, Zayachkivsky), and others (Sampath et al., 2014), found that immediately after PHI-treatment, there is a significant reduction in all cortical EEG rhythms,

reported as background suppression. However, 24 hr later, all of the EEG rhythms for the HI-treated animals returned to control levels, except beta and gamma, which stayed suppressed until monitoring ended at P10. We performed PSD analysis on this same time frame, P7-P10, but were unable to identify the same background suppression. There are multiple differences between the two experiments that could explain the discrepancies. (1) There might be a difference in the amount of cortical damage that has occurred between the two data sets. However, this is unlikely to be the cause based on the variable damage we have observed within this study. For the previous study, it is difficult to state the amount of damage an animal will develop as an adult by only examining their brain at P10. At that early time point, the damage is widespread and has yet to coalesce into a well-defined lesion. Injury observed at P10 could develop into atrophied brain regions (minor damage), or complete loss of those brain regions (major damage), but it is not possible to determine that early. Additionally, background suppression can recover within a few days, suggesting that the underlying pathology may be depolarization block, preventing neuronal activity, and not just the loss of cells. (2) The difference could be a result of the different recording methods. The previous study used a single-channel system that had a differential recording method, compared to our two-channel system that used a referential (single ended) recording method. The difference between these two methods is that the differential recording method is more likely to cancel out any ambient noise, which would be included in the referential recording. This would result in our study having a higher amount of baseline noise which could over power any background suppression, making it indistinguishable on the raw trace and lost in the averaging of the PSD analysis. (3) The discrepancy could be caused by the difference in recording equipment. The previous study (Zayachkivsky et al., 2013) was performed in small recording chambers with the pup isolated from the dam and littermates, while our study was performed in much larger recording chambers that included the dam and littermates. Having a larger recording chamber means the receiver is much larger, which could increase the introduction of ambient electrical noise. In addition, having the dam and littermates included in the recording could also increase movement artifacts that would also over power any noticeable background suppression. (4) It is possible that the continued suppression of beta and

gamma is not a suppression, but actually an increase in beta and gamma in the control animals. In the data figures for the Zayachkivsky et al. study, there is a “bump” or increase in the power of the beta range that also increases gamma slightly in the sham controls. It is this bump that leads to the significant difference in Zayachkivsky et al., but is absent in our sham control animals. Hypothetically, by removing the pups from the dam and placing them into a novel environment (the small recording chamber), there is an increase in mental alertness and attentiveness to this external stimuli, resulting in an increase in the power of beta and gamma in the controls. However, because of the HI-induced brain damage, the HI-treated animals are unable to have arousal of the cortex to a higher state of alertness and do not get an increase in beta or gamma rhythms as they are placed into a new environment. Thus, our study, which does not remove the pups from the dam, does not measure an increase in beta or gamma in the sham controls.

Interictal Spikes Preceding Seizures

Within the epilepsy field, there is a desire to find biomarkers as a way to predict the onset of epilepsy prior to seizure onset (Engel et al., 2013; Schmidt and Sillanpää, 2016). The most promising aspect of a biomarker in acquired epilepsy is the interictal spike (Staley et al., 2011). Although not the main focus of this study, we did monitor for interictal spikes while analyzing for seizures. We found that only 2 out of 15 PHI-treated animals were positive for spikes. Importantly, neither animal was the 1 epileptic animal confirmed to have SRSs, and we do not have video-EEG monitoring long enough to determine that these 2 animals will develop SRSs. However, both animals that did have interictal spiking, without the onset of seizures, did have brain damage, implying that they would have SRSs had we monitored long enough (Kadam et al., 2010). A possible hypothesis in regard to the difference in interictal spiking between our study and theirs is that the recording electrodes were in different regions. In Kadam et al. (2010), the electrode placement was more anterior than our placement, over forelimb motor cortex, at 0.5 mm caudal to bregma compared to our 3 mm caudal to bregma, which is over hind limb motor cortex. Based on the nature of the lesion, our electrodes are more likely to be situated over the infarct, in animals with severe brain damage, as opposed to over the peri-infarct region where you would

expect spikes to originate. Our electrode placement was limited due to the size of the transmitter and the preset location of the electrodes on the transmitter. Spike-wave discharges (SWDs) occurring at 7-9 Hz have been reported as being a pathological finding in animals treated with the fluid percussion injury (FPI) model of posttraumatic epilepsy (D'Ambrosio et al., 2004). However, additional evidence suggests that these SWDs are a common finding associated with behavioral arrest in uninjured Sprague-Dawley rats (Rodgers et al., 2015). Our analysis of the EEG did not reveal any evidence of SWDs in uninjured rats, although this could be a result of the recording time period. It has been shown that in untreated Sprague-Dawley rats, only 19% of females had SWDs by 3 months of age, and males only exhibited SWDs after 3 months of age (Pearce et al., 2014).

Seizure Rate and Detection

Due to the large amount of data collected, for the seizure and spike analysis, we increased the efficiency and possibility of detecting seizures by analyzing the time points most likely to have seizures. The earliest known time point that seizures have been previously detected with the PHI animal model has been in the 2-3 month age range. However, that study found the incidence of seizures that early in the treated animals was fairly low; 2 out of 5 epileptic animals had convulsive seizures by the end of the third month (Kadam et al., 2010). Based on this, we were aware that all of our data could be within the latent period. Therefore, we decided that the last 4 weeks of data recording would be the most likely time that we would find SRSs if the animal was having seizures that early. The first week of data recorded was also examined to identify any recurring seizures from treatment that lasted into the subacute time period. This method resulted in a minimum of 840 days analyzed out of the total 1820 days recorded, or 46% of the total.

Subacute Period

The subacute period is loosely defined as the period between acute (treatment) and chronic periods. Clinically, it consists of the time period from 48 hr to 1 week poststroke where brain swelling and damage are ongoing (Kunst and Schaefer, 2011). In the PHI model, the

occurrence of seizures within the subacute period have been identified, where 25% of animals continued to have seizures 48 hr after treatment, and 0% by 72 hr (Sampath et al., 2014). Our study did not identify any residual seizures occurring within that first week posttreatment that covered 48 hr to 1 week post-HI, even though all of our animals had convulsive seizures during treatment. This might suggest that the severity of HI-treatment in our study was less severe than other studies; however, evidence of lesions in n = 11/15 animals suggests that this is not the case, especially considering the major damage incurred in 6 of those animals. Our study is the first to perform chronic EEG recordings in immature animals while they are with the dam and littermates. This reduced stress to the pup might explain why we did not observe subacute seizures, while an increase in stress from putting pups into individual recording chambers possibly led to reflex seizures in the other study.

Latent Period

Our data analysis yielded 1 animal that had SRSs, with at least 77 identified seizures within that 4-week time frame. A complete analysis of this animal decreased the previously known latent period down to as short as 25 days post-PHI. This was a drastic reduction from the previous time point. However, the finding that only 1 PHI animal out of 15 had seizures suggests that the latent period from injury to first seizure is highly variable in this animal model.

Previous findings in this animal model have demonstrated that all of the animals with brain damage develop SRSs, while none of the uninjured animals do (Kadam et al., 2010). Based on these data, we would expect that all of the animals with brain damage (n = 11/15) in our study would develop SRSs if monitoring was to continue. There are multiple possibilities for why we have a lack of seizures in the remaining 10 PHI-treated animals that do have brain damage. (1) It is possible that we are monitoring within the latent period, ending our recordings before SRSs begin. In the Kadam et al. (2010) study, only 2 out 5 epileptic animals were found to have seizures within their earliest data analysis period (2-3 months), which overlaps with our latest data analysis period. Furthermore, video analysis beginning at 1 month of age detected the first behavioral seizures also occurring at 2-3 months, at the earliest (Kadam and Dudek, 2007).

These data support the hypothesis that our recordings terminate within the latent period. While Kadam et al. (2007, 2010) detected the first seizures occurring by P90, only 5 out of 24 of our animals were monitored to P90, with a mean age of monitoring termination of P76. (2) Another possibility is that our PHI-treated animals are having seizures, but the 4-week analysis is within a prolonged interseizure interval, giving us a false negative result. Interseizure intervals in the PHI model vary widely from less than an hour to longer than a week, but the longest interseizure interval previously detected was approximately 2 weeks long, occurring early on (third month) (Kadam et al., 2010). Our 4-week data analysis was twice as long as this, greatly reducing the possibility that we analyzed within an interseizure interval. Furthermore, a small subset of animals (PHI = 2, sham = 5) were analyzed (blinded) for the entirety of their recordings and found to not have seizures, or spikes. Based on this small sample, we are confident that the first possibility is the most likely scenario and our data are still within the latent period for the majority of these animals. Regardless, in order to state that the treated animals we did not find seizures in do not have any seizures, then we need to analyze the entire set of data. Future analysis will follow up on this, discussed in Chapter 5.

Latent Period in Other Animals Models of Acquired Epilepsy

In status epilepticus (SE)-based (pilocarpine- or kainite-induced) adult models of acquired epilepsy, the reported latent period varies from 1 (Ndode-Ekane and Pitkänen, 2013) to 37 (Williams et al., 2009) days posttreatment. Although it could be argued that seizures occurring within 1 day post-SE are recurring acute seizures, the majority of reported latent periods for these models occur within the first 2 weeks (Goffin et al., 2007; Bumanglag and Sloviter, 2008; Williams et al., 2009; Heinrich et al., 2011). In models of stroke-induced epilepsy in adult animals, reported latency periods from injury to first SRS also varies widely, but can be as short as 2-4 weeks (MCA/CCAO) (Kelly et al., 2006), or as long as 26 to 181 days (photothrombosis) (Kharlamov et al., 2003). While these studies were all performed in adult animals, until our study, there have been no other studies that have used continuous monitoring to measure the latent period in pediatric models to which we can make a comparison. Regardless, it appears that the evidence

of varying latent periods in adult models of acquired epilepsy supports our conclusion that the PHI model also has a variable latent period.

Does Lesion Size Correlate with Epilepsy Probability

In a population-based study on the probability of developing epilepsy after traumatic brain injury, it was suggested that the probability to develop epilepsy increased with increasing severity of the brain damage (Annegers et al., 1998). We are unable to fully address this hypothesis in our study, since we did not have monitoring long enough to detect seizures in all of our HI-treated animals. However, the animal in our study that had seizures was part of the group with minor damage, and not major damage as one would expect based on the human data. Furthermore, seizures were not identified in animals with major damage. This would imply that the amount of damage does not increase the chance of developing epilepsy. Alternatively, the probability of developing epilepsy in relation to damage severity could follow a normal distribution curve, where there is a “sweet spot” in the middle where the probability is high. Increasing damage to the point that there is very little amount of ipsilateral brain tissue remaining (as in our group with major damage) results in a low probability to develop seizures.

Power Spectral Analysis

Cortical and hippocampal EEG rhythms are generated through the precise timing of neuronal-spike discharges that are temporally regulated by GABAergic interneurons (Cobb et al., 1995; Buzsáki et al., 2004; Klausberger and Somogyi, 2008; Buzsáki and Wang, 2012). Removal of large portions of neurons and interneurons would hypothetically result in a decrease in the amount of time various cortical rhythms (measured as power) are present in affected regions of the brain. EEG rhythms can be separated into multiple frequency bands, ranging from 1-100 Hz: 0.1-3 Hz = Delta, 4-7 Hz = Theta, 8-12 Hz = Alpha, 13-30 Hz = Beta, 31-100 Hz = Gamma. The lower frequency rhythms delta and theta (not to be confused with hippocampal theta) are generally associated with sleep, or a less active cortex, and are believed to be generated by layer V pyramidal cells and the corticothalamic network during sleep (Steriade et al., 1993; Schmidt et

al., 2016). The alpha frequency rhythm is most often associated with a relaxed state of consciousness and is thought to be generated within layer 4C and deeper cortical layers, with involvement of the corticothalamic network (Bollimunta et al., 2008, 2011), whereas the higher frequency rhythms beta and gamma are correlated with alertness, mental activity, and higher level information processing, and have been found to be generated in a wide range of network structures and cell types (Fries, 2015; Khanna and Carmena, 2015). The induction of a HI-induced infarct results in such a massive amount of brain damage affecting these brain regions that we would expect to record a consistent decrease in the power of each frequency rhythm, or at least a decrease in the higher frequency bands (beta and gamma) and an increase in the lower ones (delta and theta). A comparison of PHI vs. sham control animals, as well as ipsilateral vs. contralateral hemispheres within HI-treated animals, identified no difference in the running means of any of the frequency bands from the time the transmitter was implanted (P8-10) until the recording was terminated approximately 70 days later. It was surprising to us that PHI animals showed no difference in the running means between contralateral and ipsilateral hemispheres, especially considering some of these animals in the major damage group were missing a large portion of their ipsilateral cortex. A possible explanation for this is that the cortical activity from the contralateral hemisphere conducts through the cerebral spinal fluid in the ipsilateral hemisphere where it is recorded from that electrode. This would result in the ipsilateral hemisphere having the same types of rhythms as the contralateral hemisphere. It is also possible that in the minor damage group, there is enough surviving cortical neurons and interneurons to maintain normal functioning rhythms.

Due to the variability in the size of the lesion that develops after PHI, we decided to split the PHI groups into minor damage and major damage for the power spectral density (PSD) analysis. This was an attempt to prevent any loss of significance that might be present. The unfortunate consequence of splitting the groups was that it reduced the sample size for each group, leading to wide 95% confidence intervals, making it difficult to detect any difference in the means between groups. Another variable that led to wide 95% confidence intervals was the large fluctuation in the power of each EEG rhythm from day-to-day. There was no correlation between

sleep, or any specific behavior, and these fluctuations. Therefore, the source of the fluctuations may be from electrical noise, recording artifacts that are introduced into the wireless system, or just normal variance in activity throughout the day-to-day life of the animal.

Conclusion

When considering all of our results together: the earliest time point of SRSs at P32, the lack of detected seizures in the other PHI-treated animals, and the similarities in EEG rhythms between PHI and sham animals, we conclude that our study was conducted within the latent period of epileptogenesis. We find that there is no specific time point at which nonconvulsive or convulsive seizures are set to begin, and that the latent period can be variable depending on the time course of the epileptogenic changes. Furthermore, as will be described in more detail in Chapter 4, the progressive nature of the seizures (becoming more severe and frequent over time), and the presence of smaller subtle seizures that are difficult to detect, suggest that the development of chronic epilepsy in this model is continuous, supporting the hypothesis that latent period of acquired epilepsy is a continuous function (Dudek and Staley, 2011).

Figure 3.1: A 6-day-old pup after implantation and 5-weeks later as an adult. These experiments aimed to provide proof-of-concept data to demonstrate that young pups can be implanted with a miniature telemetry device for continuous recording into adulthood. The pup in this experiment was implanted at postnatal day 6 (P6) (left) with a miniature wireless EEG telemetry transmitter (Epoch™ from Epitel, Inc.). Immediately upon implantation, continuous video-EEG monitoring was conducted for 71 days. Implantation of the device did not impede normal development of the rat, and the animal grew to the size of rats that had not been implanted. The device did appear to cause any discomfort (right).

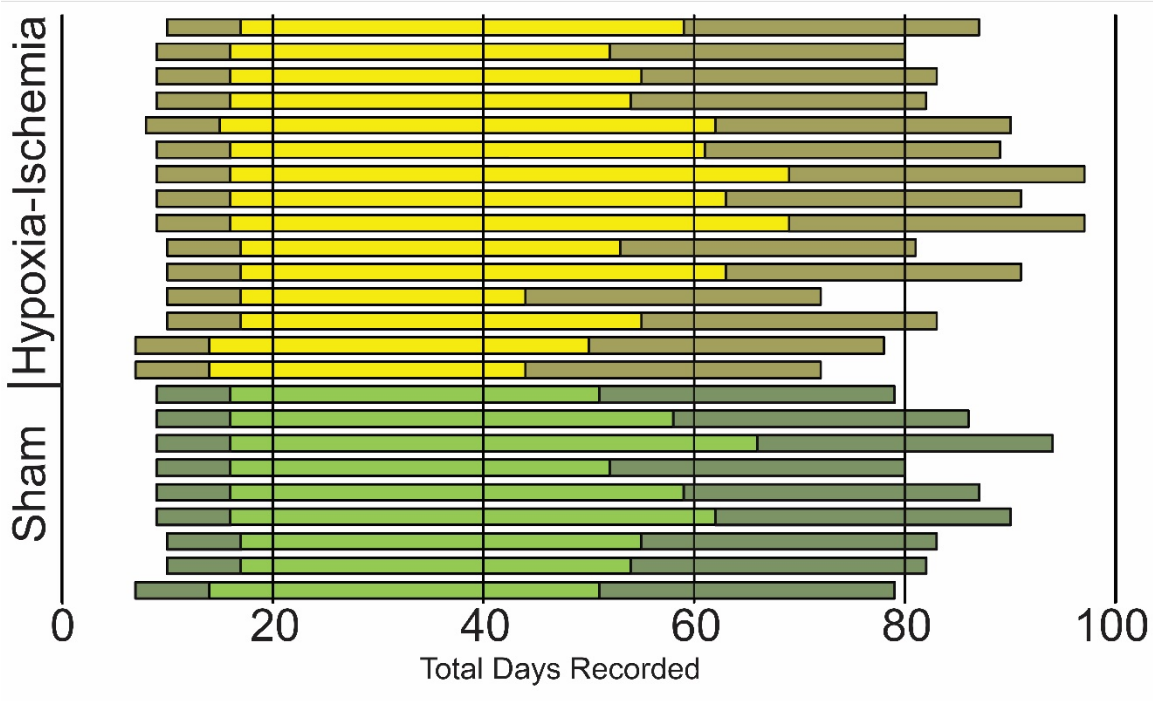

Figure 3.2: Gantt chart showing the days recorded with video-EEG for the PHI vs sham groups, and the portions that were analyzed (gray). All animals in the PHI (yellow, n=9) and sham (green, n=15) groups were implanted with miniature wireless transmitters at either P8, P9 or P10 and were recorded continuously with video-EEG until the battery died for each individual transmitter. Each bar represents a single animal and shows the ages that were monitored for that animal (gray), which included the first 7 days and the last 28 days per rat.

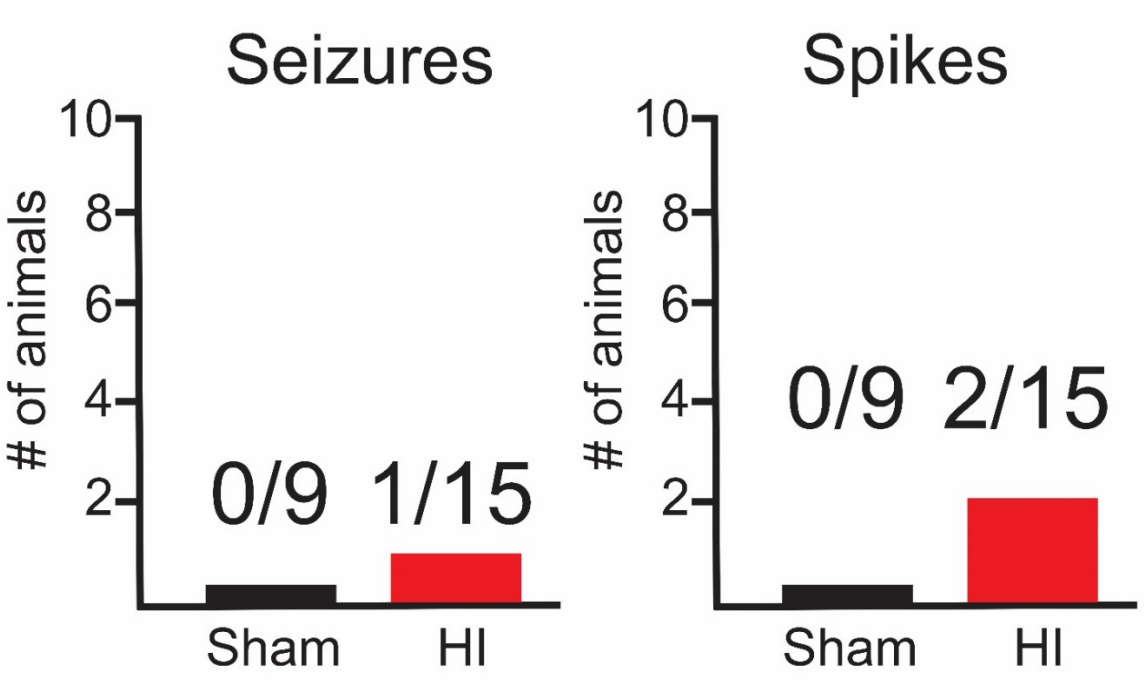

Figure 3.3: Incidence of PHI and sham animals with seizures and spikes. Seizure incidence was low during the time periods of seizure monitoring, with only one PHI-treated rat experiencing seizures and no sham controls. The number of animals with abnormal spikes was also low, with 2 PHI animals having identifiable spikes, and none of the sham controls. The animal with seizures was not one of the animals with spikes.

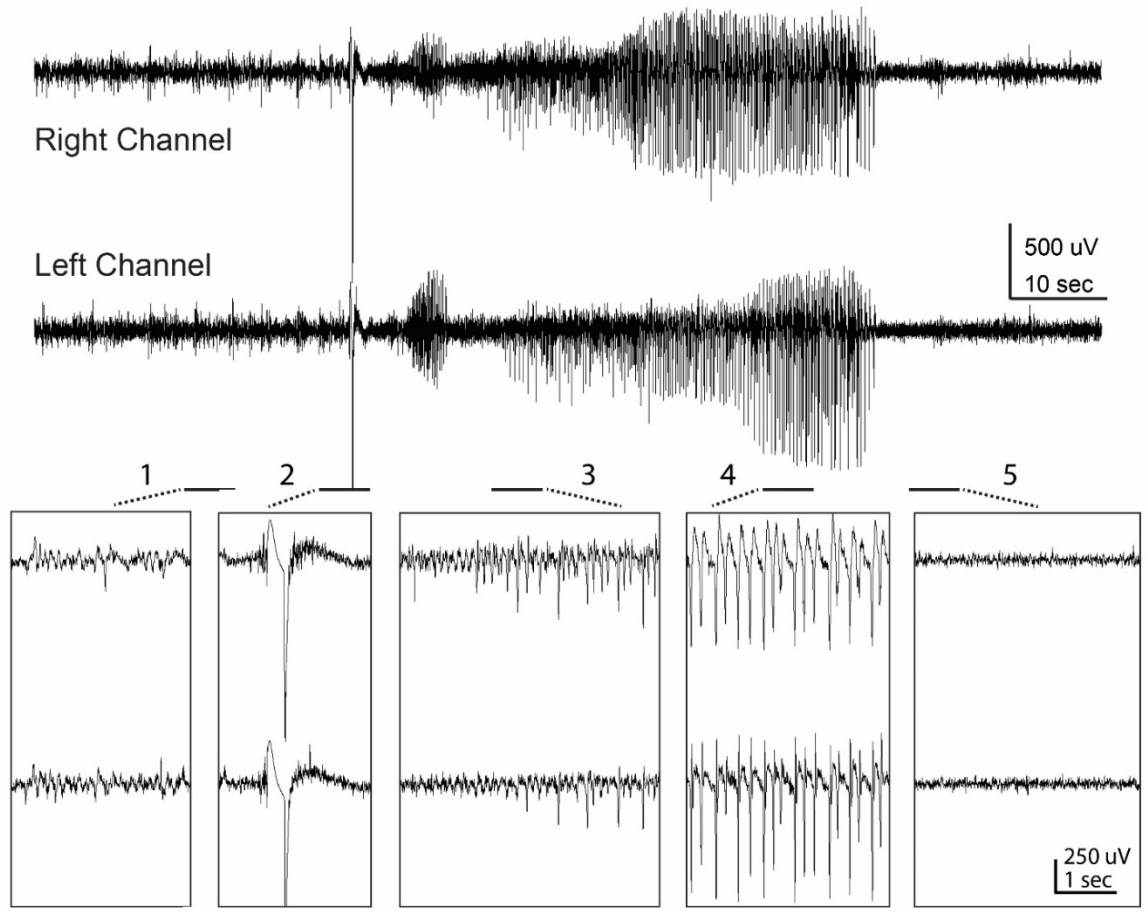

Figure 3.4: Electrographic activity of a typical spontaneous recurrent convulsive seizure in a PHI-treated animal. This type of seizure began as early as 27 days after PHI treatment when the animal was P34. These seizures were accompanied with tonic-clonic behaviors and were most often scored a 3 on the Racine scale. Expansions at the bottom show normal-amplitude pre-ictal baseline (**1**). The onset of the tonic portion of the seizure began with a large-amplitude sentinel spike (**2**), followed seconds later by the transition to the clonic phase with rhythmic spiking activity that began on the right side ipsilateral to the infarct (**3**). As the seizure progressed, the rhythmic spiking activity increased in amplitude and frequency (**4**). The seizure ended with a period of post-ictal suppression (**5**).

Figure 3.5: Two different types of spiking were detected in two different PHI-treated animals. A, Raw trace of the two channels recorded in a PHI animal including ipsilateral (right) and contralateral (left) sides. Expanded trace shows contralateral spike-wave discharges similar to the spike-wave activity seen during the clonic phase of a seizure recorded in the contralateral hemisphere of this PHI animal. Spike activity was absent in the hemisphere ipsilateral to the cortical damage. Interestingly, this particular animal had major cortical damage and was missing almost all of its ipsilateral hemisphere. **B,** Raw trace of the two channels recorded in a PHI-treated animal including ipsilateral (right) and contralateral (left) sides. Expanded trace shows ipsilateral large-amplitude, low-frequency spike activity with a long interspike interval. Spike-wave activity was not present in contralateral lead.

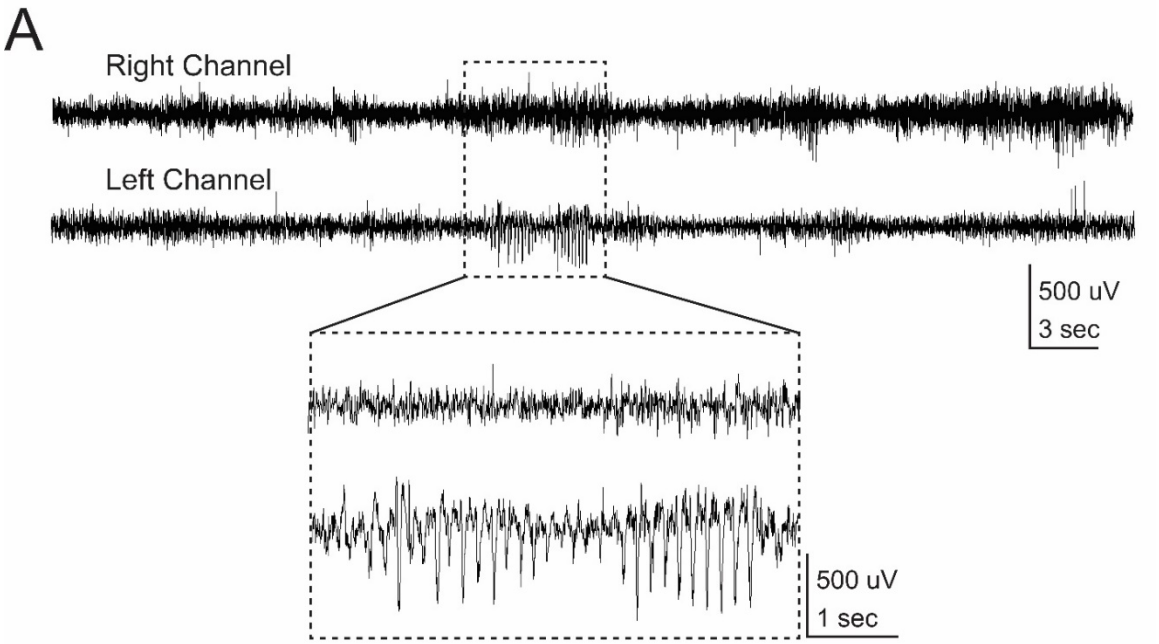
A
Right Channel
Left Channel
500 uV
3 sec
500 uV
1 sec

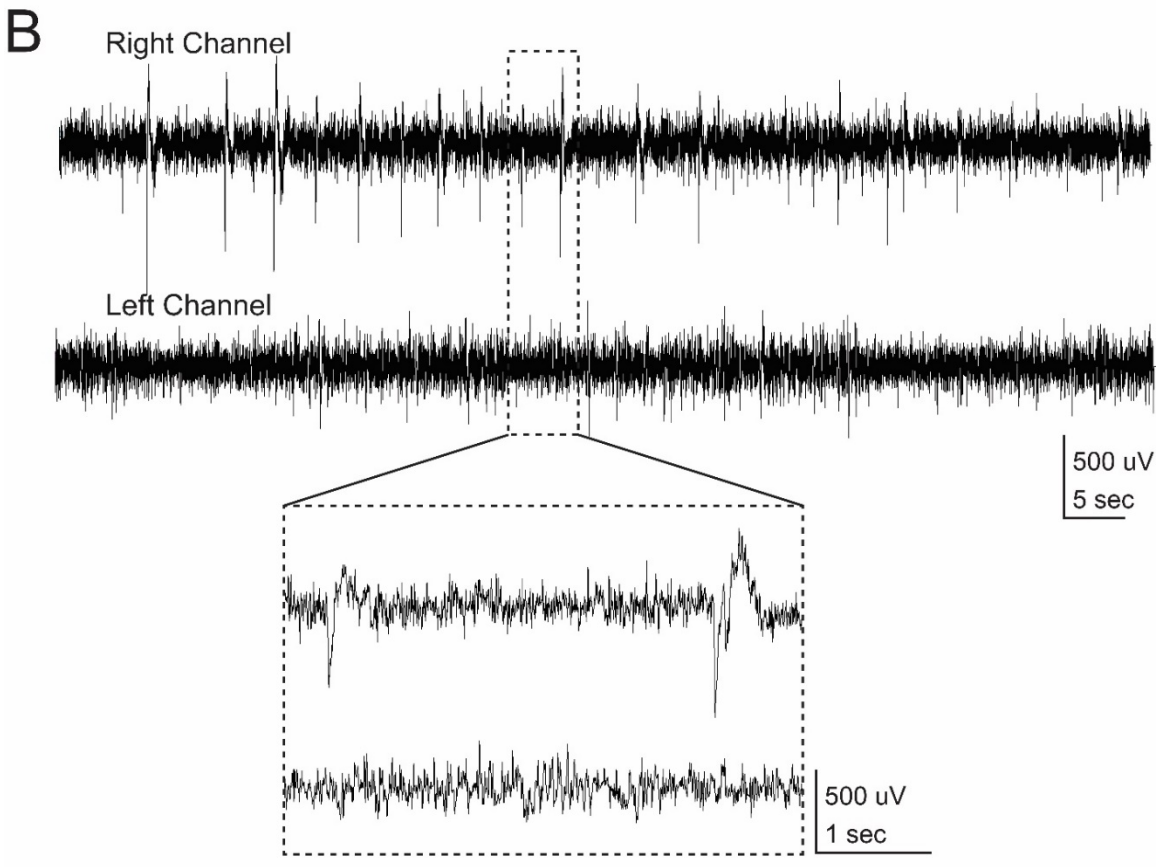
B
Right Channel
Left Channel
500 uV
5 sec
500 uV
1 sec

Figure 3.6: Recording artifacts that resembled spikes during EEG review. A, Repetitive high-amplitude, high-frequency synchronous biphasic spiking that has identical morphology and duration in each channel. This spiking was a recording artifact that resulted when the animal slept with its head sideways and the transmitter perpendicular to the receiver base. **B,** Abnormal spiking with slightly higher frequency and amplitude than baseline. This artifact was different than the artifact seen in A, but it was caused by the same activity of having the side of the transmitter parallel to the recording base. **C,** High-amplitude intermittent triphasic spiking activity that is separated by periods of normal baseline activity. These spikes occurred in both channels, but not always at the same time. This artifact was caused from the animal touching the wire top of the cage and shorting out EEG transmission. **D,** High-amplitude, high-frequency spiking that is nonsynchronous. These spikes regularly appeared with higher frequency in the right channel of PHI-treated and sham control animals making them appear real. However, this spiking artifact always correlated with the animal drinking.

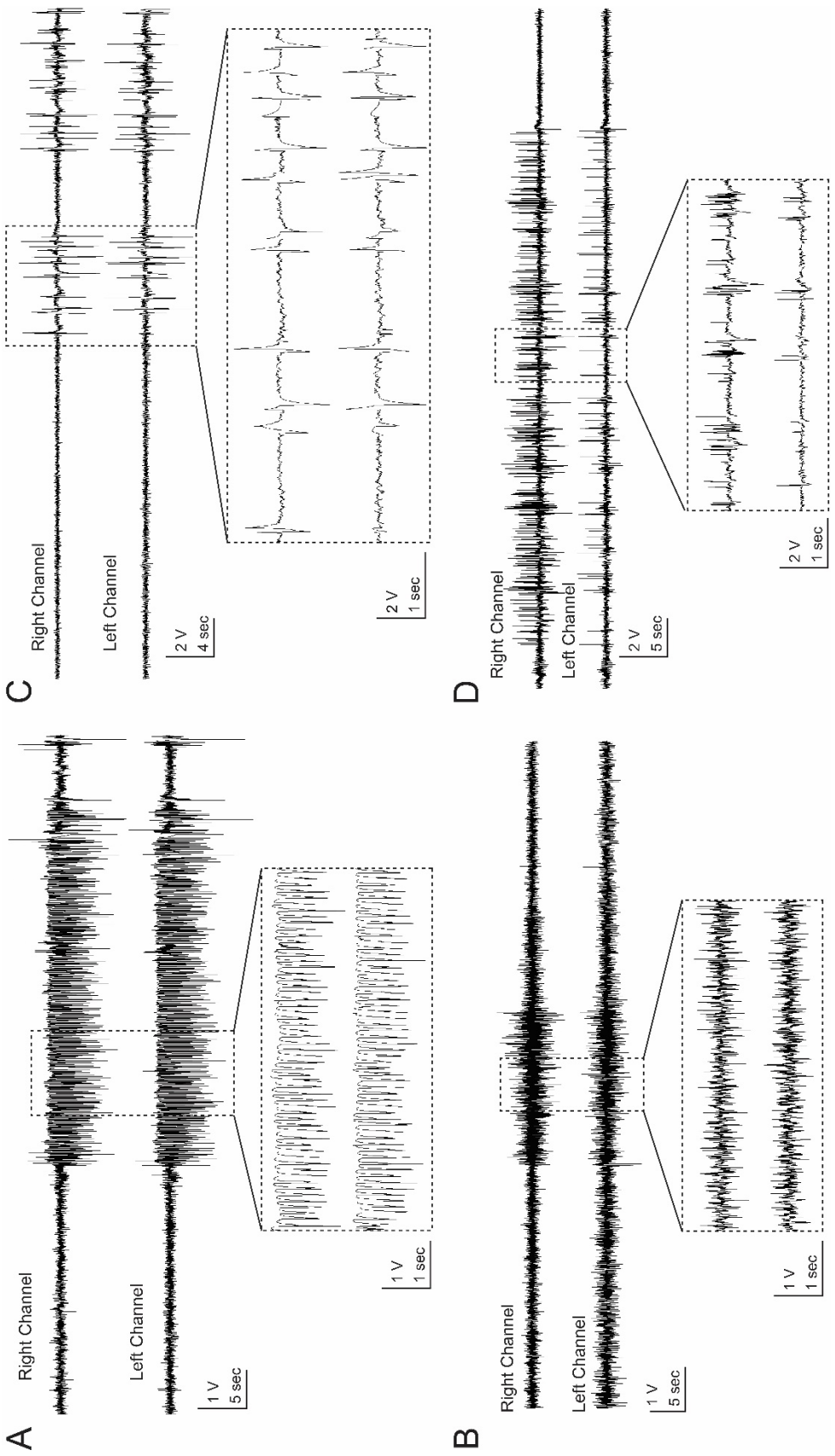
A
Right Channel
Left Channel
1 V
5 sec
1 V
1 sec
B
Right Channel
Left Channel
1 V
5 sec
1 V
1 sec
C
Right Channel
Left Channel
2 V
4 sec
2 V
1 sec
D
Right Channel
Left Channel
2 V
5 sec
2 V
1 sec

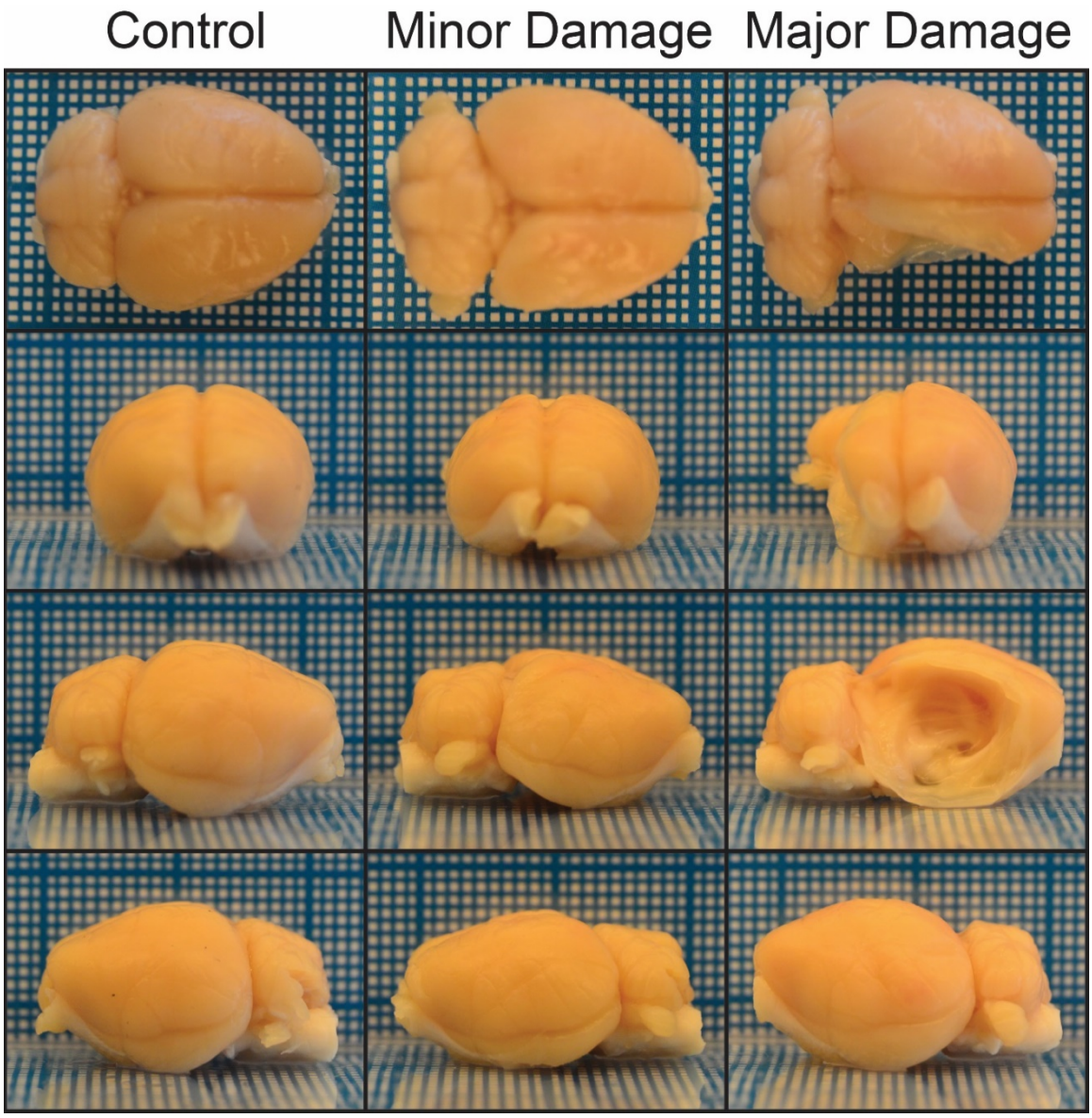

Figure 3.7: Gross anatomical view of the three categories of brain pathologies: sham control, PHI with minor damage, and PHI with major damage. The sham control brains (left column) included in the PSD study were all clear of any anatomical defects, and were symmetrical along all anatomical planes. PHI animals with minor damage (middle column) had no obvious cystic infarcts, but did have an atrophied ipsilateral hemisphere that is obvious in the horizontal (top) and coronal (second from top) views. PHI animals with major damage (right column) had large cystic infarcts that occupied the majority of the ipsilateral hemisphere.

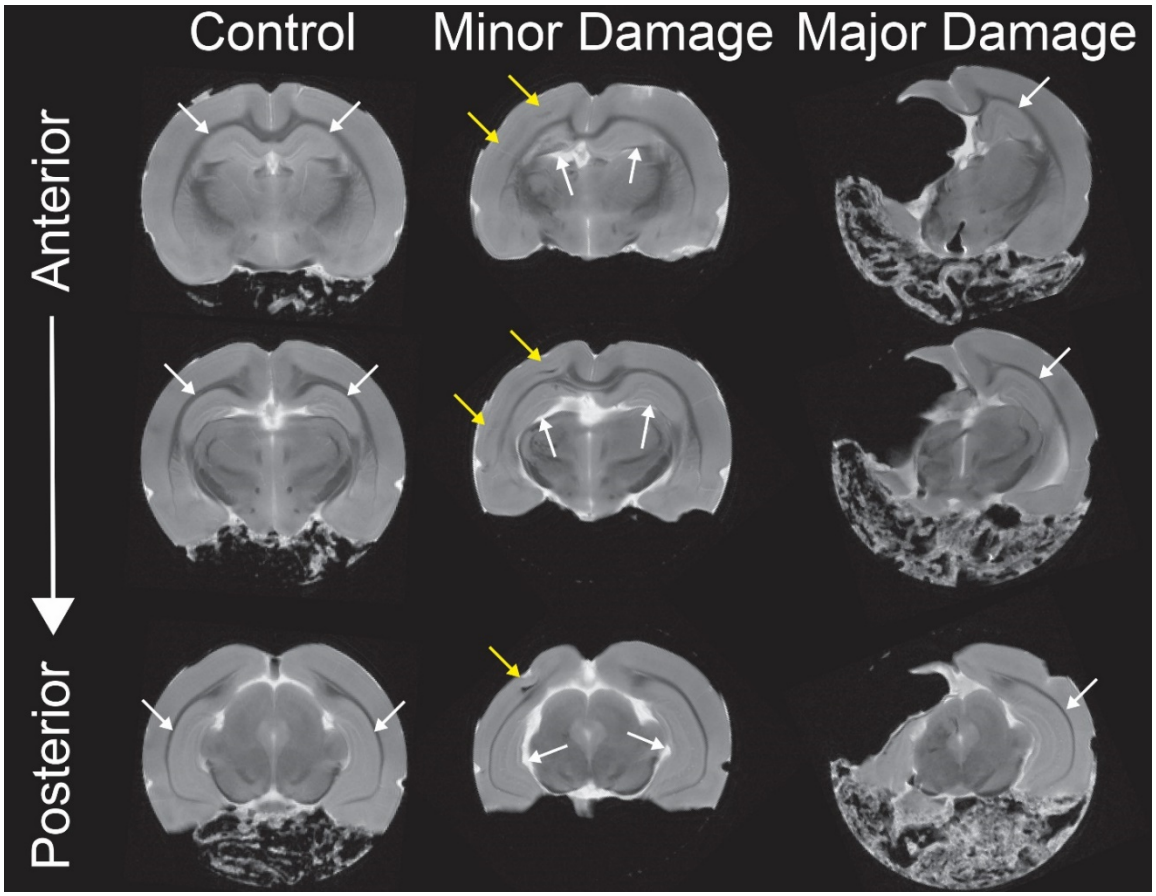

Figure 3.8: Magnetic resonance imaging of the three categories of brain pathologies: sham control, PHI with minor damage, and PHI with major damage. The sham control brains (left column) had normal underlying pathology with no abnormalities or atrophy of the cortical layers, the hippocampi (white arrows), thalamus, and other subcortical structures. The sham control brains were symmetrical between ipsilateral and contralateral hemispheres. PHI brains with minor damage (middle column) had atrophied ipsilateral dorsal hippocampi with relatively preserved ventral hippocampi (white arrows). The ipsilateral cortex showed signs of cellular loss within the middle cortical layers (yellow arrows). The contralateral hippocampi (white arrows) and cortex of the PHI brains with minor damage remained unchanged. PHI brains with major damage (right column) had near complete loss of the ipsilateral hippocampi, cortex, and other subcortical structures. The contralateral hemisphere showed signs of warped but normal looking hippocampi (white arrow), cortex, and subcortical structures.

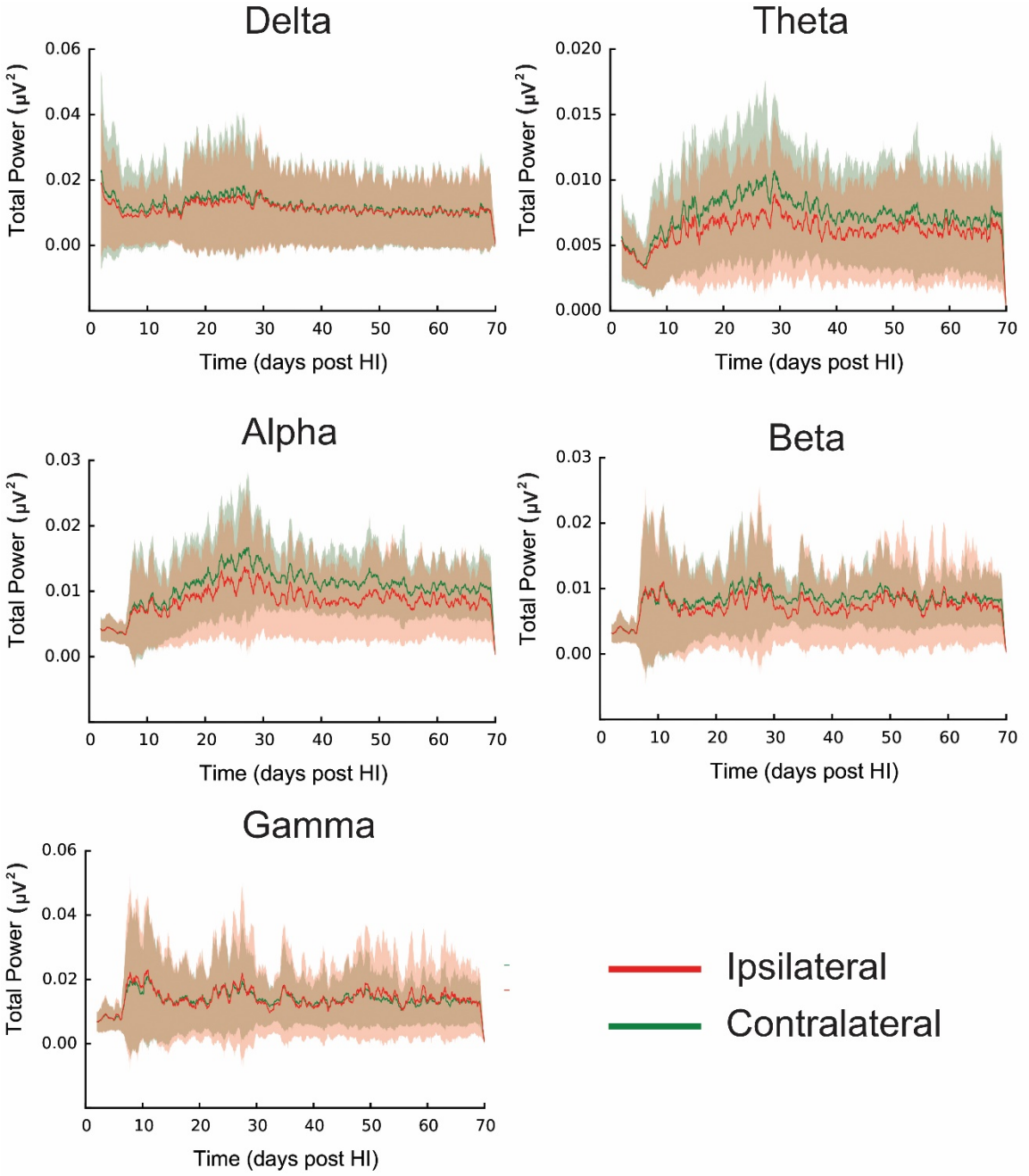

Figure 3.9: Running mean of powers in EEG frequency bands from juvenile to adult for PHI animals with major damage between ipsilateral and contralateral hemispheres. Total power of each EEG frequency band (Delta, Theta, Alpha, Beta, and Gamma) over the course of 70 days starting at the time of transmitter implantation (P8-10). There was no statistically significant difference in the running means between ipsilateral (red) and contralateral (green) hemispheres at any point during the development of the animal for any frequency band. Shaded regions (red and green) are 95% confidence intervals for each respective group.

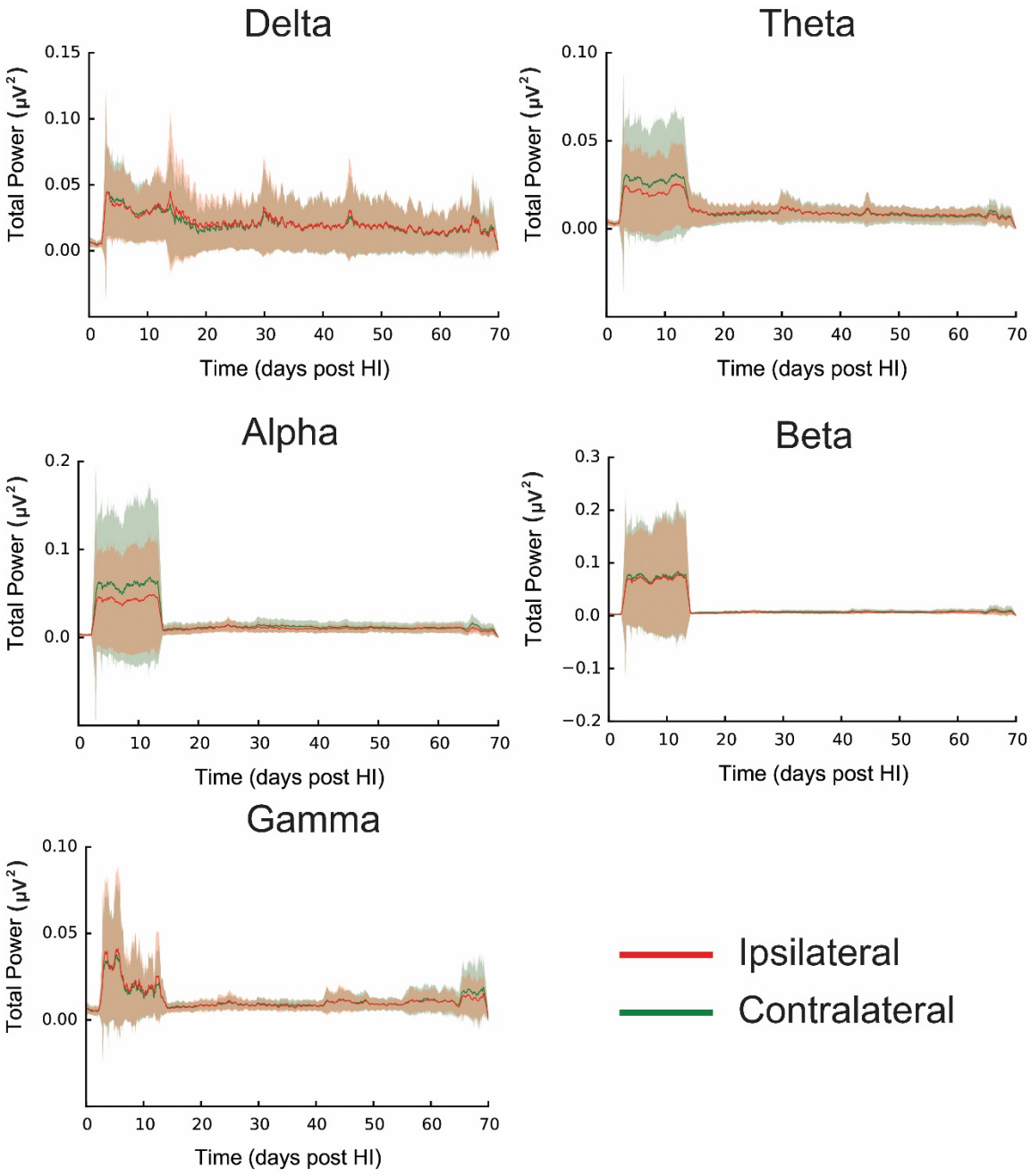

Figure 3.10: Running mean of powers in EEG frequency bands from juvenile to adult for PHI animals with minor damage between ipsilateral and contralateral hemispheres. Total power of each EEG frequency band (Delta, Theta, Alpha, Beta, and Gamma) over the course of 70 days starting at the time of transmitter implantation (P8-10). There was no statistically significant difference in the running means between ipsilateral (red) and contralateral (green) hemispheres at any point during the development of the animal for any frequency band. Shaded regions (red and green) are 95% confidence intervals for each respective group.

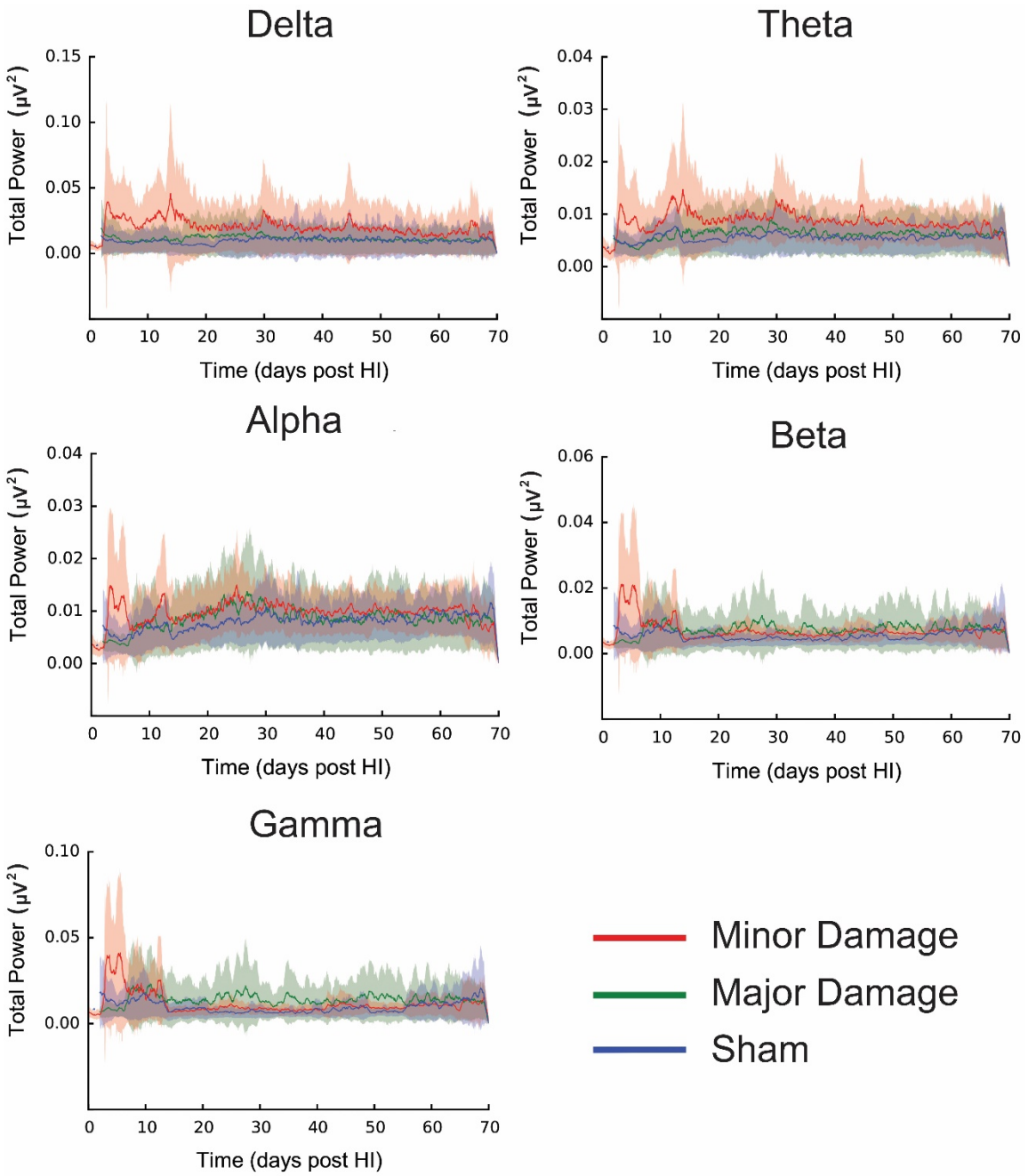

Figure 3.11: Running mean of powers in EEG frequency bands from juvenile to adult for PHI minor damage, PHI major damage, and sham controls. Total power of each EEG frequency band (Delta, Theta, Alpha, Beta, and Gamma) comparing ipsilateral hemispheres over the course of 70 days starting at the time of transmitter implantation (P8-10). There was no statistically significant difference in running means between PHI minor damage (red), PHI major damage (green), and sham controls (blue) at any point during the development of the animal for any frequency band. Shaded regions (red, green, and blue) are 95% confidence intervals for each respective group.

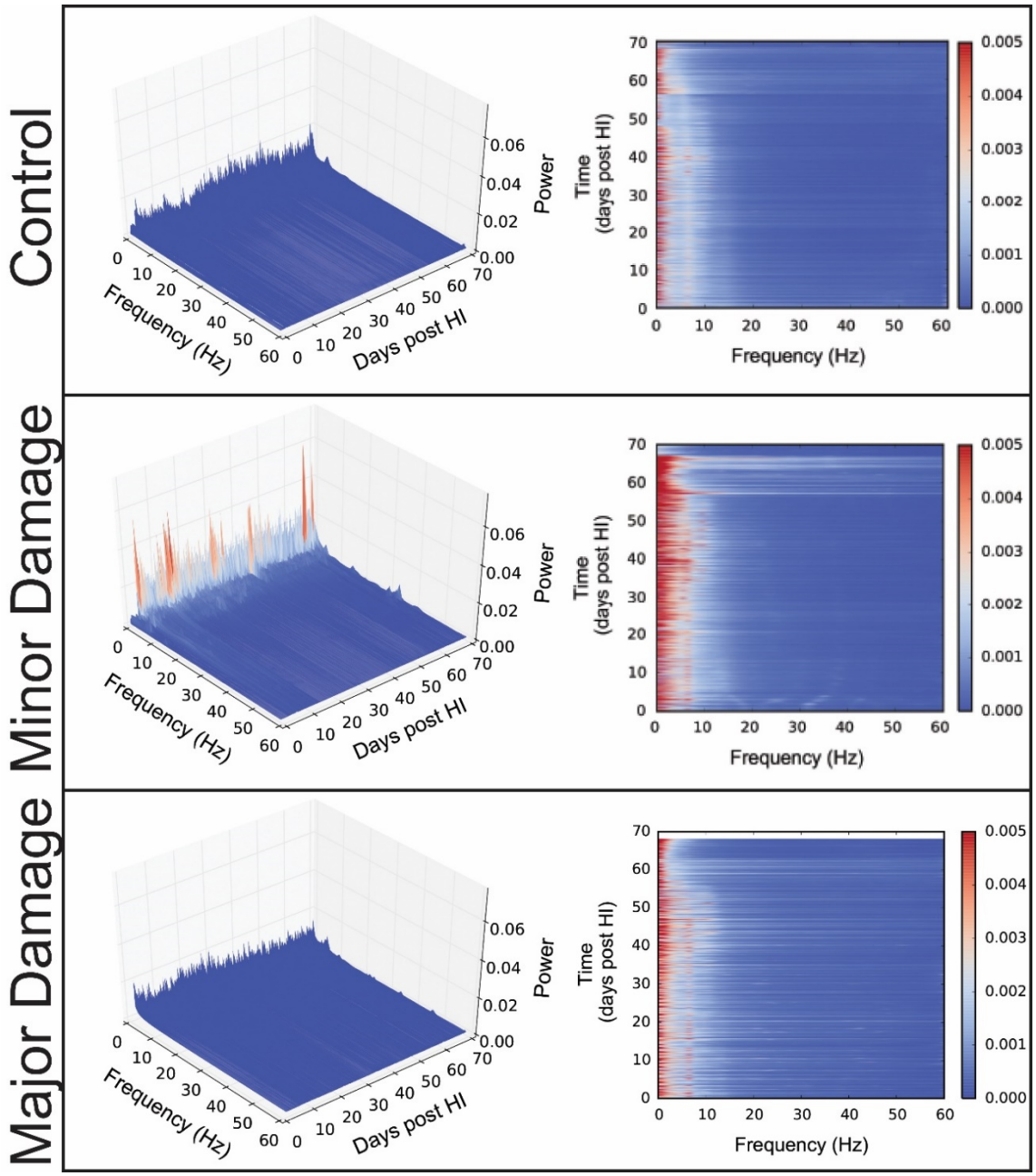

Figure 3.12: : 3D plots and heat maps of mean powers in EEG frequency bands from juvenile to adult for PHI minor damage, PHI major damage, and sham controls. Total power of continuous EEG frequency bands from 1-60 Hz covering Delta, Theta, Alpha, Beta, and Gamma bands. A comparison of ipsilateral hemispheres over the course of 70 days, starting at the time of transmitter implantation (P8-10), showed PHI minor damage (middle column) has a higher power in the 1-10 Hz frequencies compared to sham (left column) and PHI major damage (right column). This is identifiable in the 3D plot (top row) and heat map (bottom row) where a larger percentage of the plots between 1-10 Hz is above 0.02 and 0.004 μv^2, respectively. There was no statistically significant difference between PHI minor damage (middle column), PHI major damage (right column), and sham controls (left column) at any point during the development of the animal for any frequency band.

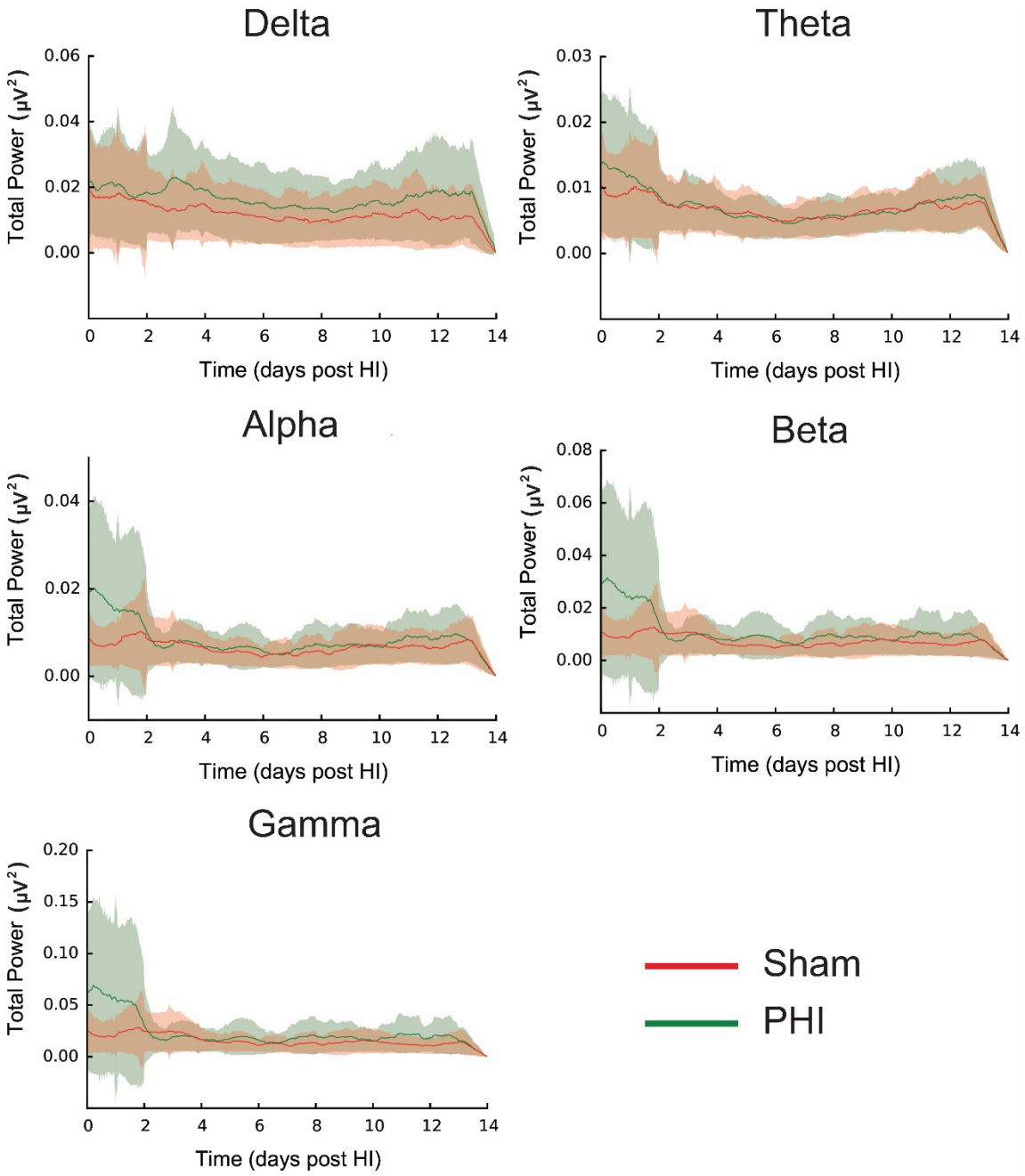

Figure 3.13: Running mean of powers in EEG frequency bands for all PHI animals compared to sham controls at ages P7-21. Total power of each EEG frequency band (Delta, Theta, Alpha, Beta, and Gamma) for the ipsilateral hemispheres over the course of 14 days starting at P7 immediately after PHI-treatment. While there was no significant difference between PHI (green) and sham (red) animals, there was a trend towards an increase in power for Theta, Alpha, Beta, and Gamma bands for the first 2 days following PHI-treatment. Increased sample size is needed to determine any significant difference. Shaded regions (red, and green) are 95% confidence intervals for each respective group.

Table 3.1: All PHI and Sham animals included in the EEG seizure analysis. The following is a list of each animal monitored and analyzed in the seizure detection portion of this paper along with their gender, age of implantation, total number of days monitored, and the age at the end of the recording.

Treatment	sex	Age Implanted	Number of Days Monitored	Age at End of Recording
PHI	male	6	66	72
PHI	female	6	72	78
PHI	male	10	73	83
PHI	male	10	62	72
PHI	female	10	81	91
PHI	male	9	72	81
PHI	male	9	88	97
PHI	female	9	82	91
PHI	female	9	88	97
PHI	male	9	80	89
PHI	male	8	81	90
PHI	male	9	73	82
PHI	male	9	74	83
PHI	male	9	71	80
PHI	female	10	77	87
sham	male	6	73	79
sham	female	10	72	82
sham	female	10	73	83
sham	female	9	81	90
sham	female	9	78	87
sham	male	9	71	80
sham	female	9	85	94
sham	female	9	77	86
sham	male	9	70	79

CHAPTER 4

A NOVEL CASE OF BRIEF, EARLY-ONSET, CONVULSIVE SEIZURES IN AN ANIMAL MODEL OF ACQUIRED EPILEPSY AFTER PERINATAL HYPOXIC-ISCHEMIC ENCEPHALOPATHY

J.D. Bastar[1], M. Lehmkuhle[2], P. Roper[2], F.E. Dudek[2]

Departments of Physiology[1] and Neurosurgery[2]

University of Utah School of Medicine

Salt Lake City, UT

Corresponding Author:

F. Edward Dudek, Ph.D.
Department of Neurosurgery
University of Utah School of Medicine
383 Colorow, Suite 383
Salt Lake City, UT 84108

Email: ed.dudek@hsc.utah.edu

Office phone: (801) 587-5880
FAX: (801) 581-8075
Cell: (970) 690-4022

Abstract

Perinatal hypoxia-ischemia (PHI) predisposes infants to later-in-life neurological deficits, such as impaired cognition, cerebral palsy, and epilepsy. In an animal model of PHI-induced epilepsy, spontaneous recurrent seizures (SRSs) have been reported to begin as early as 2 months postinjury and to be progressive in nature, steadily becoming more frequent and severe as the rat ages. These seizures routinely last 35-100 sec; convulsive seizures are usually slightly longer than the nonconvulsive seizures. In the process of further characterization of the latent period between injury and SRS in the PHI model, a new phenotype of short-lasting *convulsive* seizure was present in a single animal. A 2-channel miniature wireless telemetry device was implanted in neonatal rat pups at postnatal day 6 (P6) prior to induction of PHI at P7 using the Rice-Vannucci model. A single rat pup (n=1 out of a total n=15 HI-treated rats) with the novel short-duration seizures was monitored continuously with video-EEG while simultaneously being reared by its dam. At P21, the animal was weaned and video-EEG monitoring continued for a total of 72 days. Blinded analysis of the EEG was done partially (50%) with a custom-written computer algorithm based on auto-correlation, and partially (50%) by manual visual inspection. Typical Racine grade 3 seizures exhibiting immobility with forelimb clonus and lordotic posturing were detected by the custom-written computer algorithm prior to 3 months of age. Electrographic activity consisted of a large-amplitude sentinel spike, indicating onset of the seizure, followed by rhythmic spiking activity that increased in amplitude during the seizure, before ending in a period of post-ictal depression. Prior to 2 months of age, seizures were commonly found lasting <10 sec, within a single animal. The middle portion of the seizure consisted of a few repetitive bilateral high-amplitude spikes followed by low-amplitude synchronous spike activity predominantly on the ipsilateral side. There was no discernable post-ictal phase at the end of the seizure. Although short in duration, these seizures were not similar to traditional spike-and-wave discharges (i.e., absence seizures). All of the brief seizures were *convulsive* with corresponding electrographic activity that was a shorter version of the longer seizures. SRSs have been recorded in a variety of animal models of acquired epilepsy using chemoconvulsants, traumatic brain injury, and PHI. A similar phenotype of seizures present in all these models involves convulsive seizures lasting >20

sec. The single animal in this study is the first animal we have discovered in any model of acquired epilepsy to have brief convulsive seizures lasting <10 sec. Because the convulsive component was also <10 sec in duration, these brief seizures were unlikely to be an artefact derived from the seizure occurring at a remote site. Although this is an n=1, this distinctive seizure phenotype is a novel finding that illustrates that brief convulsive seizures are at least possible, even though these events appear to be a rare occurrence.

Introduction

Epilepsy afflicts nearly 1% of the world's population, and is characterized by the occurrence of spontaneous recurrent seizures (SRSs) (Duncan et al., 2006). A large number of these patients, roughly 30%, suffer medically intractable seizures (Duncan et al., 2006). Animal models, although imperfect, offer the best opportunities to develop potential pharmaceutical and therapeutic treatments to treat this population. However, a large limitation with animal models of acquired epilepsy is that there needs to be proper characterization of the SRSs that develop following an injury.

Within the experimental side of epilepsy, there is an ongoing debate involving what is and is not an appropriate seizure for the type of epilepsy being modeled (D'Ambrosio and Miller, 2010; Dudek and Bertram, 2010). While it has been suggested that "the practice of defining away experimental seizures that have subtle behavioral manifestations or short duration may significantly hamper the development of better treatments" (D'Ambrosio and Miller, 2010), we disagree and believe that intense scrutiny should be in place for experimental models of epilepsy. An incorrectly identified model of epilepsy would be misleading and waste research resources.

Using an animal model based on perinatal hypoxic-ischemic (PHI) encephalopathy, a translationally relevant model of pediatric stroke-induced epilepsy (Kadam and Dudek, 2007), we identified a previously undescribed type of convulsive seizure with an unusually brief duration. Even though it has been suggested before that short-duration electrographic seizures in experimental models should be considered seizures, these specific examples have a mild behavioral correlate (D'Ambrosio et al., 2009), and recent studies show that they are present in

control animals. Although the seizures in this study were brief, almost all of them were accompanied by convulsive behavioral.

Methods

Animals

All surgical procedures were performed under protocols approved by the University of Utah Animal Care and Use Committee. Pregnant Sprague-Dawley adult female rats (14 days gestation) were received from Charles River (Wilmington, MA). Pups were born in the animal facility ~1 week after the arrival of the pregnant female (University of Utah, Salt Lake City, UT). The litter size was culled to 8 pups at P3. Animals were housed with the dam and littermates, and at P7, they were treated with HI. The weight of the pup at the time of treatment was 16-18 g. Due to high mortality rates with early transmitter implantation, pups were implanted at P8-10 to allow for an adequate increase in body weight to compensate for transmitter weight. At the time of transmitter implantation, the litter was further culled to a total of 4 pups to enhance survival of the implanted pup. Environmental enrichment items such as a block of wood were added to the cage to occupy the dam's desire to chew and entice her away from chewing the transmitter.

Perinatal HI

To model human neonatal hypoxic-ischemic encephalopathic cortical infarcts, the modified Levine's method (Levine, 1960; Rice et al., 1981) was performed on P7 rat pups. Both male and female rat pups 7 days of age were anesthetized with 2-4% isoflurane. The ventral cervical region was aseptically prepared with betadine scrub and the ventral midline infused with bupivacaine (0.5%, 0.25 ml). A 1-cm midline incision was made over the trachea, and the right carotid artery isolated and permanently ligated with a cautery pen. The incision was closed with 4-0 vicryl suture and the pup was allowed to recover for 2 hr with the dam and littermates. Age-matched sham controls had the carotid artery exposed under identical procedures but not ligated.

After a 2-hr recovery period, the rat pups with the ligated carotid artery were placed into an air-tight temperature and humidity controlled chamber. They were subjected to hypoxia

(humidified 8% oxygen, balanced nitrogen) and maintained at 37 °C for 2 hr, and then allowed to recover in normal air before being returned to the dam and littermates. Age-matched sham-operated controls were placed into a separate air-tight temperature (37 °C) and humidity controlled chamber for 2 hr, but did not receive hypoxic conditions.

Telemetry Unit Implantation

Pups were housed and reared with the dam and implanted at 8-10 days of age with a 2-channel miniature wireless telemetry device. During this procedure, animals were anesthetized with 2-4% isoflurane, and placed onto a water-circulating heating pad on a stereotaxic unit. The stereotaxic unit was sprayed with 70% alcohol, and surgical tools were sterilized by autoclaving and maintained in 70% ethanol. The rat pup was placed in the stereotaxic unit using small-animal ear bars. The surgical site was prepped with betadine scrub and solution, and the incision site was isolated with sterile surgical drapes. Once the pup was anesthetized, a 0.5 inch incision was made on the top of the head using a scalpel, and the skin was separated using hemostats. Periosteum was removed from the skull, and surface bleeding was cauterized. Three holes were drilled using a 0.7mm burr, one over each bilateral hemisphere at approximately 3 mm caudal to bregma and 2.5 mm lateral to the sagittal suture for the recording electrodes, and one over the cerebellum at approximately 1 mm caudal lambda and along midline for the reference electrode. The electrode wires of the transmitter were trimmed to an adequate length and placed at a target depth of the dura. The transmitter was attached to the skull using a cyanoacrylate adhesive (Loctite 454) with accelerator (Loctite 7452). The skin was then closed with Vicryl 4-0 around the implant and cleaned with betadine solution. Animals were treated with local anesthetic and allowed to recover with the dam and littermates.

Data Acquisition and Recording

Animals began 24-hr Video-EEG monitoring immediately after the implantation of the transmitters. The unsexed male and female Sprague Dawley rat pups were housed with their dam and 3 littermates in cages under a 12 hr light/dark cycle (6:00am – 6:00 pm), until the age at

which they could be weaned and individually housed. The transmitters (three Platinum-Iridium alloy electrodes) have two channels referenced to a common electrode. EEG is transmitted wirelessly on a frequency-modulated carrier centered at 6 kHz using capacitive coupling to a receiver base situated below the animal's housing. Signals were bandpass filtered (0.1 - 100 Hz, 8 dB per octave), amplified (2000x gain), digitized at 500 Hz per channel (BIOPAC MP150, Goleta, CA), and stored on a PC computer using Acqknowledge software version 4.1.1. (BIOPAC). Each animal was simultaneously video monitored with video cameras and IR lighting for the duration of the EEG recording. Video and EEG recordings were time stamped and new recordings were started at 2 hr epochs to maintain temporal congruency. Video was stored on 4-terabyte external desktop hard drives (WD Green).

Grading of Seizures

Behavioral movements associated with electrographic seizures were classified using the Racine scale (grades 1-5) to identify the severity of the motor seizure (Racine, 1975): grade 1, immobility with open eyes and/or “wet-dog shakes” associated with facial automatisms; grade 2, same behaviors as grade 1 with head bobbing; grade 3, forelimb clonus with a lordotic posture; grade 4, continued forelimb clonus with rearing; grade 5, same behavior as grade 4 with falling over from rearing. Electrographic seizure activity associated with no abnormal behavior was classified as a grade 0.

Experimental Design

Unsexed male and female rats were monitored (n=24, 13 male, 11 female). Implantation times were staggered as a result of high mortality when implanted early: 3 rats were implanted at P6, 1 rat was implanted at P8, 14 rats were implanted at P9, and 6 rats were implanted at P10. Of the 24 implanted rats, 9 were randomly selected male and female sham controls, and 15 were randomly selected male and female HI-treated animals all from separate litters. All rats yielded data for the duration of their wireless transmitter’s battery life, which was estimated to be

approximately 2 months. Animals were monitored for an average of 75.8 ± 1.3 d (minimum 62, maximum 88). The total number of video-EEG recording days in this study was 1820.

EEG analysis was blinded, leaving the reviewer without the knowledge of the treatment or the degree of possible brain damage. Seizure detection was performed half by manual visual inspection, half using a custom written computer algorithm based on auto-correlation. Any seizures that were identified by the algorithms were visually confirmed by eye on the EEG and video.

Seizure duration was measured in two ways. Duration of EEG was the length of the spike-wave discharges that was identifiable on EEG. Duration of the behavioral seizure was often longer and encompassed the large amplitude sentinel spike, the space between the large-amplitude sentinel spike to the beginning of the spike-wave activity, and a portion of the right sided slow waves that occur after spike-wave activity. Duration of the behavioral seizure was from the beginning of the seizure activity, always awakening from sleep, until the animal resumed normal movement.

Results

The following results are from the analysis of a single implanted and HI-treated animal (n=1) that exhibited a unique phenotype of seizures previously not described in the literature on animal models of acquired epilepsy.

Anatomical Lesion

The HI insult at P7 produced a profound infarcted lesion in the ipsilateral hemisphere. The ipsilateral hemisphere was intact with no obvious porencephalic cyst. Based on the gross anatomical assessment, the ipsilateral hemisphere of the brain was estimated to be roughly 50% smaller in volume compared to the contralateral hemisphere (Figure 4.1). The core of the lesion was within the perfusion territory of the middle cerebral artery (MCA), with sparing of the cingulate and paracingulate cortices, which are perfused by the anterior cerebral artery (ACA). The size of

the lesion for this animal would be classified as moderate, based on the large amount of hemispheric atrophy, but the absence of complete cellular loss resulting in a cystic cavity.

Magnetic Resonance Imaging

The use of the small animal magnetic resonance imaging (MRI) allowed for the study of the underlying pathology of the cortical layers and the subcortical structures in the intact HI-treated brain. As previously reported in this animal model, cortical dysplasia exists in the form of microgyri, deep laminar cell loss, and cortical layering abnormalities in animals with lesions (Kadam and Dudek, 2016). MRI of this particular animal identified the presence of deep laminar cell loss in the ipsilateral cortex, and the presence of a microgyrus at the border of the infarct and peri-infarct region (Figure 4.2). Marked atrophy was present in the ipsilateral dorsal hippocampus, whereas the ventral hippocampus was spared. Expansion of the ipsilateral lateral ventricle and diffuse cell loss occurred within various subcortical structures, such as the thalamus and the internal capsule (Figure 4.2). The contralateral cortex and subcortical structures were intact with no atrophy or obvious cellular loss.

Seizure Frequency and Severity

Due to the relatively large size of the DSI radiotelemetry transmitters used in previous studies, the earliest time point at which HI-treated animals were known to have electrographic and/or behavioral seizures was 2-3 months of age (Kadam et al., 2010). The animal in this study had its first observable seizure at P32, or 25 days posttreatment. Previous work has shown that the epilepsy in this animal model is progressive in nature, and the seizures often tend to cluster (Kadam et al., 2010). The seizures in this animal did not appear to occur in clusters; instead, the seizures occurred almost every day. From the time of the first observable seizure, 46 days were monitored for seizures until the transmitter battery expired. Of those 46 days, only 6 days were void of any observable seizures. Of the 40 days that had seizures, 32 of them had 2 or more seizures per day, with a maximum of 9 seizures identified in a single day. There was a total n=128 seizures, which were predominantly Racine grade 3 seizures. While the first few seizures

were predominantly nonconvulsive or Racine grade 1, there was a mix of Racine grade 1-4 seizures over the course of the 46 days with a slight pattern of increasing severity and duration. All seizures, both convulsive and nonconvulsive, occurred while the animal was asleep, resulting in the animal rapidly awakening from sleep before initiation of a seizure. Behaviorally, there were 3 nonconvulsive seizures, 6 Racine grade 1, 4 Racine grade 2, 111 Racine grade 3, and 4 Racine grade 4.

Seizure Duration

Seizure durations in this animal were observed to be variable, compared to previous work in this model. We observed two different types of electrographic seizure activity that were both accompanied by convulsive seizures. The first type of electrographic seizure activity consisted of the typical large-amplitude rhythmic spiking activity that lasted 10s of seconds (n = 67) (Figure 3.4). These seizures were all predominantly Racine grades 3-4 and occurred as early as age P34, but became more common as the animal aged. The second type of electrographic seizure activity was a shorter version of the longer seizure (Figure 4.3), lasting 10 sec or less (n = 61), and even as short as 5 sec. These unique, short, convulsive seizures were difficult to identify by visual observation, and were not detected by the auto-detection algorithm. The defining features of these seizures that made them possible to identify were that they generally began with a large-amplitude sentinel spike, and ended with post-ictal large-amplitude slow waves located predominantly in the ipsilateral cortex. These seizures were not always accompanied by spike activity during the middle portion of the seizure. The behavioral component to these short seizures was most commonly Racine grade 3 seizures (80%), but also included Racine grades 1-2 (15%) and nonconvulsive seizures (5%). Approximately half of the observed seizures occurred as brief seizures where both the electrographic and convulsive behavior were $\leq$10 sec long (48%) (Figure 4.4). To see the distribution of durations, we examined epochs from ≤10 sec, 11-20 sec, and >21 sec (Figure 4.5). Of the 128 total seizures, 61 were ≤10 sec, 38 were 11-20 sec, and 29 were >21 sec. The seizures that were ≤10 sec began the earliest, and occurred most frequently.

However, the amount of seizures that occurred as the animal aged seemed to increase at the same rate in all three epochs (Figure 4.5).

Discussion

Previous studies of animal models of acquired epilepsy based on status epilepticus (Williams et al., 2009), perinatal HI (Kadam et al., 2010), and posttraumatic epilepsy (Statler et al., 2009; Kelly et al., 2015) have reported convulsive seizures lasting 10s of seconds (e.g., typically about 25-70 sec). Our study found that not only can an animal model, such as PHI, have typical convulsive seizures lasting >10 sec, but short-duration convulsive seizures are also possible. While this is – to our knowledge – the first report of convulsive seizures lasting <10 sec, we hypothesize that they may occur in other animal models as well. Common methods for data analysis of raw EEG traces involve reviewing large amounts of EEG in a condensed time viewing window. The short seizures in our study evaded detection by the seizure detection computer algorithm and were only detected by manual inspection. Typical seizures seen in most animal models tend to stand out against background activity and artifact amongst other EEG traces (Figure 4.6). However, the short seizures in this study did not do so, and were difficult to identify against other EEG traces (Figure 4.7). Based on this, it is possible that these types of seizures might have gone undetected in other animal models, as they may have previously in this animal model. The inability to detect these seizures can lead to a false interpretation of the duration of the latent period, and the progression of the latent period.

Progression of Epileptogenesis

Our data also support the hypothesis that, at least in this single animal, PHI-induced epilepsy is progressive (Dudek and Staley, 2011). In this particular animal, the first seizures were predominantly nonconvulsive, or Racine grade 1-3, and were virtually all <10 sec. As the animal aged, the seizures progressively became longer. Although short seizures still occurred, the seizures became longer than 20 sec at about P40 (Figure 4.4). Seizures of the three different duration ranges all increased in frequency at a similar rate as the animal became older.

Brief Seizure Durations; due to Occurrence at Remote Locations?

It is possible that the brief electrographic activity is not from short seizures, but rather from seizures occurring at a distant or electrically remote site. However, the behavioral convulsive component to the brief electrographic seizures persisted for the same duration as the electrographic activity, suggesting that the short-duration seizures occurred completely at the site of the recording and were not from a remote site.

Seizure Focal Point

HI-induced lesions are variable in size, but most often include some degree of cellular loss in the cortex, dorsal hippocampus, and thalamus (Figure 4.2). All of these regions could be the site of seizure initiation in the PHI model. EEG recordings with leads over the infarct, peri-infarct region, and ipsilateral hemisphere suggest that the onset of seizures occurs within the peri-infarct region (Kadam et al., 2010). Additionally in the cortex, the formation of polymicro gyri, deep layer cellular loss (Kadam and Dudek, 2007), and a high susceptibility to evoked epileptiform discharges (Kadam and Dudek, 2016) further supports that notion. However, the hippocampus also experiences cellular loss within the dentate gyrus, CA3, and CA1 (Williams et al., 2004) followed by mossy fiber sprouting in the ipsilateral and contralateral hippocampi (Williams et al., 2004; Kadam and Dudek, 2007), a feature commonly associated with epilepsy (Houser, 1992; Dudek and Sutula, 2007; Buckmaster, 2014). In this study, we find that the durations for the electrographic activity was the same duration as the convulsive behavioral component. This implies that the recording electrodes are directly over the seizure onset zone, supporting the notion that the seizure onset is in the cortex, although further studies with simultaneous recordings of cortex and hippocampus are necessary to determine the exact seizure focal point in PHI.

Relevance to the Debate on What is an Appropriate Seizure for a Model of Acquired Epilepsy

Previous controversies about what types of synchronous epileptiform events are actual seizures arising from brain injury (i.e., acquired epilepsy) have focused on brief events that are typically <10-15 sec and have subtle “blank stare” type behaviors (i.e., are nonconvulsive). These events have been seen in the lateral fluid percussion injury model of posttraumatic epilepsy (D’Ambrosio and Miller, 2010), in a model of hypoxia-induced seizures in immature rats (proposed to represent neonatal seizures) (Rakhade et al., 2011), and in a model of hyperthermia-induced seizures also in immature rats (a model of febrile seizures) (Dubé et al., 2006). Whether the electrographic events in these models actually represent bona fide seizures with the characteristics of acquired epilepsy has been the source of considerable debate (Kelly, 2004; Kelly et al., 2006; Dudek and Bertram, 2010; Pearce et al., 2014; Rodgers et al., 2015). The basis for this debate is that the previous reports of brief, nonconvulsive seizures did not adequately consider the possibility that the events were absence seizures, which are genetic in nature, seen in some control rats, and have a duration of <10 sec. However, these possible absence seizures have a different distribution of durations, with the most prominient range of durations only being one to a few seconds (Dubé et al., 2006; Rakhade et al., 2011; Eastman et al., 2015). Importantly, in the present data, the brief seizures (i.e., <10 sec) were almost always *convulsive* in nature. Similar brief convulsive seizures have not been described in the literature, suggesting that at least this particular animal had unique epileptogenic features.

Latent Period for Epileptogenesis

Previous studies using this PHI model have reported estimates of the latent period of approximately 2 months post-HI, although this was based on a relatively small number of animals (Kadam and Dudek, 2007; Kadam et al., 2010). In this study, the only animal with detectable SRSs had a latent period of 25 days, which was substantially shorter than previously reported. On the other hand, seizures were not detected in most of the rats with PHI-induced brain injury, even though Kadam and coworkers (2010) reported that virtually all rats with PHI-induced brain

damage developed epilepsy. It is possible that PHI-treated rats had seizures during the periods that were not analyzed; however, this seems unlikely because the period of monitoring was longer than any of the interseizure or intercluster intervals described by Kadam and coworkers. This observation suggests that either some animals with large PHI-induced brain lesions do not develop epilepsy or that the latent period in the PHI model can be several months. We are inclined to favor the latter possibility, because of the consistent finding by Kadam and coworkers (2010) that all animals with a PHI-induced infarct eventually developed epilepsy.

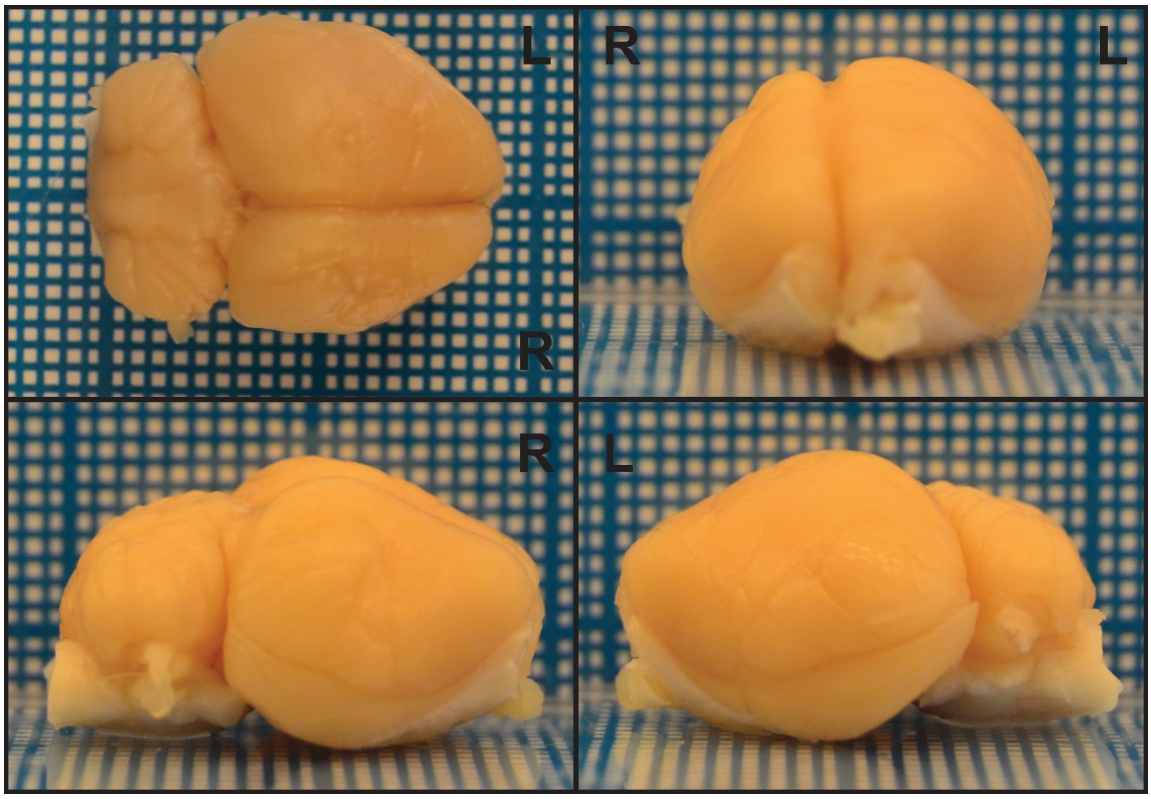

Figure 4.1: Gross anatomical views of the brain from rat subjected to HI at P7. In order to identify the presence of a HI-induced lesion, the brain was examined from the top, front, left side, and right side. What is evident from the top view (top left), and the front view (top right) is that the right hemisphere is greatly atrophied compared to the left hemisphere, with an approximate 50% reduction in volume.

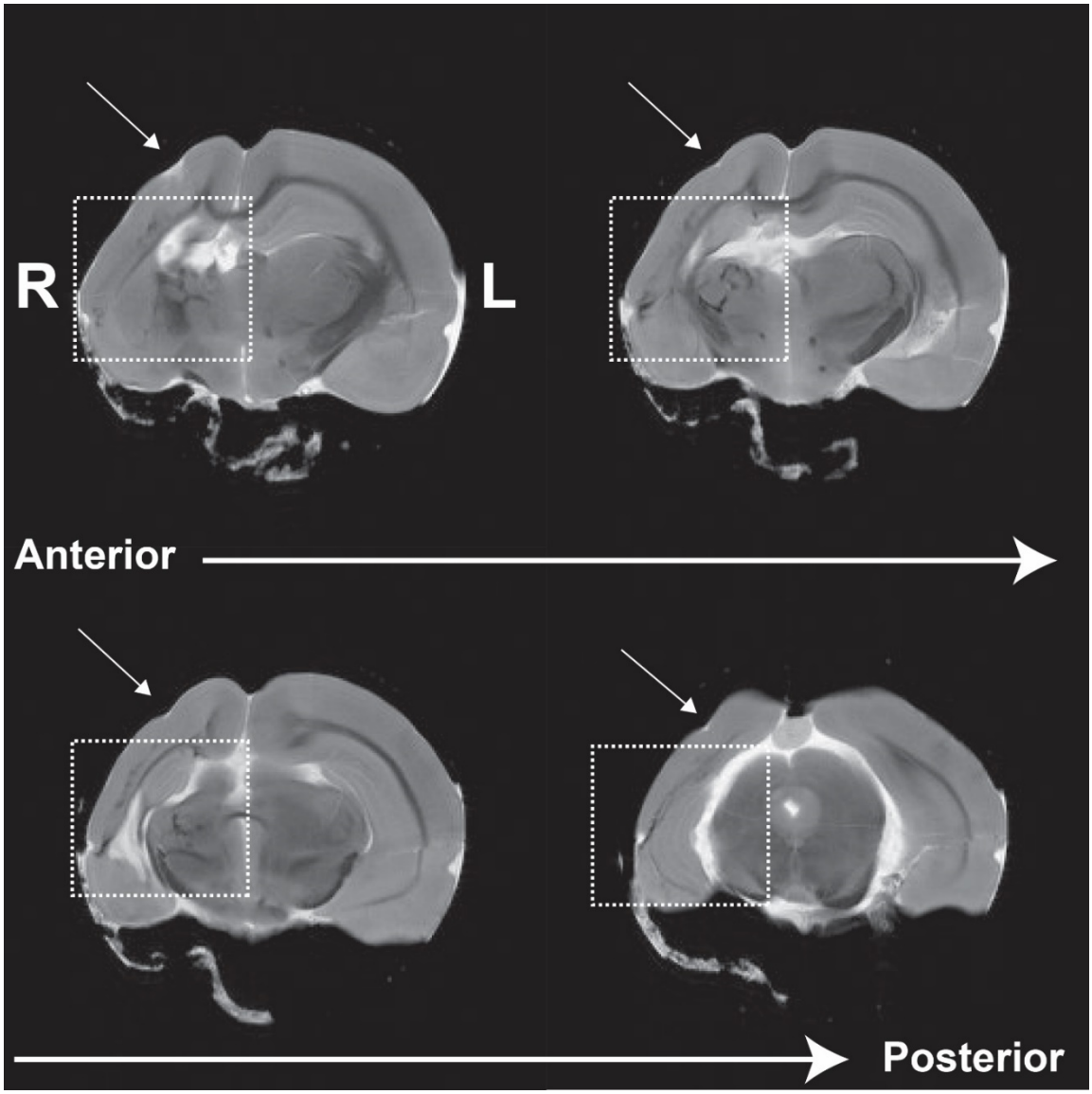

Figure 4.2: Magnetic resonance imaging of the HI-treated brain. MRI was used to identify damage to the cortical layers and subcortical structures, which was difficult to identify on the gross anatomical view. These images are coronal cross sections at four locations along the anterior (top left) to posterior (bottom right) plane. Anatomical abnormalities common to this animal model were identified, such as polymicro-gyri (white arrow), loss of ipsilateral deep cortical layers (white dotted box), and an atrophied ipsilateral dorsal hippocampus (white dotted box).

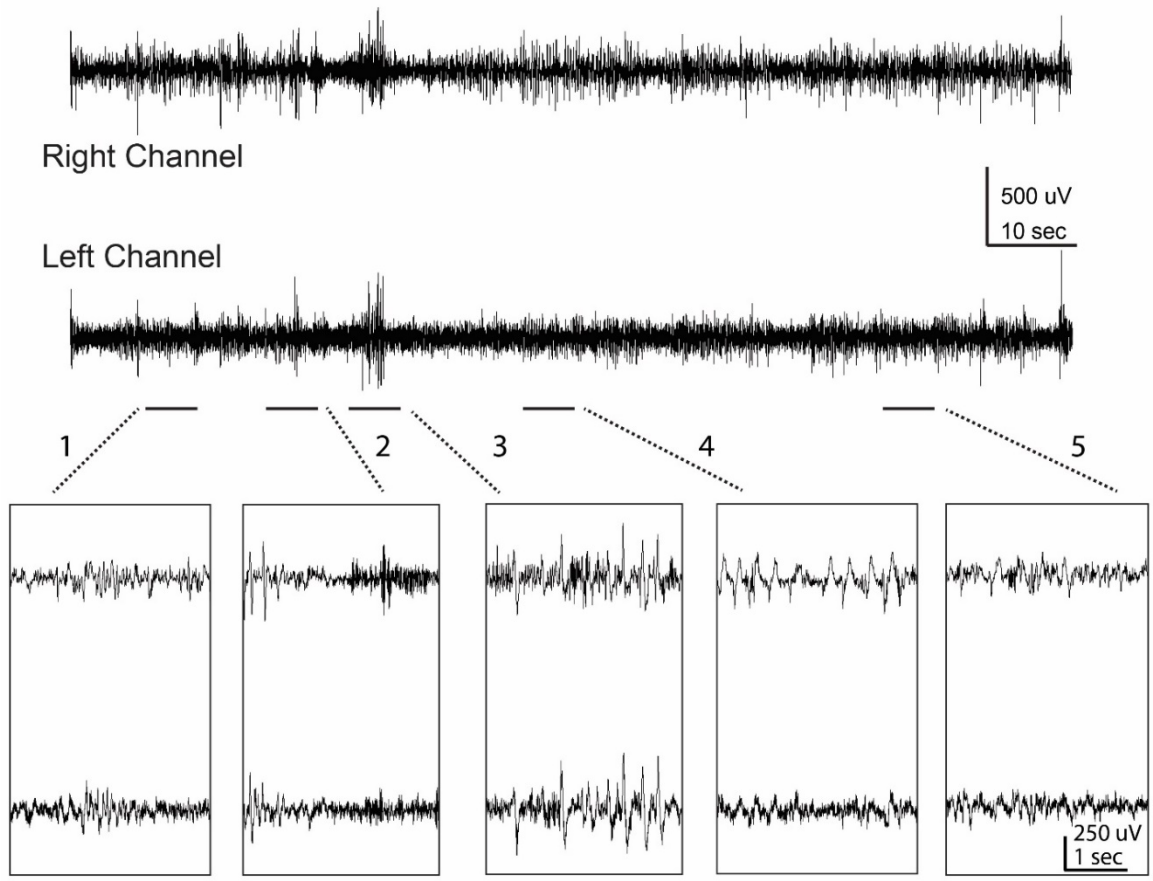

Figure 4.3: Electrographic activity of a uniquely brief spontaneous convulsive seizure in a PHI-treated animal. This type of seizure began as early as 25 days post-HI treatment when the animal was an age of P32 and occurred more frequently than the typical longer duration seizures. These seizures were accompanied with tonic-clonic convulsions, most often as a 3 on the Racine scale and often lasted <10 sec. The electrographic evolution of electrical activity during these short seizures are a similar, but abbreviated, version of the seizures that are typically 10s of seconds. Expansions along the bottom show normal amplitude pre-ictal baseline (1). The onset of the tonic portion of the seizure began with a large-amplitude sentinel spike (2), followed seconds later by the transition to the clonic phase with rhythmic spiking activity that occurred almost simultaneously in each channel (3). Instead of transitioning into large-amplitude, synchronous spiking activity, the seizure ended and the electrographic activity turned into post-ictal high-amplitude slow-wave activity existing predominantly in the ipsilateral right channel (4). At the conclusion of the seizure, the activity returned to normal baseline without a period of post-ictal suppression (5).

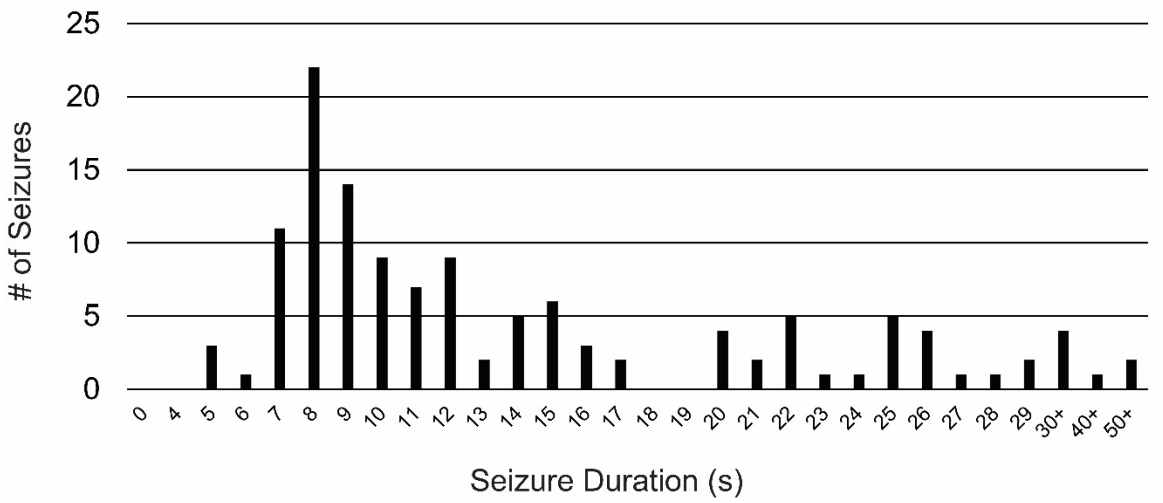

Figure 4.4: Total number of seizures per duration. Between age P32 (when seizures began to occur) and P77 (when the recording stopped), a total of 128 seizures were identified. The distribution of durations ranged from 5 sec to 56 sec. Many of the seizures were <10 sec with the most common seizure duration being 8 sec.

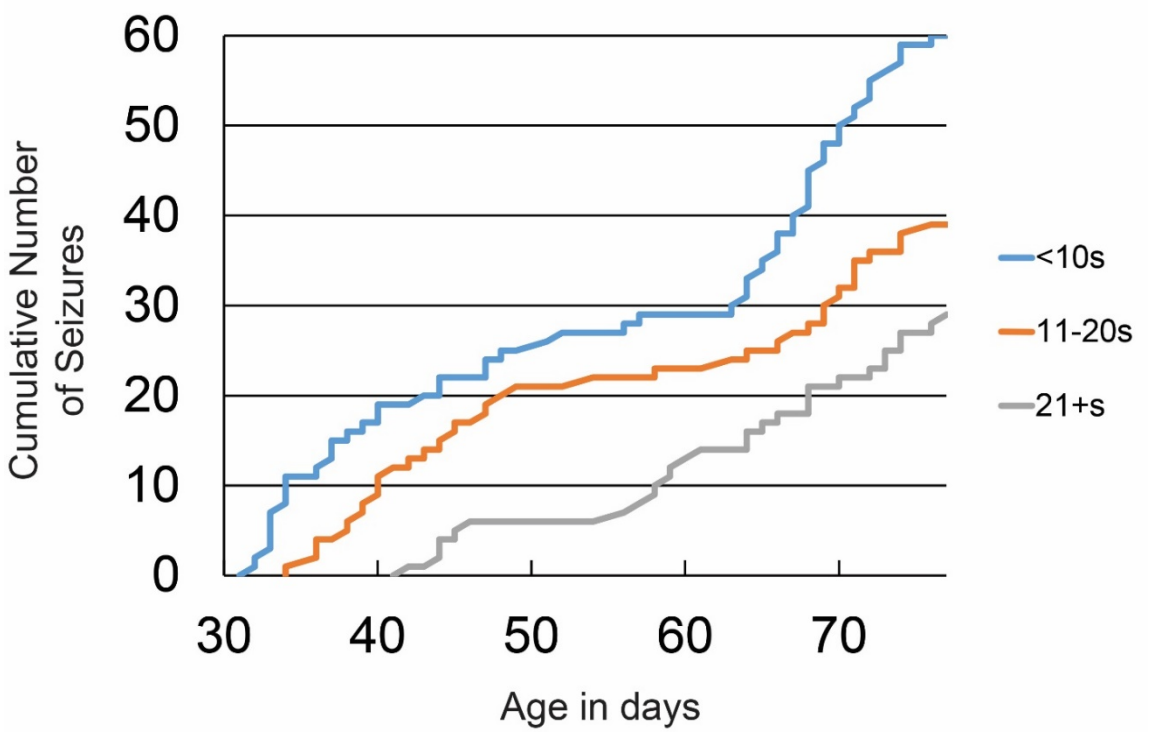

Figure 4.5: Cumulative number of seizures per day plotted in epochs of seizure duration. Breaking down seizure durations into three epochs revealed that most of the seizures were short-duration. Seizures lasting ≤10 sec (blue line) began at P32, and were the most prominent (n=61). Seizures lasting 11-20 sec (orange line) started at P34 and occurred with the second highest frequency (n=38). Seizures lasting >21 sec (grey line) started later at P42 and occurred with the lowest frequency (n=29). The rate at which the frequency of seizures increased was similar across all epochs.

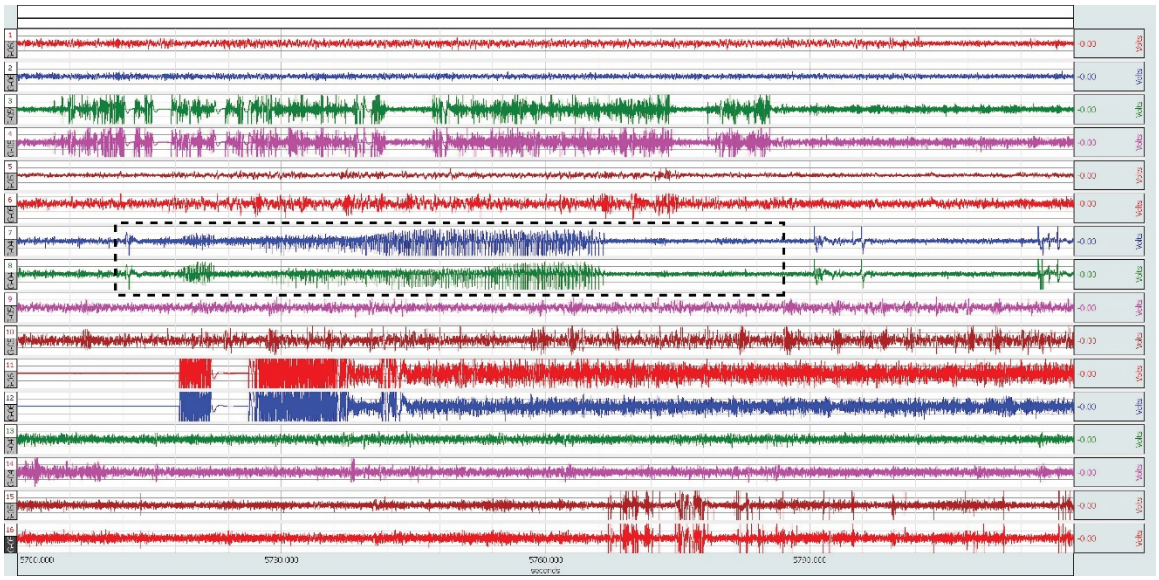

Figure 4.6: EEG trace showing the identification of a typical tonic-clonic seizure from the electrographic activity in the middle of an EEG window. Large-duration electrographic activity that lasts 10s of seconds makes it easier to detect during EEG review. The typical method for reviewing EEG is to set the time scale at 30 sec/division and to scroll through while trying to pick out seizures by eye. The seizure in this trace (black dotted box) is easy to detect against the normal background and other large-amplitude artifact. This demonstrates that these types of seizure are generally the ones that get included into studies of seizure development, which may lead to a false sense of latent period duration.

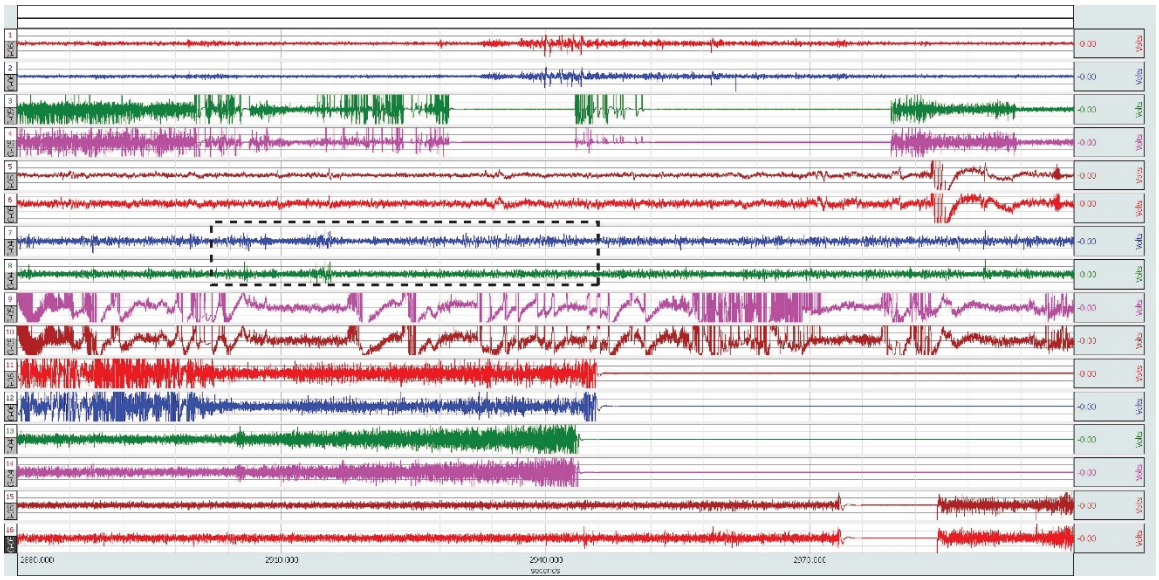

Figure 4.7: EEG trace showing the difficulty of identifying short-duration abbreviated seizures in the middle of an EEG window. The smaller the electrographic activity is for the seizure, the more difficult it is to detect during EEG review. The typical method for reviewing EEG is to set the time scale at 30 sec/division and to scroll through while trying to pick out seizures by eye. The seizure in this trace (black dotted box) is smaller and shorter than most of the artifact. The small amplitude and duration of this particular seizure makes it hard to detect against the normal background. This demonstrates that these types of seizure may go undetected in other animal models leading to a false sense of latent period duration.

CHAPTER 5

DISCUSSION

The Fundamental Problems Addressed by This Research

Clinical, and experimental, observations on the development of posttraumatic epilepsy following an initial injury (stroke, traumatic brain injury, tumor, etc.) identify a seizure-free silent period between the precipitating injury and the onset of the first spontaneous recurrent seizures (SRSs) that is referred to as the latent period. The majority of research on the latent period is performed in adult status epilepticus (SE)-based models of temporal lobe epilepsy, but because mechanisms of epileptogenesis may be very different between the adult population and the pediatric population, it is necessary to have models that study the latent period in the pediatric population. The PHI animal model is a clinically relevant model that mimics the human disease anatomically, and histologically (Kadam and Dudek, 2007). Prior to our study, there were no successfully completed chronic electroencephalographic studies of the latent period in any pediatric model of epilepsy. The numerous limitations and disadvantages of recording in a neonatal rodent prevented these studies from occurring. The development of a wireless 2-channel telemetry EEG device that is small enough and light enough to implant in a neonatal rat allowed for 24-hr continuous video-EEG recording with the dam. Without the development of this technology, it was not possible to record from animals this young, in the presence of the dam, or continuously for 24 hr. The ability to successfully record from the neonatal pup was not solved solely with the development of the miniature wireless EEG telemetry device. There was a lot of troubleshooting that was still needed to improve the tolerance of the dam to the transmitter.

Even though we addressed many questions relating to latent period of epileptogenesis, and anatomical and electrophysiological changes that occur during the latent period, the fundamental problem addressed by this research was in performing chronic long-term EEG studies in immature animals that covered the entirety of the latent period.

The Latent Period and Progressive Epileptogenesis

An issue related to latent periods is whether they exist at all (Sloviter and Bumanglag, 2013; Löscher et al., 2015), implying that seizures continue to occur immediately after the initial injury (Sloviter, 2008; Mazzuferi et al., 2012). Although the evidence for this assumption is based on adult models of temporal lobe epilepsy, we can attempt to address this in our study using the perinatal hypoxic-ischemic (PHI) animal model. As described in Chapter 3 and 4, our results suggest that there is indeed a latent period following PHI. Of the 15 HI-treated animals in our study, only 1 developed epilepsy, starting at P32. Although, we cannot completely rule out seizures in the other animals for the periods that were not analyzed, we can for sure state that none of the HI-treated or sham-treated animals had subacute seizures in the first week of monitoring. Furthermore, complete analysis was done on 3 HI-treated animals and found that for 2 of the animals, there was no evidence of seizures, convulsive or nonconvulsive, for up to 80 days postinjury. Couple this with previous work (Kadam et al., 2010) where only a portion of HI-treated animals had convulsive (n = 2/5), or nonconvulsive (n = 4/5) seizures by 3 months of age, and we have evidence of a variable, but existent, latent period.

With evidence of a variable latent period, we were interested in determining the progressive nature of the latent period. More specifically, are there anatomical and physiological changes that precede the development of SRSs that might be considered mechanisms of epileptogenesis. In Chapter 2, we identified an acute loss of both excitatory and inhibitory synaptic activity that then had a rapid recovery to normal levels 2 weeks later. Immunohistological data confirmed a loss of neurons and interneurons, supporting the reduction in synaptic activity. We were then unable to find any significant difference in synaptic activity at 4 m of age, and no other differences in cortical rhythms in the injured animals. This suggests that the

electrophysiological changes leading to an epileptic network are potentially complete by 2 weeks postinjury. If the changes are complete by 2 weeks postinjury, then why would it take months for seizures to appear? This could be the difference between mechanisms of epileptogenesis, and mechanisms of ictogenesis. While the network is primed early on for being epileptic, there are additional mechanisms that are needed to induce the onset of a seizure, such as further network synchronization or a shift in Cl^- gradient leading to depolarizing effects of GABA (Szabadics et al., 2006). If the cascade leading to posttraumatic epilepsy is complete at such an early time point, then the time frame for preventing epileptogenesis is relatively short. This would have large implications for the need to understand the latent period, and for clinical treatment of injuries that are known to increase the probability of epilepsy. Further evidence for the progressive nature of the latent period is that nonconvulsive seizures commonly precede convulsive seizures in the PHI animal model (Kadam et al., 2010). The presence of nonconvulsive seizures suggests that the mechanisms are in place for epilepsy while the mechanisms of ictogenesis are being enhanced.

Sprouting as the Cause of Epilepsy

The rapid recovery of synaptic activity that may precede the development of SRSs could be a result of axonal sprouting from the remaining neurons and interneurons. This could be an explanation for an epileptogenic, but not ictogenic, mechanism. Historically, axonal sprouting and synaptic reorganization within the hippocampus has been a pathological finding associated with experimental models of temporal lobe epilepsy. In models of chemoconvulsant-induced chronic SRSs, it has been shown that the hippocampus exhibits extensive neuronal loss followed by reorganization in the form of mossy fiber sprouting of dentate granule cells (Buckmaster and Dudek, 1997), as well as sprouting of CA1 pyramidal cell axons (Smith and Dudek, 2001). Inhibitory interneurons also exhibit an increase in sprouting in the hippocampus identified initially as an increase in GABAergic terminal labeling within the dentate gyrus (Thind et al., 2010), and later as fluorescently labeled O-LM inhibitory cells in the CA1 sprouting across the hippocampal fissure and functionally innervating granule cells in the outer molecular layer of the dentate gyrus (Peng et al., 2013). Even in the PHI animal model, Timm staining has revealed mossy fiber

sprouting within the ipsilateral and contralateral hippocampus of epileptic animals (Williams et al., 2004). Evidence of axonal sprouting occurring in cortical layers is nonexistent, potentially due to the difficulty in identifying it, or from the lack of experimental interest. However, if cellular loss can induce sprouting in the hippocampus then it is likely that it can induce sprouting in the cortex, thus warranting future investigation.

Interneurons as Seizure Generators

If axonal sprouting, as a way to maintain basal levels of synaptic activity, is a mechanism of epileptogenesis, then the increased innervation of a greater number of pyramidal neurons by fewer interneurons could be the potential mechanism of ictogenesis (Houser, 2014). The hypothesis being that as a region of cortex dies there will be a loss of both pyramidal neurons and inhibitory interneurons. Since interneurons are local network cells that generally make short distance synaptic connections, an increase in sprouting from them would lead to greater synaptic control of the local network from fewer interneurons than before. Interneurons are the primary generators of hippocampal and cortical rhythms (Freund, 2003; Whittington and Traub, 2003; Klausberger and Somogyi, 2008; Whittington et al., 2011). Therefore, an increase in synaptic connections from fewer interneurons that control the synchronization of hippocampal or cortical rhythms could lead to these regions being the focal onset of ictogenesis. Observed within the hippocampus of epileptic mice, prior to the onset of electrographic seizure activity, there is a progressive increase in the firing rate and synchrony to theta and gamma oscillations from subpopulations of interneurons (Grasse et al., 2013; Toyoda et al., 2015), indicating a potential role of interneurons in the ictogenesis of seizures. Parvalbumin (Pv)-positive interneurons form synaptic connections on the somas of excitatory pyramidal neurons, and have the most control over their firing rate. It has been experimentally shown that activation of Pv interneurons not only causes the postsynaptic inhibition, but induces a postinhibitory rebound spiking in pyramidal neurons leading to ictal generation and increased neuronal synchrony (Sessolo et al., 2015). A secondary mechanisms of ictogenesis from interneurons may be from axo-axonic interneurons that synapse directly on the axon initial segment (AIS), site of action potential generation, in

pyramidal neurons. When the reversal potential for Cl^- is depolarizing, in the event of low density of potassium chloride cotransporter 2 (KCC2) expression in the AIS, axo-axonic interneurons have been shown to be excitatory and capable of initiating action potential events (Szabadics et al., 2006). All of these hypotheses in which interneurons are ictogenic still suggest that interneurons maintain a typical role of providing inhibition and can thus create normal inter-ictal rhythms.

Background Suppression

The presence of background abnormalities in the EEG has been associated clinically with a negative outcome (Amorim et al., 2016; Latal et al., 2016; Topjian et al., 2016; Weitzel et al., 2016). Being able to identify these abnormalities as preceding and predicting the development of epilepsy allows for early detection and the use of a preventative treatment. Experimental work in the PHI animal model both in our lab (unpublished, Zayachkivsky), and a separate lab (Sampath et al., 2014), have identified a reduction in the power of all EEG frequency bands of injured animals immediately after treatment, with some bands (beta and gamma) staying suppressed for up to 3 days later. Neither of these studies did chronic monitoring to determine if the suppression lasted longer than 3 days or if it was predictive of SRSs. In our study, we did chronic monitoring and were able to cover that time frame. We looked for background suppression in our experiments and were unable to find any evidence for background suppression immediately after HI-treatment (Figure 5.1), discussed in Chapter 3. However, although our EEG power analysis does not support the finding of background suppression, our slice electrophysiology data (Chapter 2) does. The reduction in inhibitory and excitatory synaptic activity along with the loss of neurons and interneurons occurs at the same time point as background suppression, and is possibly the underlying pathology. Recovery of delta, theta, and alpha occur within 2 days post-HI, suggesting the initial loss is potentially from depolarization block. However, the question still remains as to whether the background suppression of beta and gamma would fully recover, as our synaptic activity did at 2 weeks post-HI, or would the loss of cells keep it suppressed. To

answer this, we need to return to using a more sensitive technique with differential recording electrodes to improve the signal-to-noise ratio.

Alterations During Sleep

In clinical studies of human epilepsies, it has been observed that spontaneous seizures regularly occur during sleep (Niedermeyer, 1996; Shouse et al., 1996). Aside from the generalized epilepsies, that share a common pathway of initiation with sleep (thalamocortical pathway), the relationship between seizures and sleep is vastly understudied both clinically and experimentally, resulting in very little understanding as to the cause of this relationship. There is data that suggest that seizures are more likely to occur during periods of inactivity (Hellier and Dudek, 1999), and in relation to the circadian regulatory system (Quigg et al., 1998). We found a similar observation in our study. In the animal in our experiments that had seizures, all of the seizures started when the animal was asleep. Abnormalities in the EEG during sleep were not unique to this animal either. The majority of the animals that were later identified as having a lesion, also had occasional differences between hemispheres in EEG frequency and amplitude during REM sleep. These findings suggest that the PHI animal model could be useful in the study of seizures, sleep, and circadian rhythms.

Incidence of Seizures in the PHI Animal Model

Throughout this study, we refer to Kadam et al. (2010), where they found that 100% of the animals that had lesions, and 0% of the animals (sham and HI-treated) that did not, developed SRSs. This finding allows us to correlate brain damage with SRSs and infer that those animals will become epileptic. This is particularly necessary when studying potential mechanisms of epileptogenesis where it is important to do the experiments between the injury and the onset of the first seizure. However, other animal models of posttraumatic epilepsy do not have a similar occurrence of seizures. This is potentially due to the severity of the injury in PHI and the time at which it occurs (early in development). In a population-based study of traumatic brain injury, it was found that the increase in cumulative probability of developing SRSs increased in relation to

the severity of the injury (Annegers et al., 1998). The amount of brain damage that occurs in the PHI animal model can be very severe compared to other animal models. Coupled with the timing of the injury occurring early in development, this leads to a high probability of developing SRSs. Similar, although controversial, rates of epilepsy have been reported in other models of pediatric epilepsy (i.e., hypoxia alone) with less injury (Rakhade et al., 2011).

Future Directions

Paired Electrophysiology Recordings

One hypothesis for the recovery of the synaptic activity in the first 2 weeks post-HI is that it is due to axonal sprouting. Furthermore, there has been no direct empirical evidence indicating axonal sprouting occurs within the cortex. Due to the nature of intra- and interhemispheric neuronal connections in the cortex, immunohistological labeling is not sufficient to detect sprouting. Therefore, we propose using paired recordings from synaptically coupled cortical neurons in the peri-infarct region of PHI-treated animals in acute brain slices. Simultaneously patching neuron-neuron, and interneuron-neuron, pairs would allow us to depolarize the first cell to initiate an action potential that we can measure in the second cell. The amplitude of the response in the second cell will give an indication of the number of synaptic connections on that cell from the primary cell. If the remaining cells in the peri-infarct region are sprouting and forming an increased number of synaptic connections on other cells in the region, then there would be an increase in the amplitude of the stimulated response compared to coupled cells in the sham-treated animals.

Rigorous In-Depth Analysis of EEG Data

In this study, we chose to analyze the chronic EEG data in the most efficient and time effective way possible by selecting portions of the data that were most likely to have seizures. The limitation to this method is that it allows for false negatives in the data. We reduced the possibility of having false negatives as best we could by incorporating a seizure detection algorithm that had a high selectivity of false positives, over 500,000 for 1820 days worth of EEG.

In the conclusion of our EEG study, we are careful to not state that these animals do not have seizures at all, partly because we have not monitored far enough into the chronic period, and partly because we have not analyzed every minute of EEG we collected. Although the likelihood that there are seizures in the remaining unanalyzed data is low, we would like to be certain of this. Therefore, we have plans for follow-up analysis aimed at reviewing every minute of the 1820 days manually. An estimate of the time needed to complete this analysis would be 171 weeks, or 2.3 years (3 EEG days analyzed per day for 5 working days a week). This time can be shortened by reviewing multiple animals at a time, but this will increase the chance of false negatives. If we are able to analyze 4 animals at a time, it will still take approximately 1 year of full-time EEG analysis. Thus, this follow up analysis will take a considerable amount of time.

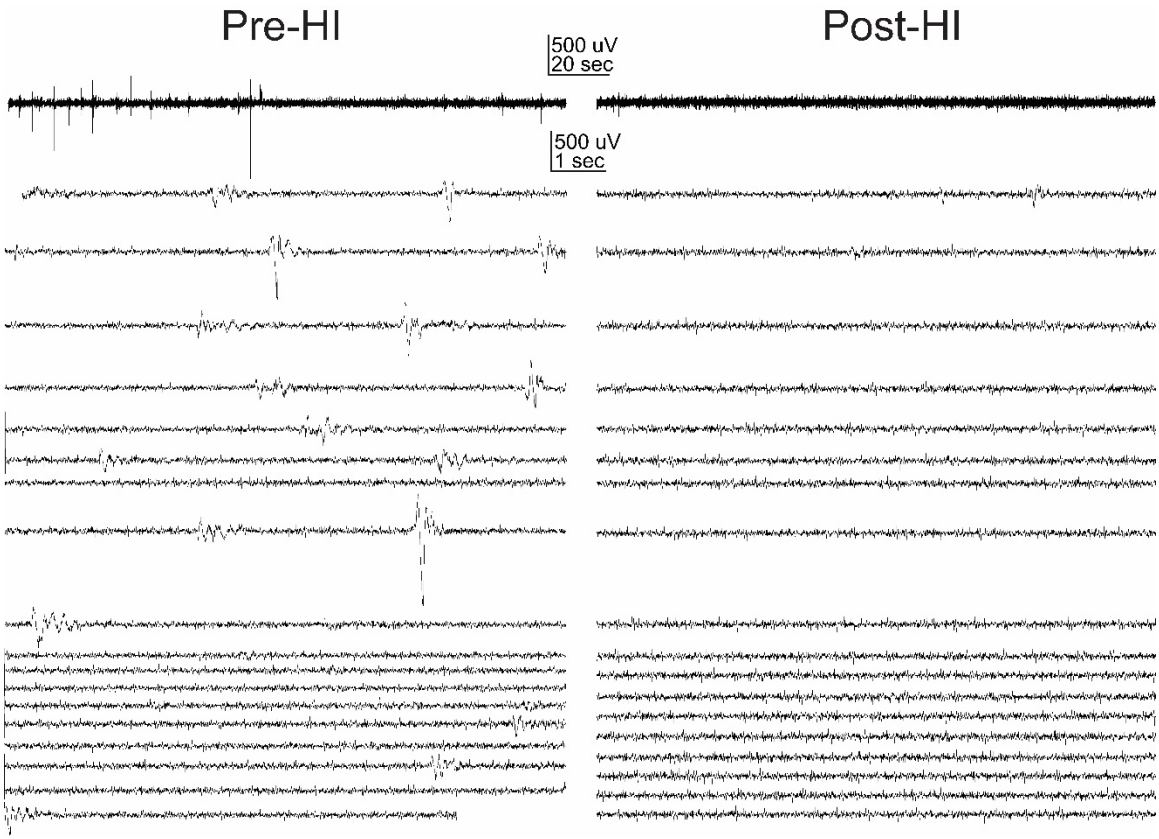

Figure 5.1: Baseline EEG pre- and posttreatment with hypoxia-ischemia. The raw EEG trace of a PHI-treated animal 5 min before the onset of hypoxia (left), and 5 min after the end of hypoxia (right) indicate that there is no obvious difference in the amplitude or frequency of baseline activity. The top single trace is the condensed version of all the traces below it. The spikes in the pre-HI trace are normal activity observed in both pre- and post-HI traces. This individual trace is from the animal that developed spontaneous recurrent seizures.

REFERENCES

van der Aa NE, **Northington FJ**, **Stone BS**, **Groenendaal F**, **Benders MJNL**, **Porro G**, **Yoshida S**, **Mori S**, **de Vries LS**, **Zhang J**. Quantification of white matter injury following neonatal stroke with serial DTI. *Pediatr Res* 73: 756–62, 2013.

Aggarwal M, **Burnsed J**, **Martin LJ**, **Northington FJ**, **Zhang J**. Imaging neurodegeneration in the mouse hippocampus after neonatal hypoxia-ischemia using oscillating gradient diffusion MRI. *Magn Reson Med* 72: 829–840, 2014.

Alkan T, **Kahveci N**, **Buyukuysal L**, **Korfali E**, **Ozluk K**. Neuroprotective effects of MK 801 and hypothermia used alone and in combination in hypoxic-ischemic brain injury in neonatal rats. *Arch Physiol Biochem* 109: 135–44, 2001.

Amorim E, **Rittenberger JC**, **Zheng JJ**, **Westover MB**, **Baldwin ME**, **Callaway CW**, **Popescu A**, **Post Cardiac Arrest Service**. Continuous EEG monitoring enhances multimodal outcome prediction in hypoxic-ischemic brain injury. *Resuscitation* 2016.

Annegers JF, **Hauser WA**, **Coan SP**, **Rocca WA**. A population-based study of seizures after traumatic brain injuries. *N Engl J Med* 338: 20–4, 1998.

Aridas JDS, **Yawno T**, **Sutherland AE**, **Nitsos I**, **Ditchfield M**, **Wong FY**, **Fahey MC**, **Malhotra A**, **Wallace EM**, **Jenkin G**, **Miller SL**. Detecting brain injury in neonatal hypoxic ischemic encephalopathy: Closing the gap between experimental and clinical research. *Exp Neurol* 261: 281–290, 2014.

Beaulieau MJ. Leveteracetam. *Neonatal Netw* 31: 193–199, 2013.

Benjelloun N, **Renolleau S**, **Represa A**. Inflammatory Responses in the Cerebral Cortex After Ischemia in the P7 Neonatal Rat. *Stroke* 30(9) 1916-23 1999.

Binder DK, **Croll SD**, **Gall CM**, **Scharfman HE**. BDNF and epilepsy: Too much of a good thing? *Trends Neurosci* 24: 47–53, 2001.

Björkman ST, **Miller SM**, **Rose SE**. Seizures are associated with brain injury severity in a neonatal model of hypoxia-ischemia. *NSC* 166: 157–167, 2010.

Bollimunta A, **Chen Y**, **Schroeder CE**, **Ding M**. Neuronal mechanisms of cortical alpha oscillations in awake-behaving macaques. *J Neurosci* 28: 9976–88, 2008.

Bollimunta A, **Mo J**, **Schroeder CE**, **Ding M**. Neuronal mechanisms and attentional modulation of corticothalamic α oscillations. *J Neurosci* 31: 4935–43, 2011.

Bona E, **Andersson AL**, **Blomgren K**, **Gilland E**, **Puka-Sundvall M**, **Gustafson K**, **Hagberg H**. Chemokine and inflammatory cell response to hypoxia-ischemia in immature rats. *Pediatr Res* 45: 500–9, 1999.

Brown, T.H., Wong, R.K.S., Prince D. Spontaneous miniature synaptic potentials in hippocampal neurons. *Brain Res* 177: 194–199, 1979.

Brown CE, **Aminoltejari K**, **Erb H**, **Winship IR**, **Murphy TH**. In Vivo Voltage-Sensitive Dye Imaging in Adult Mice Reveals That Somatosensory Maps Lost to Stroke Are Replaced over Weeks by New Structural and Functional Circuits with Prolonged Modes of Activation within Both the Peri-Infarct Zone and Distant Sites. *J Neurosci* 29: 1719–1734, 2009.

Buckmaster PS. Does mossy fiber sprouting give rise to the epileptic state? *Adv Exp Med Biol* 813: 161–8, 2014.

Buckmaster PS, **Dudek FE**. Neuron loss, granule cell axon reorganization, and functional changes in the dentate gyrus of epileptic kainate-treated rats. *J Comp Neurol* 385: 385–404, 1997.

Bumanglag A V, **Sloviter RS**. Minimal latency to hippocampal epileptogenesis and clinical epilepsy after perforant pathway stimulation-induced status epilepticus in awake rats. *J Comp Neurol* 510: 561–80, 2008.

Buzsáki G, **Geisler C**, **Henze DA**, **Wang X-J**. Interneuron Diversity series: Circuit complexity and axon wiring economy of cortical interneurons. *Trends Neurosci* 27: 186–93, 2004.

Buzsáki G, **Wang X-J**. Mechanisms of gamma oscillations. *Annu Rev Neurosci* 35: 203–25, 2012.

Carmichael ST. Plasticity of cortical projections after stroke. *Neuroscientist* 9: 64–75, 2003.

Carmichael ST, **Chesselet M-F**. Synchronous neuronal activity is a signal for axonal sprouting after cortical lesions in the adult. *J Neurosci* 22: 6062–6070, 2002.

Ceccarelli, B., Hurlbut WP. Vesicle Hypothesis of the Release of Quanta of Acetylcholine. *Physiol Rev* 60: 396–441, 1980.

Cheng Y, **Deshmukh M**, **D'Costa A**, **Demaro JA**, **Gidday JM**, **Shah A**, **Sun Y**, **Jacquin MF**, **Johnson EM**, **Holtzman DM**. Caspase inhibitor affords neuroprotection with delayed administration in a rat model of neonatal hypoxic-ischemic brain injury. *J Clin Invest* 101: 1992–1999, 1998.

Clarkson AN, **Huang BS**, **MacIsaac SE**, **Mody I**, **Carmichael ST**. Reducing excessive GABA-mediated tonic inhibition promotes functional recovery after stroke. *Nature* 468: 305–309, 2010.

Cobb SR, **Buhl EH**, **Halasy K**, **Paulsen O**, **Somogyi P**. Synchronization of neuronal activity in hippocampus by individual GABAergic interneurons. *Nature* 378: 75–8, 1995.

Cramer SC. Repairing the human brain after stroke: I. Mechanisms of spontaneous recovery. *Ann Neurol* 63: 272–287, 2008.

Cuaycong M, **Engel M**, **Weinstein SL**, **Salmon E**, **Perlman JM**, **Sunderam S**, **Vannucci SM**. A Novel Approach to the Study of Hypoxia-Ischemia-Induced Clinical and Subclinical Seizures in the Neonatal Rat. *Dev Neurosci* 33: 241–250, 2011.

D'Ambrosio R, **Fairbanks JP**, **Fender JS**, **Born DE**, **Doyle DL**, **Miller JW**. Post-traumatic epilepsy following fluid percussion injury in the rat. *Brain* 127: 304–14, 2004.

D'Ambrosio R, **Hakimian S**, **Stewart T**, **Verley DR**, **Fender JS**, **Eastman CL**, **Sheerin AH**, **Gupta P**, **Diaz-Arrastia R**, **Ojemann J**, **Miller JW**. Functional definition of seizure provides new

insight into post-traumatic epileptogenesis. *Brain* 132: 2805–2821, 2009.

D'Ambrosio R, **Miller JW**. What is an epileptic seizure? Unifying definitions in clinical practice and animal research to develop novel treatments. *Epilepsy Curr* 10: 61–66, 2010.

Danzer SC, **Crooks KRC**, **Lo DC**, **McNamara JO**. Increased Expression of Brain-Derived Neurotrophic Factor Induces Formation of Basal Dendrites and Axonal Branching in Dentate Granule Cells in Hippocampal Explant Cultures. *J Neurosci* 22: 9754–9763, 2002.

Dijkhuizen RM, **Singhal AB**, **Mandeville JB**, **Wu O**, **Halpern EF**, **Finklestein SP**, **Rosen BR**, **Lo EH**. Correlation between brain reorganization, ischemic damage, and neurologic status after transient focal cerebral ischemia in rats: a functional magnetic resonance imaging study. *J Neurosci* 23: 510–517, 2003.

Dubé C, **Richichi C**, **Bender RA**, **Chung G**, **Litt B**, **Baram TZ**. Temporal lobe epilepsy after experimental prolonged febrile seizures: prospective analysis. *Brain* 129: 911–22, 2006.

Dudek FE, **Bertram EH**. Counterpoint to "what is an epileptic seizure?" by D'Ambrosio and Miller. *Epilepsy Curr* 10: 91–4, 2010.

Dudek FE, **Staley KJ**. The time course of acquired epilepsy: implications for therapeutic intervention to suppress epileptogenesis. *Neurosci Lett* 497: 240–6, 2011.

Dudek FE, **Sutula TP**. Epileptogenesis in the dentate gyrus: a critical perspective. *Prog Brain Res* 163: 755–73, 2007.

Duncan JS, **Sander JW**, **Sisodiya SM**, **Walker MC**. Adult epilepsy. *Lancet* 367: 1087–1100, 2006.

Dzhala VI, **Talos DM**, **Sdrulla D a**, **Brumback AC**, **Mathews GC**, **Benke T a**, **Delpire E**, **Jensen FE**, **Staley KJ**. NKCC1 transporter facilitates seizures in the developing brain. *Nat Med* 11: 1205–13, 2005.

Eastman CL, **Fender JS**, **Temkin NR**, **D'Ambrosio R**. Optimized methods for epilepsy therapy development using an etiologically realistic model of focal epilepsy in the rat. *Exp Neurol* 264: 150–62, 2015.

Engel J. Clinical evidence for the progressive nature of epilepsy. *Epilepsy Res Suppl* 12: 9–20, 1996.

Engel J, **Pitkänen A**, **Loeb JA**, **Dudek FE**, **Bertram EH**, **Cole AJ**, **Moshé SL**, **Wiebe S**, **Jensen FE**, **Mody I**, **Nehlig A**, **Vezzani A**. Epilepsy biomarkers. *Epilepsia* 54 Suppl 4: 61–9, 2013.

Fathali N, **Khatibi NH**, **Ostrowski RP**, **Zhang JH**. The evolving landscape of neuroinflammation after neonatal hypoxia-ischemia. *Acta Neurochir Suppl* 111: 93–100, 2011.

Freund TF. Interneuron Diversity series: Rhythm and mood in perisomatic inhibition. *Trends Neurosci* 26: 489–95, 2003.

Fries P. Rhythms for Cognition: Communication through Coherence. *Neuron* 88: 220–35, 2015.
Garcia JH, **Yoshida Y**, **Chen H**, **Li Y**, **Zhang ZG**, **Lian J**, **Chen S**, **Chopp M**. Progression from ischemic injury to infarct following middle cerebral artery occlusion in the rat. *Am J Pathol* 142: 623–35, 1993.

Goffin K, **Nissinen J**, **Van Laere K**, **Pitkänen A**. Cyclicity of spontaneous recurrent seizures in pilocarpine model of temporal lobe epilepsy in rat. *Exp Neurol* 205: 501–5, 2007.

Goldman JE. Lineage, migration, and fate determination of postnatal subventricular zone cells in the mammalian CNS. *J Neurooncol* 24: 61–4, 1995.

Graham EM, **Ruis KA**, **Hartman AL**, **Northington FJ**, **Fox HE**. A systematic review of the role of intrapartum hypoxia- ischemia in the causation of neonatal encephalopathy. *Am J Obstet Gynecol* 199(6): 587–595, 2008.

Grasse DW, **Karunakaran S**, **Moxon KA**. Neuronal synchrony and the transition to spontaneous seizures. *Exp Neurol* 248: 72–84, 2013.

Griesmaier E, **Stock K**, **Medek K**, **Stanika RI**, **Obermair GJ**, **Posod A**, **Wegleiter K**, **Urbanek M**, **Kiechl-Kohlendorfer U**. Levetiracetam increases neonatal hypoxic-ischemic brain injury under normothermic, but not hypothermic conditions. *Brain Res* 1556: 10–18, 2014.

Gunn AJ, **Gunn TR**, **De Haan HH**, **Williams CE**, **Gluckman PD**. Dramatic neuronal rescue with prolonged selective head cooling after ischemia in fetal lambs. *J Clin Invest* 99: 248–256, 1997.

Hadjipanayis A, **Hadjichristodoulou C**, **Youroukos S**. Epilepsy in patients with cerebral palsy. [Online]. *Dev Med Child Neurol* 39: 659–63, 1997.

Hagberg H, **Mallard C**. Effect of inflammation on central nervous system development and vulnerability. *Curr Opin Neurol* 18: 117–123, 2005.

Hauser WA. Seizure disorders: the changes with age. *Epilepsia* 33 Suppl 4: S6-14, 1992.

Heinrich C, **Lähteinen S**, **Suzuki F**, **Anne-Marie L**, **Huber S**, **Häussler U**, **Haas C**, **Larmet Y**, **Castren E**, **Depaulis A**. Increase in BDNF-mediated TrkB signaling promotes epileptogenesis in a mouse model of mesial temporal lobe epilepsy. *Neurobiol Dis* 42: 35–47, 2011.

Hellier JL, **Dudek FE**. Spontaneous motor seizures of rats with kainate-induced epilepsy : effect of time of day and activity state. *Epilepsy Res* 35: 47–57, 1999.

Hellier JL, **Patrylo PR**, **Buckmaster PS**, **Dudek FE**. Recurrent spontaneous motor seizures after repeated low-dose systemic treatment with kainate: assessment of a rat model of temporal lobe epilepsy. *Epilepsy Res* 31: 73–84, 1998.

Holmes GL, **Lombroso CT**. Prognostic value of background patterns in the neonatal EEG. *J Clin Neurophysiol* 10: 323–52, 1993.

Holtzman DM, **Sheldon RA**, **Jaffe W**, **Cheng Y**, **Ferriero DM**. Nerve growth factor protects the neonatal brain against hypoxic-ischemic injury. *Ann Neurol* 39: 114–22, 1996.

Hossain MA, **Fielding KE**, **Trescher WH**, **Ho T**, **Wilson MA**, **Laterra J**. Human FGF-1 gene delivery protects against quinolinate-induced striatal and hippocampal injury in neonatal rats. *Eur J Neurosci* 10: 2490–2499, 1998.

Houser CR. Granule cell dispersion in the dentate gyrus of humans with temporal lobe epilepsy. *Brain Res* 535: 195–204, 1990.

Houser CR. Morphological changes in the dentate gyrus in human temporal lobe epilepsy. *Epilepsy Res Suppl* 7: 223–34, 1992.

Houser CR. Do structural changes in GABA neurons give rise to the epileptic state? *Adv Exp Med Biol* 813: 151–60, 2014.

Jessberger S, **Parent JM**. Epilepsy and Adult Neurogenesis. *Cold Spring Harb Perspect Biol* 7,

2015.

Jin K, **Minami M**, **Lan JQ**, **Mao XO**, **Batteur S**, **Simon RP**, **Greenberg D a**. Neurogenesis in dentate subgranular zone and rostral subventricular zone after focal cerebral ischemia in the rat. *Proc Natl Acad Sci U S A* 98: 4710–4715, 2001.

Johnston M V., **Trescher WH**, **Ishida A**, **Nakajima W**. Novel treatments after experimental brain injury. *Semin Neonatol* 5: 75–86, 2000.

Johnston M V, **Trescher WH**, **Ishida A**, **Nakajima W**. Neurobiology of Hypoxic-Ischemic Injury in the Developing Brain. *Pediatr Res* 49: 735–741, 2001.

Kadam SD, **Dudek FE**. Neuropathogical Features of a Rat Model for Perinatal Hypoxic-Ischemic Encephalopathy with Associated Epilepsy. *J Comp Neurol* 737: 716–737, 2007.

Kadam SD, **Dudek FE**. Temporal Progresion of evoked field potentials in neocortical slices after unilateral hypoxia-ischemia in perinatal rats: correlation with cortical epileptogenesis. *Neuroscience* 316: 232–248, 2016.

Kadam SD, **Mulholland JD**, **McDonald JW**, **Comi a M**. Neurogenesis and neuronal commitment following ischemia in a new mouse model for neonatal stroke. *Brain Res* 1208: 35–45, 2008.

Kadam SD, **Mulholland JD**, **Smith DR**, **Johnston M V**, **Comi AM**. Chronic brain injury and behavioral impairments in a mouse model of term neonatal strokes. *Behav Brain Res* 197: 77–83, 2009.

Kadam SD, **White AM**, **Staley KJ**, **Dudek FE**. Continuous Electroencephalographic Monitoring with Radio-Telemetry in a Rat Model of Perinatal Hypoxia – Ischemia Reveals Progressive Post-Stroke Epilepsy. *J Neurosci* 30: 404–415, 2010.

Kanemoto K, **Kawasaki J**, **Tarao Y**, **Kumaki T**, **Oshima T**, **Kaji R**, **Nishimura M**. Association of partial epilepsy with brain-derived neurotrophic factor (BDNF) gene polymorphisms. *Epilepsy Res* 53: 255–258, 2003.

Katz B, **Miledi R**. Membrane noise produced by acetylcholine. *Nature* 226: 962–3, 1970.

Kawamura M, **Nakajima W**, **Ishida A**, **Ohmura A**, **Miura S**, **Takada G**. Calpain inhibitor MDL 28170 protects hypoxic-ischemic brain injury in neonatal rats by inhibition of both apoptosis and necrosis. *Brain Res* 1037: 59–69, 2005.

Kelly KM. Spike-wave discharges: absence or not, a common finding in common laboratory rats. *Epilepsy Curr* 4: 176–7, 2004.

Kelly KM, **Jukkola PI**, **Kharlamov EA**, **Downey KL**, **McBride JW**, **Strong R**, **Aronowski J**. Long-term video-EEG recordings following transient unilateral middle cerebral and common carotid artery occlusion in Long-Evans rats. *Exp Neurol* 201: 495–506, 2006.

Kelly KM, **Miller ER**, **Lepsveridze E**, **Kharlamov EA**, **Mchedlishvili Z**. Posttraumatic seizures and epilepsy in adult rats after controlled cortical impact. *Epilepsy Res* 117: 104–16, 2015.

Khanna P, **Carmena JM**. Neural oscillations: beta band activity across motor networks. *Curr Opin Neurobiol* 32: 60–7, 2015.

Kharlamov E., **Jukkola P.**, **Schmitt K.**, **Kelly K.** Electrobehavioral characteristics of epileptic rats following photothrombotic brain infarction. *Epilepsy Res* 56: 185–203, 2003.

Kilicdag H, **Daglioglu K**, **Erdogan S**, **Guzel A**, **Sencar L**, **Polat S**, **Zorludemir S**. The role of levetiracetam on neuronal apoptosis in neonatal rat model of hypoxic ischemic brain injury. *Early Hum Dev* 84: 355–360, 2013.

Klausberger T, **Somogyi P**. Neuronal diversity and temporal dynamics: the unity of hippocampal circuit operations. *Science* 321: 53–7, 2008.

Komur M, **Okuyaz C**, **Celik Y**, **Resitoglu B**, **Polat A**, **Balci S**, **Tamer L**, **Erdogan S**, **Beydagi H**. Neuroprotective effect of levetiracetam on hypoxic ischemic brain injury in neonatal rats. *Childs Nev Syst* 30: 1001–1009, 2014.

Kunst MM, **Schaefer PW**. Ischemic stroke. *Radiol Clin North Am* 49: 1–26, 2011.

Kurinczuk JJ, **White-Koning M**, **Badawi N**. Epidemiology of neonatal encephalopathy and hypoxic-ischaemic encephalopathy. *Early Hum Dev* 86: 329–38, 2010.

Kyng KJ, **Skajaa T**, **Kerrn-Jespersen S**, **Andreassen CS**, **Bennedsgaard K**, **Henriksen TB**. A Piglet Model of Neonatal Hypoxic-Ischemic Encephalopathy. *J Vis Exp* : e52454, 2015.

Lai M-C, **Yang S-N**. Perinatal hypoxic-ischemic encephalopathy. *J Biomed Biotechnol* 2011: 609813, 2011.

Latal B, **Wohlrab G**, **Brotschi B**, **Beck I**, **Knirsch W**, **Bernet V**. Postoperative Amplitude-Integrated Electroencephalography Predicts Four-Year Neurodevelopmental Outcome in Children with Complex Congenital Heart Disease. *J. Pediatr.* 16:30416-4 2016.

Lee J, **Duan W**, **Mattson MP**. Evidence that brain-derived neurotrophic factor is required for basal neurogenesis and mediates, in part, the enhancement of neurogenesis by dietary restriction in the hippocampus of adult mice. *J Neurochem* 82: 1367–1375, 2002.

Legido A, **Clancy RR**, **Berman PH**, **Legido A**, **Clancy RR**, **Berman PH**. NeurologicOutcomeAfter Electroencephalographicafly Proven Neonatal Seizures. *Pediatrics* 88, 1991.

Levine S. Anoxic-ischemic encephalopathy in rats. *Am J Pathol* 36: 1–17, 1960.

Levison SW, **Rothstein RP**, **Romanko MJ**, **Synder MJ**, **Meyers RL**, **Vannucci SJ**. Hypoxia / Ischemia Depletes the Rat Perinatal Subventricular Zone of Oligodendrocytes Progenitors and Neural stem Cells. *Dev Neurosci* 23: 234–247, 2001.

Lim DA, **Alvarez-Buylla A**. The Adult Ventricular-Subventricular Zone (V-SVZ) and Olfactory Bulb (OB) Neurogenesis. *Cold Spring Harb Perspect Biol* 8, 2016.

Lippman-Bell JJ, **Rakhade SN**, **Klein PM**, **Obeid M**, **Jackson MC**, **Joseph A**, **Jensen FE**. AMPA Receptor antagonist NBQX attenuates later-life epileptic seizures and autistic-like social deficits following neonatal seizures. *Epilepsia* 54: 1922–1932, 2013.

Liu D, **Smith CL**, **Barone FC**, **Ellison JA**, **Lysko PG**, **Li K**, **Simpson IA**. Astrocytic demise precedes delayed neuronal death in focal ischemic rat brain. *Brain Res Mol Brain Res* 68: 29–41, 1999.

Lodygensky GA, **Inder TE**, **Neil JJ**. Application of magnetic resonance imaging in animal models of perinatal hypoxic-ischemic cerebral injury. *Int J Dev Neurosci* 26: 13–25, 2008.

Lois C, **Alvarez-Buylla a**. Proliferating subventricular zone cells in the adult mammalian forebrain can differentiate into neurons and glia. *Proc Natl Acad Sci U S A* 90: 2074–2077, 1993.

Löscher W, **Hirsch LJ**, **Schmidt D**. The enigma of the latent period in the development of symptomatic acquired epilepsy - Traditional view versus new concepts. *Epilepsy Behav* 52: 78–92, 2015.

Lukaszevicz A-C, **Sampaïo N**, **Guégan C**, **Benchoua A**, **Couriaud C**, **Chevalier E**, **Sola B**, **Lacombe P**, **Onténiente B**. High sensitivity of protoplasmic cortical astroglia to focal ischemia. *J Cereb Blood Flow Metab* 22: 289–298, 2002.

Luskin MB. Restricted proliferation and migration of postnatally generated neurons derived from the forebrain subventricular zone. *Neuron* 11: 173–189, 1993.

Maiese K, **Chong ZZ**, **Li F**, **Shang YC**. Erythropoietin: Elucidating new cellular targets that broaden therapeutic strategies. *Prog Neurobiol* 85: 194–213, 2008.

Mazzuferi M, **Kumar G**, **Rospo C**, **Kaminski RM**. Rapid epileptogenesis in the mouse pilocarpine model: video-EEG, pharmacokinetic and histopathological characterization. *Exp Neurol* 238: 156–67, 2012.

Miura S, **Ishida A**, **Nakajima W**, **Ohmura A**, **Kawamura M**, **Takada G**. Intraventricular ascorbic acid administration decreases hypoxic-ischemic brain injury in newborn rats. *Brain Res* 1095: 159–166, 2006.

Napieralski JA, **Butler AK**, **Chesselet MF**. Anatomical and functional evidence for lesion-specific sprouting of corticostriatal input in the adult rat. *J Comp Neurol* 373: 484–97, 1996.

Nawashiro H, **Brenner M**, **Fukui S**, **Shima K**, **Hallenbeck JM**. High susceptibility to cerebral ischemia in GFAP-null mice. *J Cereb Blood Flow Metab* 20: 1040–1044, 2000.

Ndode-Ekane XE, **Pitkänen A**. Urokinase-type plasminogen activator receptor modulates epileptogenesis in mouse model of temporal lobe epilepsy. *Mol Neurobiol* 47: 914–37, 2013.

Neumann H, **Kotter MR**, **Franklin RJM**. Debris clearance by microglia: An essential link between degeneration and regeneration. *Brain* 132: 288–295, 2009.

Neumann J, **Gunzer M**, **Gutzeit HO**, **Ullrich O**, **Reymann KG**, **Dinkel K**. Microglia provide neuroprotection after ischemia. *FASEB J* 20: 714–716, 2006.

Niedermeyer E. Primary (idiopathic) generalized epilepsy and underlying mechanisms. *Clin Electroencephalogr* 27: 1–21, 1996.

Noh M-R, **Kim SK**, **Sun W**, **Park SK**, **Choi HC**, **Lim JH**, **Kim IH**, **Kim H**, **Eun B-L**. Neuroprotective effect of topiramate on hypoxic ischemic brain injury in neonatal rats. *Exp Neurol* 201: 470–478, 2006.

Nusser Z. MINI-REVIEW A new approach to estimate the number , density and variability of receptors at central synapses. *Eur J Neurosci* 11: 745–752, 1999.

Ohmura A, **Nakajima W**, **Ishida A**, **Yasuoka N**, **Kawamura M**, **Miura S**, **Takada G**. Prolonged hypothermia protects neonatal rat brain against hypoxic-ischemia by reducing both apoptosis and necrosis. *Brain Dev* 27: 517–526, 2005.

Ong J, **Plane JM**, **Parent JM**, **Silverstein FS**. Hypoxic-Ischemic Injury Stimulates Subventricular Zone Proliferation and Neurogenesis in the Neonatal Rat. *Pediatr Res* 58: 600–606, 2005.

Parent JM, **Vexler ZS**, **Gong C**, **Derugin N**, **Ferriero DM**. Rat forebrain neurogenesis and striatal neuron replacement after focal stroke. *Ann Neurol* 52: 802–813, 2002.

Parent JM, **Yu TW**, **Leibowitz RT**, **Geschwind DH**, **Sloviter RS**, **Lowenstein DH**. Dentate granule cell neurogenesis is increased by seizures and contributes to aberrant network reorganization in the adult rat hippocampus. *J Neurosci* 17: 3727–3738, 1997.

Pearce PS, **Friedman D**, **Lafrancois JJ**, **Iyengar SS**, **Fenton AA**, **Maclusky NJ**, **Scharfman HE**. Spike-wave discharges in adult Sprague-Dawley rats and their implications for animal models of temporal lobe epilepsy. *Epilepsy Behav* 32: 121–31, 2014.

Pearl PL, **Carrazana EJ**, **Holmes GL**. The Landau-Kleffner Syndrome. *Epilepsy Curr* 1: 39–45, 2001.

Peng J, **Li R**, **Arora N**, **Lau M**, **Wu C**, **Eubanks JH**, **Zhang L**. Effects of neonatal hypoxic-ischemic episodes on late seizure outcomes in C57 black mice. *Epilepsy Res* 111: 142–149, 2015.

Peng Z, **Zhang N**, **Wei W**, **Huang CS**, **Cetina Y**, **Otis TS**, **Houser CR**. A reorganized GABAergic circuit in a model of epilepsy: evidence from optogenetic labeling and stimulation of somatostatin interneurons. *J Neurosci* 33: 14392–405, 2013.

Perlman JM. Summary proceedings from the neurology group on hypoxic-ischemic encephalopathy. *Pediatrics* 117: S28-33, 2006.

Pisani F, **Orsini M**, **Braibanti S**, **Copioli C**, **Sisti L**, **Turco EC**. Development of epilepsy in newborns with moderate hypoxic-ischemic encephalopathy and neonatal seizures. *Brain Dev* 31: 64–8, 2009.

Plane JM, **Liu R**, **Wang T-W**, **Silverstein FS**, **Parent JM**. Neonatal hypoxic–ischemic injury increases forebrain subventricular zone neurogenesis in the mouse. *Neurobiol Dis* 16: 585–595, 2004.

Qu X, **Qi D**, **Dong F**, **Wang B**, **Guo R**, **Luo M**, **Yao R**. Quercetin improves hypoxia-ischemia induced cognitive deficits via promoting remyelination in neonatal rat. *Brain Res* 1553: 31–40, 2014.

Quigg M, **Straume M**, **Menaker M**, **Bertram EH**. Temporal Distribution of Partial Seizures : Comparison of an Animal Model with Human Partial Epilepsy. 43(6): 748-55 1999.

Racine RJ. Modification of seizure activity by electrical stimulation: cortical areas. *Electroencephalogr Clin Neurophysiol* 38: 1–12, 1975.

Rakhade SN, **Klein PM**, **Huynh T**, **Hilario-gomez C**, **Kosaras B**, **Rotenberg A**, **Jensen FE**. Development of later life spontaneous seizures in a rodent model of hypoxia-induced neonatal seizures. *Epilepsia* 52: 753–765, 2011.

Rice JE, **Vannucci RC**, **Brierley JB**. The influence of immaturity on hypoxic-ischemic brain damage in the rat. *Ann Neurol* 9: 131–41, 1981.

Rodgers KM, **Dudek FE**, **Barth DS**. Progressive, Seizure-Like, Spike-Wave Discharges Are Common in Both Injured and Uninjured Sprague-Dawley Rats: Implications for the Fluid Percussion Injury Model of Post-Traumatic Epilepsy. *J Neurosci* 35: 9194–204, 2015.

Rojas JJ, **Deniz BF**, **Miguel PM**, **Diaz R**, **Hermel ??rica do Esp??rito Santo**, **Achaval M**, **Netto CA**, **Pereira LO**. Effects of daily environmental enrichment on behavior and dendritic spine density in hippocampus following neonatal hypoxia-ischemia in the rat. *Exp Neurol* 241: 25–33, 2013.

Romijn HJ, **Janszen a W**, **Van den Bogert C**. Permanent increase of immunocytochemical reactivity for gamma-aminobutyric acid (GABA), glutamic acid decarboxylase, mitochondrial enzymes, and glial fibrillary acidic protein in rat cerebral cortex damaged by early postnatal hypoxia-ischemia. *Acta Neuropathol* 87: 612–27, 1994a.

Romijn HJ, **Janszen a W**, **van Marle J**. Quantitative immunofluorescence data suggest a permanently enhanced GAD67/GAD65 ratio in nerve endings in rat cerebral cortex damaged by early postnatal hypoxia-ischemia: a comparison between two computer-assisted procedures for quantification of confocal *Brain Res* 657: 245–57, 1994b.

Ropert N, **Miles R**, **Korn H**. Characteristics of miniature inhibitory postsynaptic currents in CA1 pyramidal neurones of rat hippocampus. *J Physiol* 428: 707–722, 1990.

Rorke LB. Anatomical features of the developing brain implicated in pathogenesis of hypoxic-ischemic injury. *Brain Pathol* 2: 211–21, 1992.

Sampath D, **White AM**, **Raol YH**. Characterization of neonatal seizures in an animal model of hypoxic-ischemic encephalopathy. 55: 985–993, 2014.

Sanches EF, **Arteni N**, **Nicola F**, **Aristimunha D**, **Netto CA**. Sexual dimorphism and brain lateralization impact behavioral and histological outcomes following hypoxia-ischemia in P3 and P7 rats. *Neuroscience* 290: 581–593, 2015.

Scharfman HE. Brain-derived neurotrophic factor and epilepsy--a missing link? *Epilepsy Curr* 5: 83–8, 2005.

Scharfman HE, **Goodman JH**, **Sollas a L**. Granule-like neurons at the hilar/CA3 border after status epilepticus and their synchrony with area CA3 pyramidal cells: functional implications of seizure-induced neurogenesis. *J Neurosci* 20: 6144–6158, 2000.

Schmidt D, **Sillanpää M**. Prevention of Epilepsy: Issues and Innovations. *Curr Neurol Neurosci Rep* 16: 95, 2016.

Schmidt SL, **Dorsett CR**, **Iyengar AK**, **Fröhlich F**. Interaction of Intrinsic and Synaptic Currents Mediate Network Resonance Driven by Layer V Pyramidal Cells. *Cereb. Cortex* Epub 2016.

Semple BD, **Blomgren K**, **Gimlin K**, **Ferriero DM**, **Noble-haeusslein LJ**. Progress in Neurobiology Brain development in rodents and humans : Identifying benchmarks of maturation and vulnerability to injury across species. *Prog Neurobiol* 106–107: 1–16, 2013.

Sen E, **Levison SW**. Astrocytes and developmental white matter disorders. *Ment Retard Dev Disabil Res Rev* 12: 97–104, 2006.

Sessolo M, **Marcon I**, **Bovetti S**, **Losi G**, **Cammarota M**, **Ratto GM**, **Fellin T**, **Carmignoto G**. Parvalbumin-Positive Inhibitory Interneurons Oppose Propagation But Favor Generation of Focal Epileptiform Activity. *J Neurosci* 35: 9544–9557, 2015.

Shaw F-Z. Is spontaneous high-voltage rhythmic spike discharge in Long Evans rats an absence-like seizure activity? *J Neurophysiol* 91: 63–77, 2004.

Shaw F-Z. 7-12 Hz high-voltage rhythmic spike discharges in rats evaluated by antiepileptic drugs and flicker stimulation. *J Neurophysiol* 97: 238–47, 2007.

Sheehan JJ, **Tsirka SE**. Fibrin-modifying serine proteases thrombin, tPA, and plasmin in ischemic stroke: A review. *Glia* 50: 340–350, 2005.

Sheldon R a, **Sedik C**, **Ferriero DM**. Strain-related brain injury in neonatal mice subjected to hypoxia-ischemia. *Brain Res* 810: 114–122, 1998.

Shi C, **Pamer EG**. Monocyte recruitment during infection and inflammation. *Nat Rev Immunol* 11: 762–74, 2011.

Shorvon S, **Guerrini R**. Acute symptomatic seizures--should we retain the term? *Epilepsia* 51: 722–3, 2010.

Shouse MN, **da Silva AM**, **Sammaritano M**. Circadian rhythm, sleep, and epilepsy. *J Clin Neurophysiol* 13: 32–50, 1996.

Silverstein FS, **Ferriero DM**. Off-Label Use of Antiepileptic Drugs for the Treatment of Neonatal Seizures. *Pediatr Neurol* 39: 77–79, 2008.

Sirimanne ES, **Blumberg RM**, **Bossano D**, **Gunning M**, **Edwards AD**, **Gluckman PD**, **Williams CE**. The effect of prolonged modification of cerebral temperature on outcome after hypoxic-ischemic brain injury in the infant rat. *Pediatr Res* 39: 591–7, 1996.

Skoff RP, **Bessert D a.**, **Barks JDE**, **Song D**, **Cerghet M**, **Silverstein FS**. Hypoxic-ischemic injury results in acute disruption of myelin gene expression and death of oligodendroglial precursors in neonatal mice. *Int J Dev Neurosci* 19: 197–208, 2001.

Sloviter RS. Hippocampal epileptogenesis in animal models of mesial temporal lobe epilepsy with hippocampal sclerosis: The importance of the “latent period” and other concepts. *Epilepsia* 49: 85–92, 2008.

Sloviter RS, **Bumanglag A V.** Defining “epileptogenesis” and identifying “ antiepileptogenic targets” in animal models of acquired temporal lobe epilepsy is not as simple as it might seem. *Neuropharmacology* 69: 3–15, 2013.

Smith BN, **Dudek FE**. Short- and long-term changes in CA1 network excitability after kainate treatment in rats. *J Neurophysiol* 85: 1–9, 2001.

Sofroniew M V. Neuroscientist Reactive Astrocytes in Neural Repair and Protection. *Neurosci.* 11(5):400-7, 2005.

Staley KJ, **White A**, **Dudek FE**. Interictal spikes: harbingers or causes of epilepsy? *Neurosci Lett* 497: 247–50, 2011.

Statler KD, **Scheerlinck P**, **Pouliot W**, **Hamilton M**, **White HS**, **Dudek FE**. A potential model of pediatric posttraumatic epilepsy. *Epilepsy Res* 86: 221–3, 2009.

Steriade M, **Nuñez A**, **Amzica F**. Intracellular analysis of relations between the slow (< 1 Hz) neocortical oscillation and other sleep rhythms of the electroencephalogram. *J Neurosci* 13: 3266–83, 1993.

Sun H, **Juul HM**, **Jensen FE**. Models of hypoxia and ischemia-induced seizures. *J Neurosci Methods* 260: 252–260, 2016.

Szabadics J, **Varga C**, **Molnár G**, **Oláh S**, **Barzó P**, **Tamás G**. Excitatory effect of GABAergic axo-axonic cells in cortical microcircuits. *Science* 311: 233–5, 2006.

Taniguchi H, **Andreasson K**. The hypoxic-ischemic encephalopathy model of perinatal ischemia. *J Vis Exp* ,19(21):955, 2008.

Tharp BR, **Scher MS**, **Clancy RR**. Serial EEGs in normal and abnormal infants with birth weights less than 1200 grams--a prospective study with long term follow-up. *Neuropediatrics* 20: 64–72, 1989.

Thind KK, **Yamawaki R**, **Phanwar I**, **Zhang G**, **Wen X**, **Buckmaster PS**. Initial loss but later excess of GABAergic synapses with dentate granule cells in a rat model of temporal lobe epilepsy. *J Comp Neurol* 518: 647–67, 2010.

Thomas Carmichael S, **Wei L**, **Rovainen CM**, **Woolsey TA**. New Patterns of Intracortical Projections after Focal Cortical Stroke. *Neurobiol Dis* 8: 910–922, 2001.

Thoresen M, **Penrice J**, **Lorek a**, **Cady EB**, **Wylezinska M**, **Kirkbride V**, **Cooper CE**, **Brown GC**, **Edwards a D**, **Wyatt JS**. Mild hypothermia after severe transient hypoxia-ischemia ameliorates delayed cerebral energy failure in the newborn piglet. *Pediatr Res* 37: 667–70, 1995.

Topjian AA, **Sánchez SM**, **Shults J**, **Berg RA**, **Dlugos DJ**, **Abend NS**. Early Electroencephalographic Background Features Predict Outcomes in Children Resuscitated From Cardiac Arrest. *Pediatr Crit Care Med* 17: 547–57, 2016.

Towfighi J, **Mauger D**, **Vannucci RC**, **Vannucci SJ**. Influence of age on the cerebral lesions in an immature rat model of cerebral hypoxia – ischemia : a light microscopic study. *Dev Brain Res* 100(2) 149-60, 1997.

Toyoda I, **Fujita S**, **Thamattoor AK**, **Buckmaster PS**. Unit Activity of Hippocampal Interneurons before Spontaneous Seizures in an Animal Model of Temporal Lobe Epilepsy. *J Neurosci* 35: 6600–18, 2015.

Tuor UI, **Qiao M**, **Morgunov M**, **Fullerton E**, **Foniok T**, **Kirton A**. Magnetization transfer and diffusion imaging of acute axonal damage in the cerebral peduncle following hypoxia-ischemia in neonatal rats. *Pediatr Res* 73: 325–31, 2013.

Tyler WJ, **Pozzo-Miller L**. Miniature synaptic transmission and BDNF modulate dendritic spine growth and form in rat CA1 neurones. *J Physiol* 553: 497–509, 2003.

Vannucci RC, **Connor JR**, **Mauger DT**, **Palmer C**, **Smith MB**, **Towfighi J**, **Vannucci SJ**. Mini-Review Rat Model of Perinatal Hypoxic-Ischemic Brain Damage. *J Neurosci Res* 163: 158–163, 1999.

Vannucci RC, **Towfighi J**, **Vannucci SJ**. Secondary Energy Failure After Cerebral Hypoxia – Ischemia in the Immature Rat. *J Cereb Blood Flow Metab* 24(10): 1090-7, 2004

Vautrin J, **Barker JL**. Presynaptic Quantal Plasticity : Katz ' s Original Hypothesis Revisited. *Synapse* 199: 184–199, 2003.

Villapol S, **Gelot A**, **Renolleau S**, **Charriaut-Marlangue C**. Astrocyte responses after neonatal ischemia: the yin and the yang. *Neuroscientist* 14: 339–344, 2008.

Volpe JJ. Brain injury in the premature infant: overview of clinical aspects, neuropathology, and pathogenesis. *Semin Pediatr Neurol* 5: 135–51, 1998.

Volpe JJ. Brain injury in premature infants: a complex amalgam of destructive and developmental disturbances. *Lancet Neurol* 8: 110–24, 2009.

Wang S, **Zhang XQ**, **Song CG**, **Xiao T**, **Zhao M**, **Zhu G**, **Zhao CS**. In vivo effects of bumetanide at brain concentrations incompatible with NKCC1 inhibition on newborn DGC structure and spontaneous EEG seizures following hypoxia-induced neonatal seizures. *Neuroscience* 286:

203–215, 2015.

Wang Y, **Cao M**, **Liu A**, **Di W**, **Zhao F**, **Tian Y**, **Jia J**. Changes of Inflammatory Cytokines and Neurotrophins Emphasized Their Roles in Hypoxic–Ischemic Brain Damage. *Int J Neurosci* 123: 191–195, 2013.

Wang Y, **Cheung P-T**, **Shen GX**, **Wu EX**, **Cao G**, **Bart I**, **Wong WHS**, **Khong P-L**. Hypoxic-ischemic brain injury in the neonatal rat model: relationship between lesion size at early MR imaging and irreversible infarction. *AJNR Am J Neuroradiol* 27: 51–4, 2006.

Watanabe K, **Hara K**, **Miyazaki S**, **Hakamada S**. The role of perinatal brain injury in the genesis of childhood epilepsy. *Folia Psychiatr Neurol Jpn* 34: 227–32, 1980.

Weitzel L-R, **Sampath D**, **Shimizu K**, **White AM**, **Herson PS**, **Raol YH**. EEG power as a biomarker to predict the outcome after cardiac arrest and cardiopulmonary resuscitation induced global ischemia. *Life Sci.* 16:3056-6, 2016

White A, **Williams PA**, **Hellier JL**, **Clark S**, **Dudek FE**, **Staley KJ**. EEG spike activity precedes epilepsy after kainate-induced status epilepticus. *Epilepsia* 51: 371–83, 2010.

Whittington MA, **Cunningham MO**, **LeBeau FEN**, **Racca C**, **Traub RD**. Multiple origins of the cortical gamma rhythm. *Dev Neurobiol* 71: 92–106, 2011.

Whittington MA, **Traub RD**. Interneuron diversity series: inhibitory interneurons and network oscillations in vitro. *Trends Neurosci* 26: 676–82, 2003.

Williams CE, **Gunn AJ**, **Synek B**, **Gluckman PD**. Delayed seizures occurring with hypoxic-ischemic encephalopathy in the fetal sheep. *Pediatr Res* 27: 561–565, 1990.

Williams PA, **Dou P**, **Dudek FE**. Epilepsy and synaptic reorganization in a perinatal rat model of hypoxia-ischemia. *Epilepsia* 45: 1210–8, 2004.

Williams P a, **Dudek FE**. A chronic histopathological and electrophysiological analysis of a rodent hypoxic-ischemic brain injury model and its use as a model of epilepsy. *Neuroscience* 149: 943–61, 2007.

Williams PA, **White AM**, **Clark S**, **Ferraro DJ**, **Swiercz W**, **Staley KJ**, **Dudek FE**. Development of spontaneous recurrent seizures after kainate-induced status epilepticus. *J Neurosci* 29: 2103–12, 2009.

Williams SR, **Mitchell SJ**. Direct measurement of somatic voltage clamp errors in central neurons. *Nat Neurosci* 11: 790–8, 2008.

Wirrell EC, **Armstrong E a**, **Osman LD**, **Yager JY**. Prolonged seizures exacerbate perinatal hypoxic-ischemic brain damage. *Pediatr Res* 50: 445–454, 2001.

Witte OW, **Bidmon HJ**, **Schiene K**, **Redecker C**, **Hagemann G**. Functional differentiation of multiple perilesional zones after focal cerebral ischemia. *J Cereb Blood Flow Metab* 20: 1149–65, 2000.

Yang Y, **Shuaib A**, **Li Q**, **Siddiqui MM**. Neuroprotection by delayed administration of topiramate in a rat model of middle cerebral artery embolization. *Brain Res* 804: 169–176, 1998.

Yasuoka N, **Nakajima W**, **Ishida A**, **Takada G**. Neuroprotection of edaravone on hypoxic-ischemic brain injury in neonatal rats. *Dev Brain Res* 151: 129–139, 2004.

Zayachkivsky A, **Lehmkuhle MJ**, **Ekstrand JJ**, **Dudek FE**. Ischemic injury suppresses hypoxia-induced electrographic seizures and the background EEG in a rat model of perinatal hypoxic-ischemic encephalopathy. 114(5):2753-63, 2015

Zayachkivsky A, **Lehmkuhle MJ**, **Fisher JH**, **Ekstrand JJ**, **Dudek FE**. Recording EEG in immature rats with a novel miniature telemetry system. *J Neurophysiol* 109: 900–11, 2013.

Zhang RL, **Zhang ZG**, **Zhang L**, **Chopp M**. Proliferation and differentiation of progenitor cells in the cortex and the subventricular zone in the adult rat after focal cerebral ischemia. *Neuroscience* 105: 33–41, 2001.

Zhu WW, **Ma XL**, **Guo AL**, **Zhao HY**, **Luo HH**. Neuroprotective effects of NEP1-40 and fasudil on Nogo-A expression in neonatal rats with hypoxic-ischemic brain damage. *Genet Mol Res* 10: 2987–95, 2011.